BOUNDING SURFACE APPROACH TO THE FATIGUE MODELING OF ENGINEERING MATERIALS WITH APPLICATIONS TO WOVEN FABRIC COMPOSITES AND CONCRETE

A Dissertation
Submitted to the Graduate Faculty
of the
North Dakota State University
of Engineering and Architecture

By

Chao Wen

In Partial Fulfillment of the Requirements
For the Degree of
DOCTOR OF PHILOSOPHY

Major Department:
Civil Engineering

March 2011

Fargo, North Dakota

North Dakota State University
Graduate School

Title

Bounding Surface Approach to the Fatigue Modeling of Engineering Materials with Applications to Woven Fabric Composites and Concrete

By

Chao Wen

The Supervisory Committee certifies that this ***disquisition*** complies with North Dakota State University's regulations and meets the accepted standards for the degree of

DOCTOR OF PHILOSOPHY

ABSTRACT

Wen, Chao, Ph.D., Department of Civil Engineering, College of Engineering and Architecture, North Dakota State University, March 2011. Bounding Surface Approach to the Fatigue Modeling of Engineering Materials with Applications to Woven Fabric Composites and Concrete. Major Professor: Dr. Frank Yazdani.

It has been known that the nucleation and growth of cracks and defects dominate the fatigue damage process in brittle or quasi-brittle materials, such as woven fabric composites and concrete. The behaviors of these materials under multiaxial tensile or compression fatigue loading conditions are quite complex, necessitating a unified approach based on principles of mechanics and thermodynamics that offers good predictive capabilities while maintaining simplicity for robust engineering calculations. A unified approach has been proposed in this dissertation to simulate the change of mechanical properties of the woven fabric composite and steel fiber reinforced concrete under uniaxial and biaxial fatigue loading. The boundary surface theory is used to describe the effect of biaxial fatigue loading. A fourth-order response tensor is used to reflect the high directionality of the damage development, and a second-order response tensor is used to describe the evolution of inelastic deformation due to damage. A direction function is used to capture the strength anisotropic property of the woven fabric composite. The comparisons between model prediction results and experimental data show the good prediction capability of models proposed in this dissertation.

ACKNOWLEDGEMENTS

I would like to thank my advisor, Dr. Frank Yazdani, for the guidance, encouragement, personal development and patience he always provided during the course of this work. I especially appreciate the in-depth explanation of the fundamental principles that generated new insight and ideals. His technical and editorial advice was essential to the completion of this dissertation.

I would also like to thank my other committee members, Dr. Alan Kallmeyer, Dr. Magdy Abdelrahman, and Dr. Yail (Jimmy) Kim, for their help during my course studies and valuable suggestions on my dissertation.

The friendship with my colleagues at school and at Black & Veatch Corp. is very much appreciated and has made the many hours of work bearable. The discussions and support from Na Zhang, Kamal Thapa, and Rick Yang are invaluable.

Last, but not least, my deepest gratitude goes to my parents, Yusong Wen and Yuefang Xiao. Their unconditional love and support are in the end what made everything possible.

TABLE OF CONTENTS

LIST OF TABLES

LIST OF FIGURES

1. INTRODUCTION

1.1. Material fatigue

The tendency of material to break under repeated stress is called material fatigue. Usually, the applied maximum stress is less than the ultimate tensile strength of the material. Material fatigue, especially metal fatigue, which has caused a large percentage of engineering failures, has been intensively studied, after researchers began to notice this phenomenon in the early 19th century. (Refer to Figure 1.1.)

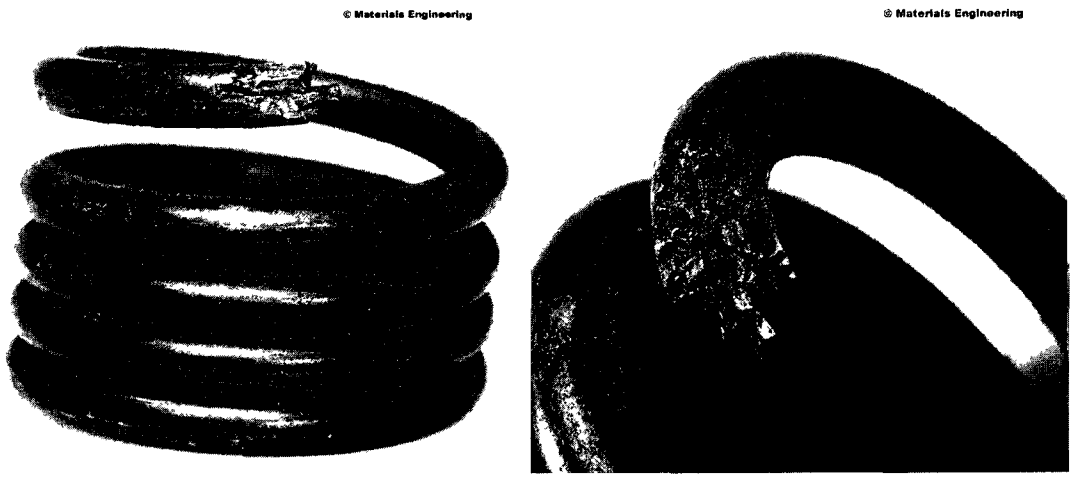

Figure 1.1. Fatigue failure in spring (http://materials.open.ac.uk/mem/mem_mf.htm)

However, the research and studies on material fatigue are still highly limited, because of the complex nature of the fatigue process and the number of influencing factors, such as the uncertainty of real loading cycles, variations of loading combinations, change of temperature, impact of corrosive environment, and different rates of material degradation. For example, the spring shown on Figure 1.1 suffers a

complex loading combination of bending, torsion and fatigue in the working environment. Fortunately, design data have been accumulated for different engineering metals and alloys, and a series of rules, empirical or based on scientific understanding, has been set up for design.

To meet higher engineering requirements, many new materials have been developed and widely applied, such as composite material, because they show very different mechanical properties from those of traditional metal and alloy, especially under fatigue conditions. For example, as shown on Figure 1.2, composites are only about 12 percent of the total materials by weight in the Boeing 777 plane. However, composites and fiberglass are about 50 percent of the total materials by weight in the newer Boeing 787 plane.

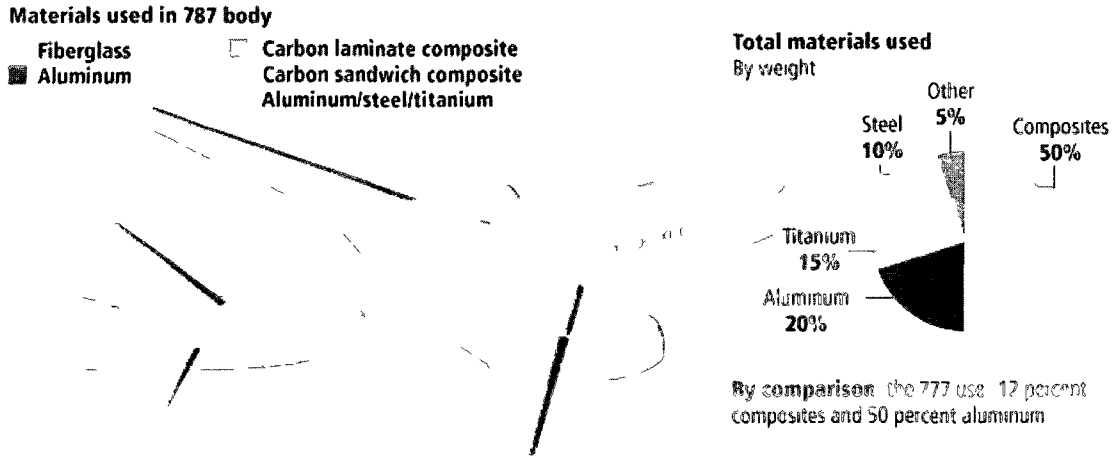

Figure 1.2. Application of composites in aerospace: Material used in 787 body. (http://seattlepi.nwsource.com/boeing/787/787primer.asp)

Although composites' micro-structure and fabrication processes are very different than metallic materials, the methods used to study the fatigue of these materials are similar. Therefore, the application of the existing design methodology for the new materials may become questionable and even unsafe. Lack of understanding of the mechanical properties of the new materials has led to many engineering failures, such as the rudder of the Airbus A310 shown on Figure 1.3 that is a composite reinforced 28 feet high structure and fell off just after the aircraft took off.

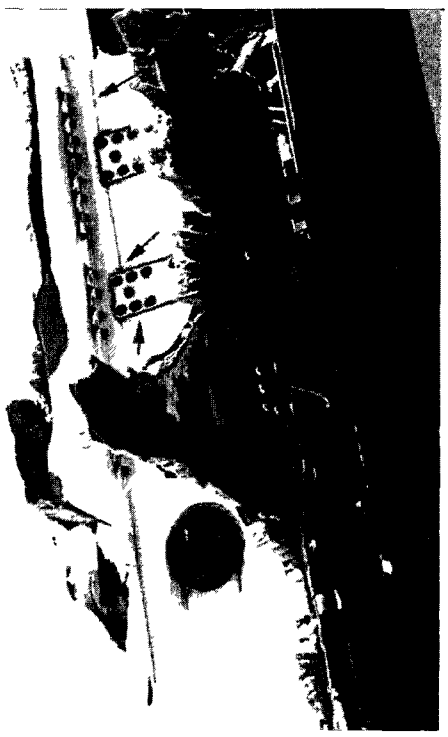

Figure 1.3. Rudder failure of Airbus A310 model plane. (http://www.yachtsurvey.com/composite_troubles_in_aircraft.htm)

1.2. Composite materials

Composite materials consist of two or more physically distinct and mechanically separable constituents. The term "composite" implies that the constituents are not only different at the molecular level but also have distinctive component properties, and they are generally mechanically separable. Usually, the composite material is a combination of a reinforcing material, such as a particle or a fiber, and a matrix or a binder material. The largest subdivision of composites is the fiber reinforced plastics (FRP) in which the matrix is a polymer (or plastic) and the reinforcement is always a fiber. With superior properties of fiber, the FRP displays many advantages over the traditional materials. These advantages include lower corrosion, lower density, higher specific stiffness and strength, better opportunity to tailor material properties by choosing different fibers. Other design objectives may be met also by varying fiber resin ratio or resin formulation, selecting different processes, and applying various fabrication methods. With these advantages the FRP has been widely used especially in weight critical and corrosion related industries. The comparison of mechanical properties between composite materials and conventional materials is listed in Table 1.1.

The most commonly used fiber-reinforcement forms are uni-directional lamina and woven fabric (Figure 1.4). Woven fabric composite is widely used in engineering applications for its better mechanical properties than the uni-directional lamina. Woven fabrics have higher resistance to impact loading, show high strength

and dimensional stability, offer high heat and fire resistance, and are preferred in applications where a biaxial stress state exists.

Table 1.1. Composite Materials v.s. Conventional Materials

Material	Density, ρ (g/cm^3)	Modulus, E_t (GPa)	Strength, σ_t (GPa)	ε_{fra} (%)	E/ ρ (GPa/Kg)	σ_t/ ρ (GPa/Kg)
Al-Zn-Mg Alloy	2 8	72	503	11	25 7	180
Low Alloy Steel	7 85	207	2050-2600	11-28	26 4	261-276
Nylon 66	1 14	2	70	60	1 8	61
Carbon/Epoxy	1 62	220	1400	0 8	135	865
Glass/Polyester	1 93	38	750	1 8	19 7	390

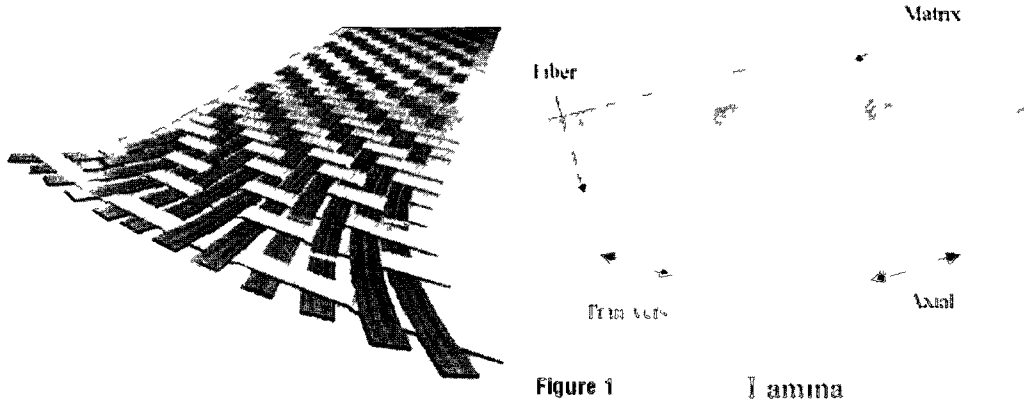

Figure 1 4 Woven fabric composite (http //nathanscars wordpress com/2008/08/04/)

However, due to a more complex reinforcement form and production technique, the mechanical behaviors of the woven fabric composite are much more complicated than those of uni-directional composite, especially under fatigue loading

conditions. Figure 1.5 shows some common reinforcing forms of woven fabrics, and Figure 1.6 shows the properties of woven fabrics with different reinforcing forms. It can be seen that one specific reinforcing form may show excellent properties in some aspects but very poor properties in some other aspects.

1.3. Fatigue behaviors of woven fabric composites

Fatigue damage in metallic materials usually begins initially from a single micro-crack or micro-defect, and propagates as one crack until the final failure without warning. In common low-level stress fatigue, only the metal properties in the vicinity of the crack are impacted, and those far away from the crack almost has no change.

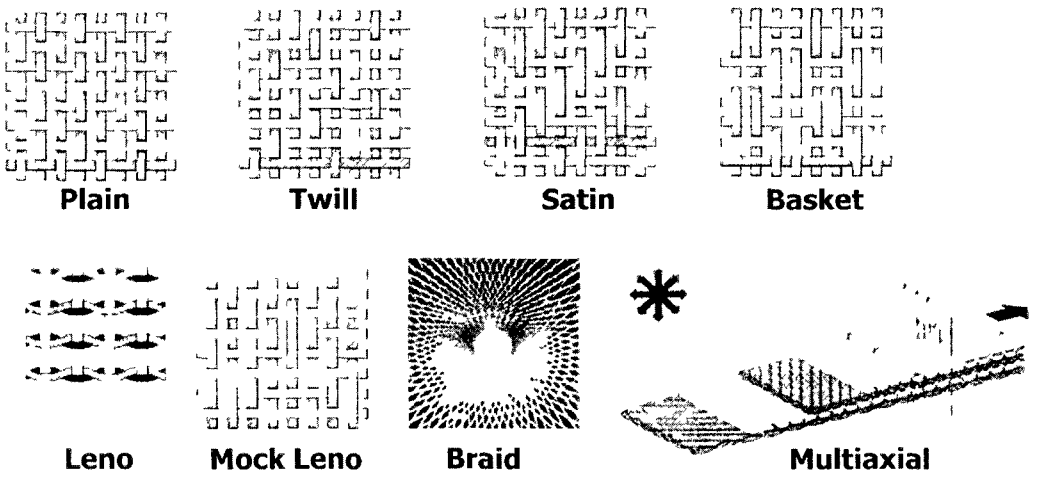

Figure 1.5. Reinforcement forms of woven fabric composites. (http://autospeed.com/cms/title_Complete-Guide-to-Composites-Part-4/A_108696/article.html)

Property	Plain	Twill	Satin	Basket	Leno	Mock leno
Good stability	****	***	**	**	*****	***
Good drape	**	****	*****	***	*	**
Low porosity	***	****	*****	**	*	***
Smoothness	**	***	*****	**	*	**
Balance	****	****	**	****	**	****
Symmetrical	*****	***	*	***	*	****
Low crimp	**	***	*****	**	**/*****	**

***** = excellent, **** = good, ***= acceptable, ** = poor, * = very poor

Figure 1.6. Properties of woven fabric composites with different reinforcement forms. (http://autospeed.com/cms/title_Complete-Guide-to-Composites-Part-4/A_108696/article.html)

The fatigue in woven fabric composites is quite different from that in metallic materials. The reinforcement plays an important role in determining the fatigue behaviors of composite materials due to the presence of reinforcement/matrix interface. The interface determines the inter-laminar shear strength, delamination resistance, fatigue resistance, and corrosion resistance, and makes the damage a strong directionality process as shown in Figure 1.7.

There are three types of interfaces in woven composites: resin-rich area to longitudinal fiber group, resin-rich area to transverse fiber group, and longitudinal fiber group to transverse fiber group. When the fatigue load is applied in the longitudinal direction, it is shown (Smith and Pascoe, 1989) that only the first and third types of interfaces described above tend to stop the development of cracks

perpendicular to the loading direction. This is attributed to the strength and stiffness of the longitudinal fiber group. The resultant stress concentration would then lead cracks into the weak interface area around the longitudinal fiber group and promote the breaking of interfaces between adjacent layers. After a number of the weak interfaces are broken down, and resultant separate interface areas are joined together, delamination emerges.

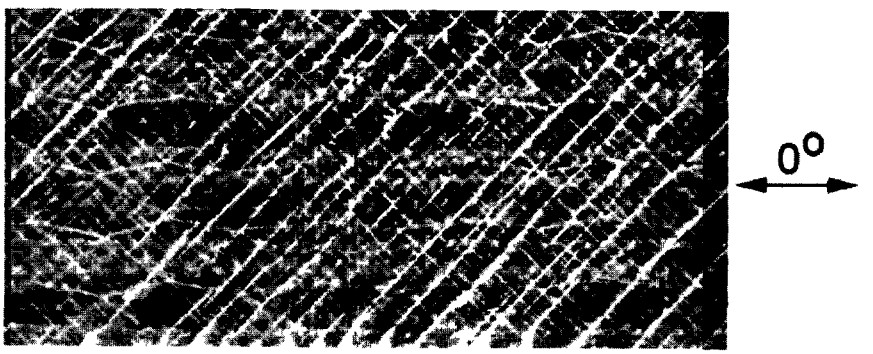

Figure 1.7. Damage directionality. (Samborsky, 2008)

Under these complex phenomena, several different damage modes are present: micro-cracking, cracking, debonding, delamination, fiber fracture, etc. (Smith and Pascoe 1989). These damage modes can be divided into two groups: micro-structural damage mechanisms within the impregnated strand, and macro-structural damage mechanisms between different phases. The first type includes matrix micro-cracking, fiber/matrix interfacial debonding, fiber breakage and crack coupling. The second type of damage mechanisms includes transverse cracking, shear failure in longitudinal fibers, cracking in pure matrix regions, delamination between adjacent layers, longitudinal fiber tensile failure and final fracture.

Many observations show that the fatigue process can be divided into three stages (Hansen, 1999; Natarajan et al., 2005), as shown on Figure 1.8. The abscissa is the loading cycles, and the y-axis can be several mechanical properties and variations, such as longitudinal specimen stiffness (Hansen, 1999), expended energy (Natarajan et al., 2005). In the first stage, the main damage modes are micro damage mechanisms. The rapid damage accumulates and stiffness reduces attribute to the release of the geometrically stress and strain concentrations. This rapid reduction in stiffness is called as the "knee effect." as shown in Figure 1.9. The square dots are the experimental data of the longitudinal stiffness at different number of loading cycles of one fatigue test (Hansen, 1999.) This process continues until the micro-crack saturates, which means that the geometrically stress and strain concentrations are almost totally released.

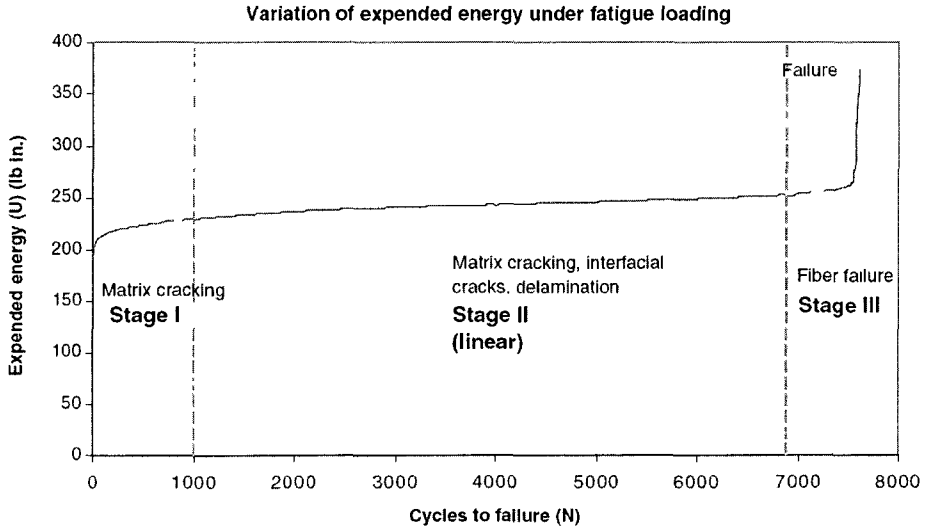

Figure 1.8. Three stages of fatigue process in woven fabric composite. (Natarajan et al., 2005)

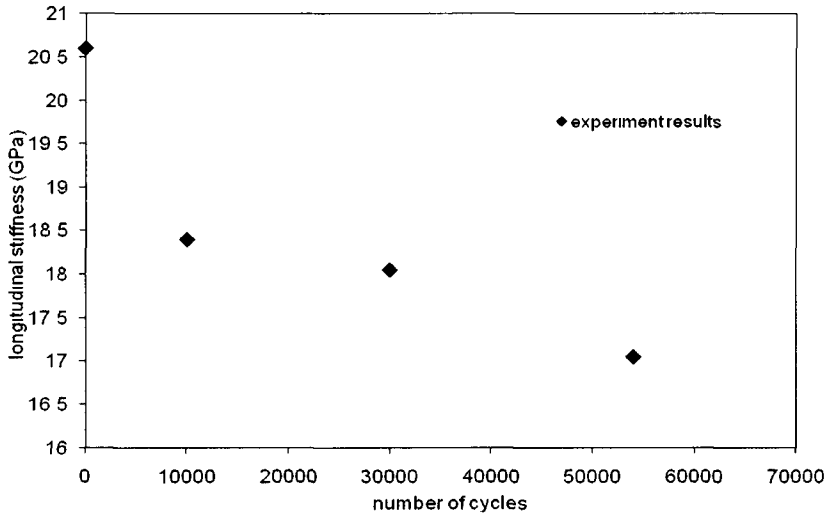

Figure 1.9. Illustration of "knee effect". (Hansen, 1999)

The second stage is controlled by a combination of matrix cracking, interfacial cracking and delamination. In this stage, damage accumulates slower and more stable rate than the first stage due to the interlock between different phases, such as between longitudinal and transverse fibers. The mechanical properties change approximately in a linear rule under logarithmic coordinates. (Natarajan et al., 2005)

With further loading, at over-stressing or over-straining concentrations, the last stage occurs. During the last stage, various kinds of damage mechanisms grow rapidly and cause a high rate of damage accumulations. When the stress or strain states reach critical values, fiber fracture occurs and the composite fabric fails.

Another important characteristic of woven fabric is the strength anisotropy. Fiber type or fiber density of woven fabric can be different in different directions to meet various strength requirements, especially in weight-critical situation. Thus, the

strength of the woven fabric is anisotropy as shown in Figure 1.10. The square dots are the experimental data of ultimate tensile strengths of woven fabric in various biaxial loadings (Franklin 1968.) All of these phenomena demonstrate that the fatigue of woven composites is a very complex process.

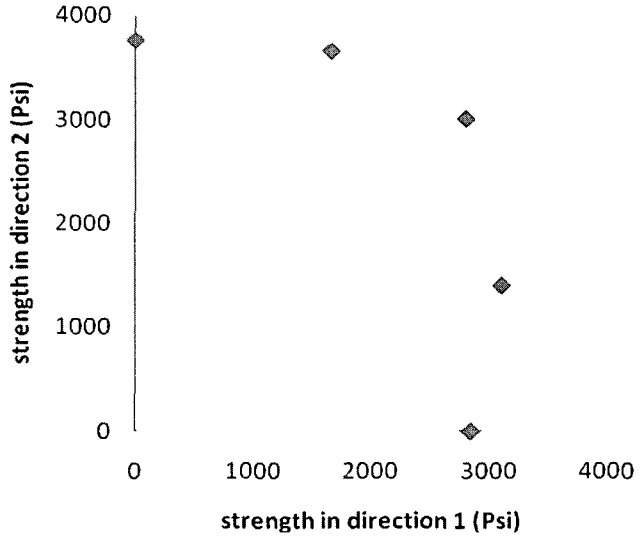

Figure 1.10. Strength anisotropy. (Franklin 1968)

2. LITERATURE REVIEW

2.1. Introduction

The complex properties and damage modes make the modeling of the fatigue process a very difficult task. However, many researchers have put much effort into this area, and many models have been proposed during the last several decades. Based on the different main parameters, these models can be divided into three categories: fatigue life models, phenomenological residual strength/stiffness models, and progressive damage models (Degrieck et al., 2001).

2.2. Categories of existing models

2.2.1 Fatigue life models

The fatigue life models are the earliest type of models. This type does not consider the damage accumulation, but extracts the information about the fatigue life from the "S-N" curves or Goodman-type diagrams. Although this type cannot show the details of the fatigue damage development, it gives the information that most concerns the industry. Thus, this type is widely used in many computer codes, such as ANSYS, and in many engineering standards.

The basic forms of "S-N" curves are power function and logarithm function. The first one can be shown as

$$e^{aS}N = c \tag{2.1}$$

where a and c are material constants that are determined by material properties, specimen configurations, and loading methods; e is the base of natural

logarithm; S is the applied stress; and N is the fatigue life corresponding to the applied stress. Taking the natural logarithm to both sides of Equation 2.1, one obtains

$$aS\lg e + \lg N = \lg c \tag{2.2}$$

Setting $a\lg e = A$, $\lg c = B$, one obtains

$$AS + \lg N = B \tag{2.3}$$

This equation shows that the applied stress, S, and fatigue life, N, are in a linear relation in the semi-logarithm coordinate system.

The logarithm function can be written as

$$S^a N = c \tag{2.4}$$

where a and c are material parameters that are also determined by material properties, specimen configurations, and loading methods; S is the applied stress; and N is the fatigue life corresponding to the applied stress. Taking the natural logarithm to both sides of Equation 2.4, one obtains

$$a\lg S + \lg N = \lg c \tag{2.5}$$

This equation shows that the applied stress, S, and fatigue life, N, are in a linear relation in the bi-logarithm coordinate system.

Based on these two basic forms, many models proposed with considerations of some other factors that affect the material fatigue life, such as the stress ratio between maximum applied stress and minimum applied stress, mean stress, and fatigue limit.

Caprino and Giorleo (1999) established a model with the influence of the stress ratio.

$$N = \left[1 + \frac{1}{\alpha \cdot (1-R)} \cdot \left(\frac{\sigma_0}{\sigma_{max}} - 1\right)\right]^{1/\beta} \tag{2.6}$$

where R is the stress ratio; α and β are material parameters determined experimentally; σ_0 is the monotonic tensile strength of virgin material; σ_{max} is the maximum applied stress; N is the fatigue life. This model shows good correlations for long life prediction as shown on Figure 2.1, but for short life prediction the results are not sure.

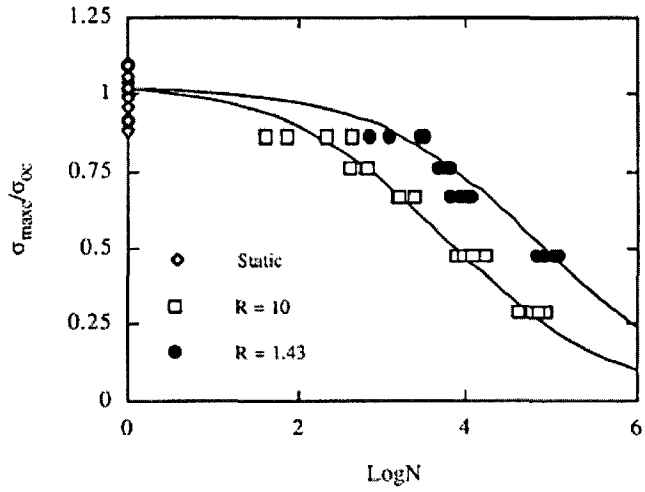

Figure 2.1. Semi-log plot of the non-dimensional maximum applied stress- the number of cycles to failure. Continuous lines: theoretical predictions. (Caprino and Giorleo, 1999)

2.2.2. Phenomenological models

Phenomenological models are also called as Continuum Damage Mechanics (CDM) models and can be divided into two categories: residual stiffness model and residual strength model.

Residual stiffness models describe the degradation of the elastic properties of material during the fatigue process. A variable D is often used to name damage, but different people used different definitions for D. In the uniaxial fatigue condition, one popular definition is $D=1-E/E_0$, where E_0 is the initial or undamaged Young's modulus. Although these models use D as a damage variable, they do not take the actual damage mechanisms into account, but use a macro scale mathematical expression to describe the change of the damage rate, dD/dN. It seems desirable and accurate to predict the fatigue behaviors by monitoring the development of an individual crack; nevertheless it is formidable, if not impossible, because the crack-developing manner of woven fabric is not only an increase of the crack length, as it happens in metals, but also a multiplication of the crack numbers. And the latter dominates the main part (first and second stages) of the fatigue life, due to the stunting of the interlock between different phases. Therefore, the macro scale mathematical expression of the damage seems to be a good implement to simulate the fatigue development of composites.

The residual strength models describe the fatigue process through the degradation of the material strength and generally assume that the material fails when the residual strength reaches the applied stress. Two types of residual strength models can be distinguished: sudden death model and wearout model. The former one is suitable for high strength unidirectional composites where the residual strength acts as a function of the number of cycles with nearly the same value as the initiation and decreases dramatically when the number of cycles reaches the number of failure. The

latter one is more suitable for lower level states of stress where the residual strength decreases more gradually.

The two kinds of models have their advantages and disadvantages. The residual stiffness models show the whole fatigue process with a real material property which can be used in structural analysis and material evaluation, but it is difficult for these models to provide the final failure criteria. On the other hand, the residual strength models give a very clear failure criterion, but cannot show the fatigue process with a meaningful parameter through which the degraded material properties for a given loading cycle number can be determined. Considering these advantages and disadvantages, some researchers developed models that combined the advantages of these two models. Since it is difficult to divide these models into either group, they are not specifically categorized in this paper. The following models can be either kind or a combination of both.

Van Paepegem and J. Degrieck (2001) proposed a CDM model to predict the stiffness degradation. The model was too simple to be used in complex conditions, and the model had no theoretical background.

In the next year, they proposed another model (Van Paepegem et al., 2002). In this model, the authors considered the advantages and disadvantages of residual stiffness models and residual strength models, and took their advantages to simulate the stiffness degradation and give the final failure criteria. They developed a set of equations to picture the damage growth, and modified the Tsai-Wu static failure criterion as their failure criterion. The results were well correlated with the

experimental data as shown on Figure 2.2. However, the model still had no theoretical background but was just established based on experimental results. Also, this model had five parameters that needed to be determined and did not include the influence of either fiber direction or stress direction.

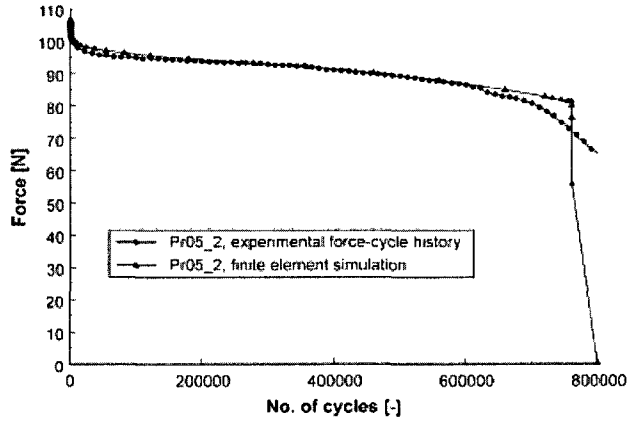

Figure. 2.2. Experimental and simulated force-cycle history. (Van Paepegem et al., 2002)

One year later, Paepegem et al. (2003) developed their model by taking the impact of stress directions and possible permanent strain into account. This model derived a multi-dimensional damage relationship from a one-dimensional damage relationship. The developments of the damages in different directions were expressed in a matrix form, and every element was given in a specific form. However, the expressions of damage developments made the model quite complex, although the predictions well matched the experimental data as shown on Figure 2.3.

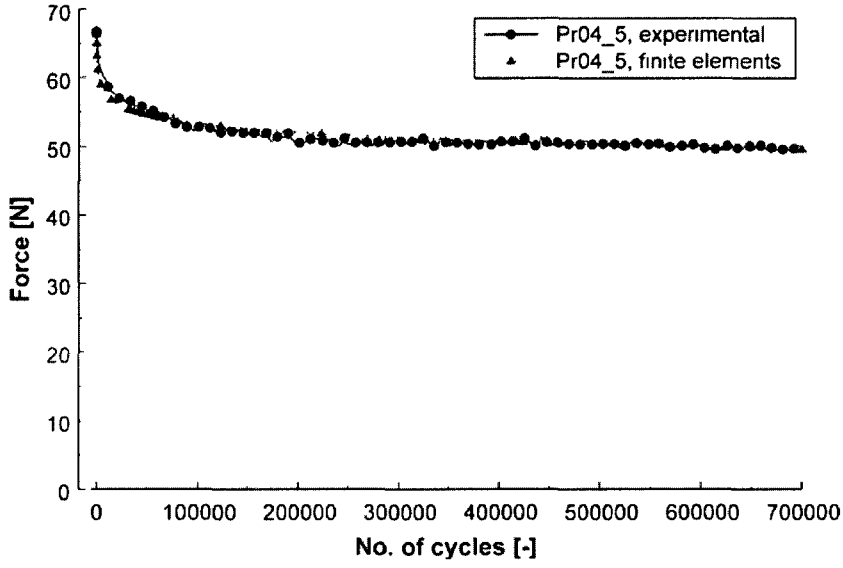

Figure 2.3. Experimental and simulated force-cycle history for the [#45°]8 speciman Pr04-5. (Paepegem et al. 2003)

Mao and Mahadevan (2002) proposed a model with a new damage variable for considering the influence of the final Young's modulus E_f and used a fatigue damage accumulation equation as follow

$$D = \frac{E_0 - E}{E_0 - E_f} \tag{2.7}$$

$$D = q\left(\frac{n}{N}\right)^{m_1} + (1-q)\left(\frac{n}{N}\right)^{m_2} \tag{2.8}$$

where q, m_1, and m_2 are material dependent parameters.

Their predictions were good for woven composites as shown on Figures 2.4. However, the three parameters are defined by three other equations, and their model did not consider the difference between uniaxial loading and multiaxial loading

conditions. This disadvantage severely undermined the capability of the model, although the damage variable, D, is often used as nondimensional.

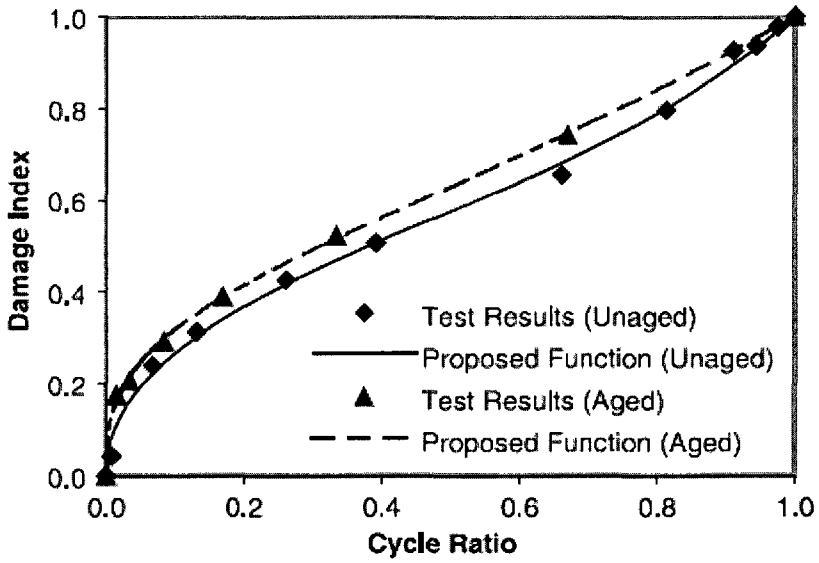

Figure 2.4. Experimental observation and model prediction for the AS4/PR500 woven composite. (Mao and Mahadevan, 2002)

Hansen (1999) pointed out that the impact on the surface of composite material plays an important role in the fatigue behavior of composite material. Thus, he used 3 levels of impact damage: undamaged, barely visible impact damaged (BVID), and penetrated damaged, in both static and fatigue testing. Hansen applied continuum damage mechanics to simulate the fatigue process. He considered a linear elastic isotropic solid for which the mechanical properties changed with the number of fatigue cycles. The change in mechanical properties was described through a

damage parameter β. He assumed the following relationship between the mechanical properties and β.

$$E = E_0(1-\beta) \text{ and } \nu = \nu_0(1-\beta) \tag{2.9}$$

where E_0 and ν_0 are the initial Young's modulus and Poisson's ratio.

Furthermore, the model was given a damage evolution function of the form

$$\beta = A\int_0^N \left(\frac{\varepsilon_e}{\varepsilon_0}\right)^n dN \qquad \beta \le \beta_{\lim} \tag{2.10}$$

where A and n are material parameters; ε_e is the effective strain measure given as $\varepsilon_e = \sqrt{\boldsymbol{\varepsilon} : \boldsymbol{\varepsilon}}$, and where ε_0 corresponds to the peak strain level during a fatigue cycle.

Based on these theories, Hansen predicted the degradation of the longitudinal stiffness with respect to the number of cycles as shown in Figure 2.5. Although Hansen's model was based on continuum damage mechanics and easy to be fulfilled by a computer program, the model did not involve the impact of the fiber directions and the stress directions, and the prediction results were not as good as those of other models.

2.2.3. Progressive damage models

These models differ from the models mentioned above because of the chosen damage variables, such as damage area, crack surface, and strain energy release rate, to describe the degradation of the materials.

Natarajan et al. (2004) proposed a fatigue damage model which was based on the internal strain energy release rate. They gave the formula of the energy release rate as

$$\frac{dU}{dN} = a\left(\frac{\varepsilon_{\max}}{\varepsilon_{ult}}\right)^{b} \tag{2.13}$$

where ε_{max} is the maximum induced strain of the material, ε_{ult} is the static ultimate strain of the material, and a and b are the fatigue coefficients.

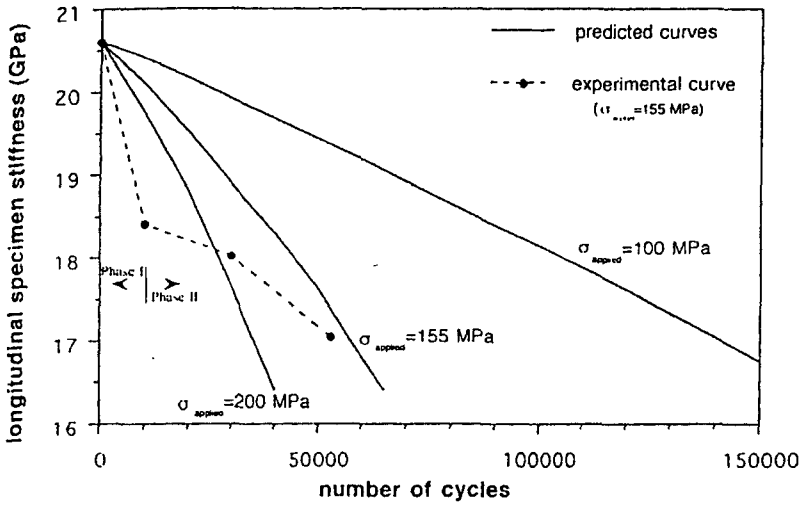

Figure 2.5. Prediction modulus reduction with number of cycles at three different applied stress levels. The experimentally measured modulus reduction at an applied stress of 155MPa as shown. (Hansen, 1999)

Based on this expression, the failure life was predicted as

$$N_f = \frac{0.5U_0}{a(\varepsilon_{\max}/\varepsilon_{ult})^{b}} \tag{2.14}$$

where U_0 is the initial internal strain energy. This model has a good correlation with the experiments as shown in Figure 2.6. However, for different loading types and materials, different formulas of strain energy and values of parameters are needed.

The failure criterion is assumed to be 50% increase in the total energy expended based on experimental observations.

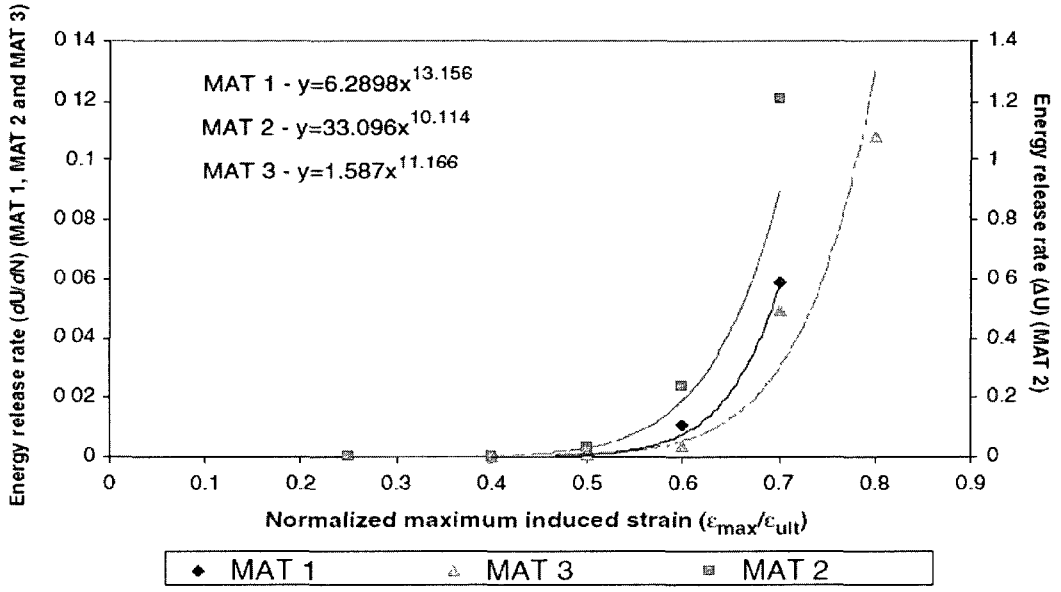

Figure. 2.6. Variation of energy release rate with percentage of ultimate strain applied for MAT 1, MAT 2, and MAT 3. (Natarajan et al., 2004)

Yoshioka and Seferis (2002) developed a model to predict the modulus deterioration based on a combination of the crimp model and the shear-lag model. With the micro level experiments, they proposed an idealized unit cell of plain woven composite containing fatigue damage as shown in Figure 2.7. With this idealized unit cell, they established equations to estimate the stiffness.

They also gave the expression of the effective transverse modulus with transverse cracking.

$$E'_2 = \frac{1 - \frac{2}{\alpha l_c}\tanh\left(\frac{\alpha l_c}{2}\right)}{1 + \frac{2}{\alpha l_c}\frac{E_2 t_2}{E_1 t_1}\tanh\left(\frac{\alpha l_c}{2}\right)} E_2 \tag{2.15}$$

where α is the shear-lag parameter, l_c is the crack spacing in the 90-deg lamina. E_1 and E_2 are the original longitudinal and transverse moduli, respectively. t_1 is the thickness of the adjacent 0-deg laminae and t_2 is the half thickness of the 90-deg lamina.

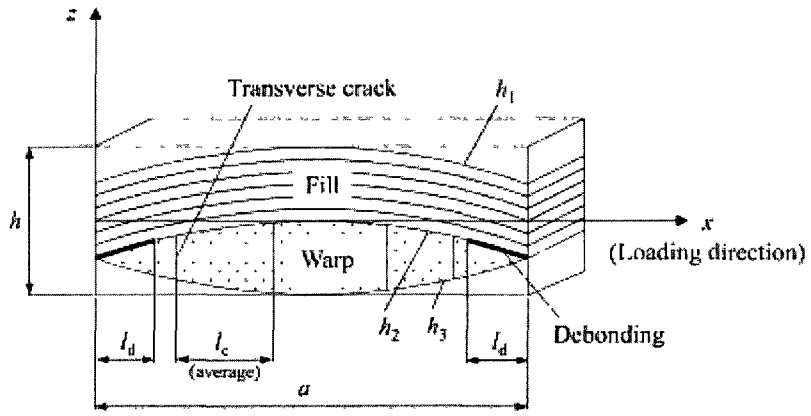

Figure. 2.7. Idealized unit cell of plain woven composite containing fatigue damage. (Yoshioka and Seferis, 2002)

This model is a very good attempt at modeling based on micro-level phenomena. However, many different phenomena are presented in the woven composite fatigue process. Therefore, modeling each phenomenon is not a practical method.

2.3. Conclusion of existing models

The fatigue life model is simple and easy to use, but it is not able to give information, such as the change of the modulus, that is required by engineering design, because of its inherent disadvantages as described above.

The progressive damage model is a good attempt to apply some new damage variables. The authors noticed that the propagation of cracks and microcracks is the main type of fatigue damage and dominates the fatigue process of composite materials; therefore, these authors logically try to picture the fatigue process by modeling the details of the evolution and growth of the crack or defect. However, from previous chapters it is obvious that modeling the evolution and growth of every crack or defect is a formidable task, if not an impossible one, because of the scatteration of the cracks and defects.

The phenomenological model gives the information which mostly interests design engineers and avoids the tedious work of monitoring every crack development and every damage mode. Therefore, the phenomenological model is a good method for modeling the composite fatigue.

2.4. Fatigue models for steel fiber reinforced concrete

Steel fiber reinforced concrete (SFRC) is a kind of composite composed of cement as the matrix, aggregate as the granular reinforcement, and steel fiber as the fiber reinforcement. Similar to the woven fabric, the properties of SFRC are also determined by the properties of matrix and reinforcement and the interfaces between

them. Before loading, micro-cracks scatteringly exist at the interfaces attribute to the cement contraction during hydration and the volume change during cement drying. During loading, the micro-cracks develop and finally connect to each other and cause the material fails. Since the fatigue load causes more micro-cracks than the monotonic load; and this effect is more pronounced in fiber reinforced concrete (Zhang et al., 1999,) successful description of the evolution of micro-cracks is essential to understand the evolution of the properties of SFRC under fatigue loadings. Based on the discussion of models of woven fabric composite, the phenomenological model or CDM model is also the best method to describe the evolution of the properties of SFRC.

2.5. Fatigue tests for woven fabric and steel fiber reinforced concrete

For better understanding of the behaviors of woven fabric composites and steel fiber reinforced concrete, calibrating parameters, and verifying proposed models, many experimental tests were performed.

Hansen (1999) performed a series of static and tension-tension proportional fatigue tests for woven fabric composites with three levels of damage, undamaged, barely visible impact damaged (BVID), and penetrated.

The specimens were made up of plain woven glass/epoxy prepreg fabrics with a lay-up sequence $[(+45\#-45)/(90\#0)]_s$. The symbol "#" indicates the bi-directional reinforcement of each prepreg. The dimension of the specimen were 100mm width, 190mm gage length, and 0.9mm thickness. Specimen manufacture consisted of

vacuum bagging and autoclaving. The Young's moduli of the woven fabric were 26.2GPa in direction 1 and 24.2GPa in direction 2, respectively. The Poison's ratio was 0.138. The tensile strengths were 400MPa in direction 1 and 381MPa in direction 2, respectively. The failure strains were 1.52% in direction 1 and 1.56% in direction 2, respectively. Hansen (1999) also measured the properties of the specimen and obtained that the tensile strength of the specimen was 330MPa, and the failure strain was 2.2%.

The impact of the BVID and penetrated specimen was performed in a drop-weight tower using a spherical indenter with a radius of 12.5mm. The impact energies were 9 Joules and 20 Joules for the BVID and penetrated specimen, respectively. All tests were performed in a servo hydraulic Instron 1333 with hydraulic grips, and a 250 KN load cell. To record overall strains and displacements, HBM 6/350XY11 strain gages and an Instron 2620-602 extensometer were used. Static testing was generally performed at an actuator speed of 1mm/min. The tensile fatigue testing was performed in load control mode at a frequency of 5 Hz and with a load ratio of $R = \sigma_{min}/\sigma_{max} = 0$. Material hysteresis at this frequency leads to specimen surface temperatures of approximately 35 degree. A thermal imaging system (IT45) was included in the experimental set-up of the present work to estimate the surface temperature of the specimen over a region of dimensions of approximately 25mm x30mm by registering the infrared radiation.

Smith and Pascoe (1989) studied the fatigue of woven fabric composites with a series of fatigue tests of nine proportional biaxial and three uniaxial stress states.

One batch of test materials was used for the whole program. The laminate was laid up from reinforcement of glass-fiber woven roving, Marglass 266 24 oz (Fothergill and Harvey Ltd), and an isophthalic polyester resin, BP 2785 CV (BP Chemicals). The warp and weft fibers were balanced and the roving had a weave of 5mm width. Lamina thickness as laid up averaged 0.9mm and the test laminate contained 13 laminae. The nominal resin content was 46 per cent. The biaxial cruciform specimens were 300mm x 300mm and of 12mm nominal thickness with a 60mm square flat working section and bolted to the four loading arms. The parallel-sided uniaxial specimens were 50mm wide and bolted to the two loading arms. Grip reinforcement with duralumin plate is used to avoid fracture in the arms.

The properties of the specimen under monotonic loadings were listed as follows. The Young's moduli of the specimen were 17.07GPa and 18.31GPa in weft and warp directions, respectively. The Poison's ratios were 0.155 and 0.167 in weft and warp directions, respectively. The tensile strengths were 238MPa and 257MPa in weft and warp directions, respectively. The failure strains were 1.7% and 2.4% in weft and warp directions, respectively.

A biaxial hydraulic servo-controlled rig developed at the Cambridge University Engineering Department was used for all the tests. This machine is able to test biaxial cruciform specimens for any phase of principal in-plane loadings up to ±200KN. A special extensometers based on bending of a short resistance-strain-gauged double cantilever beam were developed to measure and monitor the specimen strain throughout the fatigue tests. All tests were under load control with a load ratio

R equals to -1. The fatigue test frequencies were generally kept in the range 0.1 to 0.6 Hz to prevent excessive cyclic induced heating.

Yin and Hsu (1995) tested the fatigue behaviors of steel fiber reinforced concrete plates under uniaxial or proportional biaxial compressive fatigue loadings. The concrete specimens were made of type III Portland cement. The mix proportion was 1:2.16:1.88, by weight, for cement, sand, and coarse aggregate, respectively. The water cement ratio was 0.6 and the maximum size of aggregate was 0.5in. For fiber concrete specimens, the aggregate consisted of quartz and flint, with some feldspar. The carbon steel fibers were smooth, straight, slit-type, with a cross section of 0.01 x 0.022in. The length of fiber was 1in. and the percentage of fiber volume used in all fiber concrete specimens was 1.0 per cent. The average tensile strength of steel fibers was 60ksi. Concrete mixing was done in a 5-ft^3 rotary drum mixer, while the fibers were gradually sprinkled into the drum by hand. After all the fibers were added, mixing continued for about 1 minute. Two 6x6x20in and three 6x6x40in steel molds were used for casting fiber concrete blocks. One 6x6x20in mold was used for the companion plain concrete block. The molds were laid with their longest dimensions horizontally for casting. The concrete blocks were stored in a water tank in the moist-room at 780 F and 100 percent relative humidity until sawing at 1 week before testing. The plate specimens were cut from the cast concrete blocks by a precision diamond saw. The dimensions of the specimen were 6x6x1.5in. After sawing, the concrete specimens were coated with two thin layers of sealant to prevent evaporation of water. By examining the cut surfaces and failure regions of the plate specimens,

the random orientation of the fibers was verified. Companion uniaxial compression tests of the plate specimens were carried out at regular time intervals to ascertain strength gain with age.

Specimens were tested in a specially designed biaxial test machine. The load was supplied by a hydraulic actuator with the capacity of 220kips, mounted on top of the testing frame. The downward load passed through a load cell and a spherical bearing hinge, and was then resolved into a pair of forces by a load bifurcation mechanism. The load bifurcation mechanism transformed a uniaxial load into two mutually perpendicular loads, thus creating a biaxial stress condition. Brush loading platens, rather than solid platens, were used to minimize the frictional confinement of the test specimens. Deformations in the three principal axes were measured by a pair of capacitance type transducers in each direction.

Four principal compression stress ratios were used in the tests, 0, 0.2, 0.5, and 1.0. For each principal stress ratio, the first test was at the maximum stress level of 1.0. The maximum stress level means the ratio of the maximum applied stress to the compression strength of plain concrete. And subsequent stress levels were taken at 1.1, 1.2, and so on, at an increment of 0.1, up to the test where the number of cycles at failure reached 1. After that, tests were carried out at stress levels of 0.9, 0.8, 0.7, and so on, at a decrement of 0.1, down to the test where the number of cycles at failure reached 2 million. At least two specimens were tested at each stress level for each stress ratio. The load ratio R equals to 0.05. The loading rate is 1 Hz. The loading wave form is triangular.

3. OBJECTIVE

As discussed in previous chapters, many researchers have modeled material behavior under fatigue loadings. However, many of these models were based on empirical equations without solid theoretical foundations. Some researchers proposed models that were based on general theories, but did not take into account many important characteristics of the material. Others introduced so many variables that the model was too complex to be applied to engineering. To overcome these disadvantages, three new continuum damage mechanical models based on the laws of thermodynamics have been developed in this dissertation to capture the characteristics of brittle or quasi-brittle materials under fatigue loadings by introducing limited material parameters. The advantages and details of continuum damage mechanics and thermodynamics are explained in Chapter 4.

One main characteristic of fatigue damage in brittle or quasi-brittle materials is that damage development is anisotropic. Therefore, the change of the compliance or stiffness and the development of the inelastic strain, if it exists, should be anisotropic, too. A fourth-order response tensor and a second-order response tensor are introduced in Chapter 5 to capture the effects of the anisotropic damage development on the compliance and the inelastic strain, respectively.

Another main characteristic of the fatigue process is the "knee effect," which means that the stiffness of the material has a rapid drop after a very short part of the fatigue life. After that, the reduction of the stiffness becomes stable and close to linearity. In the dissertation, a damage evolutionary law is proposed in Chapter 5 to

describe the process of the change of the material state and reflect the phenomenon of the "knee effect."

Although the model presented in Chapter 5 is able to describe several aspects of the fatigue process, its scope was limited and lacks generality the present work seeks. Therefore, a new model utilizing the bounding surface theory is established in Chapter 6 to improve upon the model introduced in Chapter 5. Another advantage of the bounding surface theory is that once the limit surface is established, the fatigue life of the material under any load combination can be determined through a simple loading path, such as a uniaxial loading path. The details of the model and the bounding surface theory are discussed in Chapter 6.

Usually, components in service are not in pure uniaxial or equal multiaxial loading conditions, but in nonequal multiaxial loading conditions. Using the same fibers in different loading directions is a waste of materials for components under nonequal, biaxial loadings. Therefore, choosing different fibers or different fiber densities in different directions can save some materials and, at the same time, tailor the mechanical properties of the woven composite to match the requirements of complex loading conditions. However, this adjustment will cause strength anisotropy in woven composite materials. To model this feature, a strength function is introduced in Chapter 6.

The damage that occurs in the first cycle should be treated as quasi-static damage rather than as fatigue damage. A shape function to capture the damage in the first cycle is discussed in Chapter 6 for a composite material model, and fully

explained in Chapter 7 for a concrete model. The damage in the first cycle is negligible for composite materials, but important for concrete.

Since the model proposed is a unified approach to the damage mechanics modeling of quasi-static and fatigue loading of brittle or quasi-brittle materials in general, it is natural to apply the established model to concrete, which is also a quasi-brittle material. However, compared to composite materials that are mainly applied in tension loading conditions because of their high tensile strengths, concrete is widely used in compression conditions for its relatively high compression strength to its tensile strength. Under compression loadings, the damage develops in a different manner from that of composite material under tensile loadings. A new fourth-order response tensor and a new second-order response tensor reflecting the effect of compression loadings are introduced in Chapter 7 to explain this difference.

4. CONTINUUM DAMAGE MECHANICS AND THERMODYNAMICS

4.1. Introduction

For a successful model that is able to describe the fatigue process of materials, two kinds of modeling are necessary. One process is the kinetic or mechanical modeling that deals with the motion and the force in the material and leads to consistent definitions of stresses, strains, and equations of equilibrium; another is the phenomenological modeling that is used to characterize the fatigue process by selecting suitable variables. Therefore, an approach of thermodynamics of irreversible processes and continuum damage mechanics by introducing state variables has been used. This chapter introduces the theories that are used in the following chapters.

4.2. Continuum mechanics and thermodynamics

The approach of the thermodynamics of irreversible processes is used here for two reasons: one reason is that this approach is able to provide a formalism that is directly accessible to the methods of functional analysis, and another is that the thermodynamic framework will be useful to guide and limit the possible choices in phenomenological modeling (Lemaitre and Chaboche, 1990).

Thermodynamics was initiated by chemists and was applied to continuum mechanics by Eckart and Biot around 1950 (Lemaitre and Chaboche, 1990). Through this method, the state of material can be described by defining associated variables

from observable variables and internal variables selected to study the phenomena. This, then, leads to the state laws. The dissipation inequality furnishes the laws of evolution for the variables that describe the irreversible processes.

It should be mentioned, however, that the thermodynamics applied here is without the consideration of thermal or true dynamic effects.

4.2.1. Cauchy's first law of motion

It is assumed that the total force acting on an isolated continuum body is composed of a body force $\mathbf{f}_b$ and a contact force $\mathbf{f}_c$

$$\mathbf{f} = \mathbf{f}_c + \mathbf{f}_b \tag{4.1}$$

and further assumed that the body force could be obtained from a vector field $\mathbf{b}(\mathbf{r},t)$.

$$\mathbf{f}_b = \int_R \mathbf{b}\rho dv \tag{4.2}$$

where, R is the volume of the body, ρ is the density of the material, dv is the infinitesimal volume of the material, $\mathbf{r}$ is the position vector with respect to the origin in the Eulerian coordinates, and t is current time.

Similarly $\mathbf{f}_c$ could be obtained by a vector field representing a force per unit area, stress vector $\mathbf{t}$, acting on ∂R, the surface of the body.

$$\mathbf{f}_c = \int_{\partial R} \mathbf{t}(\mathbf{r},\mathbf{n}) ds \tag{4.3}$$

where $\mathbf{n}$ is the unit normal vector, and ds is the infinitesimal surface of the material.

The total force acting on the body causes the body to move with an acceleration $\mathbf{a}$, so

$$\mathbf{f} = \int_R \mathbf{a}\rho dv \tag{4.4}$$

Thus, the relationship in Equation 4.1 can be expressed as follows by substituting Equation 4.2, 4.3, and 4.4 into Equation 4.1

$$\int_R \mathbf{a}\rho dv = \int_R \mathbf{b}\rho dv + \int_{\partial R} \mathbf{t}(\mathbf{r},\mathbf{n})ds \tag{4.5}$$

Cauchy's fundamental theorem states that at the boundary of the body:

$$\mathbf{t} = \boldsymbol{\sigma} \cdot \mathbf{n} \tag{4.6}$$

where, $\boldsymbol{\sigma}$ is Cauchy's stress tensor.

So, with preceding equation, Equation 4.5 is as follows:

$$\int_R \mathbf{a}\rho dv = \int_R \mathbf{b}\rho dv + \int_{\partial R} \boldsymbol{\sigma} \cdot \mathbf{n} ds \tag{4.7}$$

With the application of the divergence theorem, Equation 4.5 becomes the following:

$$\int_R \mathbf{a}\rho dv = \int_R \mathbf{b}\rho dv + \int_R \boldsymbol{\sigma} \cdot \nabla dv \tag{4.8}$$

where $(\,)\cdot\nabla$ is the divergence of the function or tensor in the bracket.

Since this relation holds for any dv, Cauchy's first law of motion can be expressed as follows:

$$\mathbf{a}\rho = \mathbf{b}\rho + \boldsymbol{\sigma} \cdot \nabla \tag{4.9}$$

4.2.2. Thermodynamics

4.2.2.1. First principle of thermodynamics

The first principle of thermodynamics is the conservation of energy, which can be represented as following equation:

$$\dot{E} = P_{input} + Q_{input} \tag{4.10}$$

where $\dot{E}$ is the rate of change of the total energy of the system, P_{input} is the power input due to the mechanical work performed on the system, and Q_{input} is the heat change rate in the system.

P_{input} is the sum of the powers made by the body force $\mathbf{f_b}$ and contact force $\mathbf{f_c}$. With the same formalism used in section 4.2, P_{input} can be represented as follows:

$$P_{input} = \int_R \mathbf{b}\rho \cdot \mathbf{V} dv + \int_{\partial R} \mathbf{t} \cdot \mathbf{V} ds \tag{4.11}$$

where $\mathbf{V}$ is an arbitrary vector of displacement rate.

Q_{input} is the sum of the heat rate of internal source of the system and the heat flux through the boundary of the system, and it can be represented as follows:

$$Q_{input} = \int_R r dv - \int_{\partial R} \mathbf{q} \cdot \mathbf{n} ds \tag{4.12}$$

where r is the heat source per unit volume, and $\mathbf{q}$ is the heat fleet vector.

By applying the divergence theorem, Equation 4.12 becomes

$$Q_{input} = \int_R r dv - \int_R \mathbf{q} \cdot \nabla dv \tag{4.13}$$

With Equation 4.6, P_{input} becomes

$$P_{input} = \int_R \mathbf{b}\rho \cdot \mathbf{V} dv + \int_{\partial R} \mathbf{V} \cdot \boldsymbol{\sigma} \cdot \mathbf{n} ds \tag{4.14}$$

With the divergence theorem which has been applied in preceding section, P_{input} becomes

$$P_{input} = \int_R \mathbf{b}\rho \cdot \mathbf{V} dv + \int_R (\mathbf{V} \cdot \boldsymbol{\sigma}) \cdot \nabla dv \tag{4.15}$$

It can be demonstrated that

$$(\mathrm{V}\cdot\sigma)\cdot\nabla = \mathrm{V}\cdot(\sigma\cdot\nabla)+Tr[(\mathrm{V}\nabla)\cdot\sigma] \tag{4.16}$$

Thus, Equation 4.15 becomes to

$$\mathrm{P}_{input} = \int_R \mathbf{b}\rho\cdot\mathbf{V}dv + \int_R (\boldsymbol{\sigma}\cdot\nabla)\cdot\mathbf{V}dv + \int_R \mathrm{Tr}[(\mathbf{V}\nabla)\cdot\boldsymbol{\sigma}]dv$$

$$= \int_R (\mathbf{b}\rho+\boldsymbol{\sigma}\cdot\nabla)\cdot\mathbf{V}dv + \int_R \mathrm{Tr}[(\mathbf{V}\nabla)\cdot\boldsymbol{\sigma}]dv \tag{4.17}$$

Introducing Equation 4.9 into Equation 4.17, we obtain

$$\mathrm{P}_{input} = \int_R \rho\mathbf{a}\cdot\mathbf{V}dv + \int_R \mathrm{Tr}[(\mathbf{V}\nabla)\cdot\boldsymbol{\sigma}]dv$$

$$= \int_R \rho\dot{\mathbf{V}}\cdot\mathbf{V}dv + \int_R \mathrm{Tr}[(\mathbf{V}\nabla)\cdot\boldsymbol{\sigma}]dv \tag{4.18}$$

With Equation 4.13 and 4.18, the rate of change of the total energy of this system, $\dot{E}$, can be expressed as

$$\dot{\mathrm{E}} = \int_R \rho\dot{\mathbf{V}}\cdot\mathbf{V}dv + \int_R \mathrm{Tr}[(\mathbf{V}\nabla)\cdot\boldsymbol{\sigma}]dv + \int_R rdv - \int_R \mathbf{q}\cdot\nabla dv \tag{4.19}$$

In another respect, the rate of change of the total energy of this system, $\dot{\mathrm{E}}$, is the sum of the rate of change of internal energy and rate of change of kinetic energy. This relationship can be expressed as below

$$\dot{\mathrm{E}} = \int_R \dot{u}dv + \frac{1}{2}\frac{\mathrm{d}}{\mathrm{dt}}\int_R \rho\mathbf{V}\cdot\mathbf{V}dv$$

$$= \int_R \dot{u}dv + \int_R \rho\dot{\mathbf{V}}\cdot\mathbf{V}dv \tag{4.20}$$

where $\dot{u}$ is the rate of change of internal energy per unit volume.

With Equation 4.19 and 4.20, the following relationship is established

$$\int_R \dot{u}dv + \int_R \rho\dot{\mathbf{V}}\cdot\mathbf{V}dv = \int_R \rho\dot{\mathbf{V}}\cdot\mathbf{V}dv + \int_R \mathrm{Tr}\left[(\mathbf{V}\nabla)\cdot\boldsymbol{\sigma}\right]dv + \int_R rdv - \int_R \mathbf{q}\cdot\nabla dv \tag{4.21}$$

Since this relationship holds for any dv, the first law of thermodynamics can be represented as

$$\dot{u} = \mathrm{Tr}\left[(\mathbf{V}\nabla)\cdot\boldsymbol{\sigma}\right] + r - \mathbf{q}\cdot\nabla \tag{4.22}$$

By decomposing $\mathbf{V}\nabla$ into its symmetric and anti-symmetric parts, we obtain the rate of deformation tensor **D** and the rate of rotation tensor **W** as follows

$$\mathbf{D} = \frac{1}{2}\left[\mathbf{V}\nabla + (\mathbf{V}\nabla)^T\right]$$

$$\mathbf{W} = \frac{1}{2}\left[\mathbf{V}\nabla - (\mathbf{V}\nabla)^T\right] \tag{4.23}$$

For most of the fatigue life of brittle or quasi brittle materials concerned in this work, the strains are small, so that, $\mathbf{D} = \dot{\boldsymbol{\varepsilon}}$, and Equation 4.22 becomes

$$\dot{u} = \boldsymbol{\sigma} : \dot{\boldsymbol{\varepsilon}} + r - \mathbf{q}\cdot\nabla \tag{4.24}$$

where ":" represents the tensor contraction operation.

4.2.2.2. Second principle of thermodynamics

The second principle states that the rate of entropy production of the system is always greater than the rate of heating divided by the absolute temperature.

$$\frac{d}{dt}\int_R sdv \geq \int_R \frac{r}{T}dv - \int_{\partial R}\frac{\mathbf{q}}{T}\cdot\mathbf{n}ds \tag{4.25}$$

where s is the entropy, T is the absolute temperature, $\frac{r}{T}$ is the rate of change of entropy by internal heat source, and $\frac{\mathbf{q}}{T}$ is the rate of change of entropy by heat flux.

With the divergence theorem, this equation changes to

$$\int_R \dot{s} dv \geq \int_R \frac{r}{T} dv - \int_R \frac{\mathbf{q}}{T} \cdot \nabla dv \tag{4.26}$$

Since dv is arbitrary,

$$\dot{s} \geq \frac{r}{T} - \frac{\mathbf{q}}{T} \cdot \nabla \tag{4.27}$$

The difference between the left side and right side of the preceding equation can be defined as the internal entropy production rate as follows

$$\dot{\eta} = \dot{s} - \frac{r}{T} + \frac{\mathbf{q}}{T} \cdot \nabla \geq 0 \tag{4.28}$$

So that the second law can be stated as

$$\dot{\eta} \geq 0 \tag{4.29}$$

If $\dot{\eta} = 0$, the process is said to be reversible.

With a little further deduction, Equation 4.28 can be written as

$$\dot{\eta} = \dot{s} - \frac{r}{T} + \frac{1}{T}\mathbf{q} \cdot \nabla - \frac{\mathbf{q} \cdot T\nabla}{T^2} \geq 0 \tag{4.30}$$

Including Equation 4.24 into Equation 4.30, the second principle becomes

$$\dot{\eta} = \dot{s} - \frac{\dot{u}}{T} + \frac{1}{T}\boldsymbol{\sigma} : \dot{\boldsymbol{\varepsilon}} - \frac{\mathbf{q} \cdot T\nabla}{T^2} \geq 0 \tag{4.31}$$

This equation is also known as Clausius-Duhem Inequality.

4.3. Continuum damage mechanics

Continuum damage mechanics is a class of theories that is structured to describe the weakening of solids in the presence of multiple defects. It introduces one

or more scalar or tensor damage variables into the constitutive equations as a measure of the degradation of the material. Damage can be described in the form of microcracks for surface discontinuities, or micro-cavities for volume discontinuities.

Continuum damage mechanics is primarily used to describe the evolution of the properties of materials between the virgin state and the initiation of macroscopic cracks where the evolution is in the microscopic stage. Between these two stages, the representative volume element can be treated as a continuous medium. The size of the crack that falls into the macroscopic scale is out of that of the representative volume element. Different materials have different sizes of the volume element. Usually, the size is 0.1 to 1mm for metals or polymers, 1cm for wood, and 10cm for concrete. From the initiation of a macroscopic crack to the complete failure, the best theory to describe the material behavior is fracture mechanics.

For a brittle or quasi-brittle material, most of the fatigue life is between the virgin state and the macroscopic crack initiation, because the crack develops very quickly after the macroscopic crack initiates, and the part of the fatigue life corresponding to this part is very short. Therefore, continuum damage mechanics is a suitable theory to describe the fatigue behavior of the brittle or quasi-brittle material, such as composite materials and concrete.

In the past several decades, continuum damage mechanics has been well developed and widely applied in modeling behaviors of materials (Krajcinovic, 1985; Ortiz and Popov, 1982; Ortiz, 1985; Simo and Ju, 1987 a and b; Yazdani and Schreyer, 1988; Yazdani and Karnawat, 1996; Hansen, 1999; Vojiadjis et al., 2009;

and Gude et al., 2010). Ortiz and Popov (1982) established a model in the framework of thermodynamics to study the consequences of the composite nature of concrete. Ortiz (1985) presented a novel idea of representing damage through the continuous degradation of elastic moduli. Yazdani and Schreyer (1988) presented a bi-surface plasticity and damage mechanics model for concrete in the framework of thermodynamics and on the foundation set up by Ortiz. Yazdani and Karnawat (1996) developed the model of Yazdani and Schreyer (1988) with a single flow surface unifying damage mechanics and plasticity. This set of theories has been well developed for quasi-brittle solids in general and concrete in particular under monotonic loadings. The extension of this set of theories into modeling the behaviors of quasi-brittle solids under fatigue loadings, which is the objective of this dissertation, is natural. For a better understanding of the models presented in the following chapters, the basic details of this set of theories are explained in the next subsections.

4.3.1. General constitutive equations

4.3.1.1. Thermodynamic potential

The Gibbs free energy, G, is chosen to derive the state law of the materials. The relationship between internal energy and Gibbs free energy can be expressed as follows

$$u = \boldsymbol{\sigma} : \boldsymbol{\varepsilon} + Ts - G \tag{4.32}$$

Intruducing this equation into Equation 4.31, the Clausius-Duhem Inequality becomes

$$\dot{G} - \dot{\boldsymbol{\sigma}} : \boldsymbol{\varepsilon} - \dot{T}s - \frac{\mathbf{q} \cdot T\nabla}{T} \geq 0 \tag{4.33}$$

For stress space approach, the Gibbs free energy can be written as a function of temperature, T, stress, $\boldsymbol{\sigma}$, and damage, k. Thus, $\dot{G}$ is as follows:

$$\dot{G} = \frac{\partial G}{\partial T}\dot{T} + \frac{\partial G}{\partial \boldsymbol{\sigma}} : \dot{\boldsymbol{\sigma}} + \frac{\partial G}{\partial k}\dot{k} \tag{4.34}$$

Including this equation into Equation 4.33, we get

$$\left(\frac{\partial G}{\partial T} - s\right)\dot{T} + \left(\frac{\partial G}{\partial \boldsymbol{\sigma}} - \boldsymbol{\varepsilon}\right) : \dot{\boldsymbol{\sigma}} + \frac{\partial G}{\partial k}\dot{k} - \frac{\mathbf{q} \cdot T\nabla}{T} \geq 0 \tag{4.35}$$

Since $\dot{T}$ and $\dot{\boldsymbol{\sigma}}$ are arbitrary:

$$\frac{\partial G}{\partial T} = s \tag{4.36}$$

$$\frac{\partial G}{\partial \boldsymbol{\sigma}} = \boldsymbol{\varepsilon} \tag{4.37}$$

$$\frac{\partial G}{\partial k}\dot{k} - \frac{\mathbf{q} \cdot T\nabla}{T} \geq 0 \tag{4.38}$$

Equation 4.38 is also known as the dissipation inequality.

Let us define $\mathbf{C}(k)$ as the compliance tensor of the material, $\boldsymbol{\beta}(k)$ as the tensor of thermal expansion coefficient, and $\xi(k)$ as specific heat under constant volume, so that

$$\frac{\partial G}{\partial \boldsymbol{\sigma} \partial \boldsymbol{\sigma}} = \mathbf{C}(k) \tag{4.39}$$

$$\frac{\partial G}{\partial \boldsymbol{\sigma} \partial T} = \boldsymbol{\beta}(k) \tag{4.40}$$

$$T\frac{\partial G}{\partial T\partial T}=\xi(k) \tag{4.41}$$

Then, with some deduction, the general form of Gibbs free energy can be expressed as

$$G(\boldsymbol{\sigma},k,T)=\frac{1}{2}\boldsymbol{\sigma}:\mathbf{C}:\boldsymbol{\sigma}+\boldsymbol{\sigma}:\boldsymbol{\beta}(k)(T-T_0)+\boldsymbol{\sigma}:\boldsymbol{\varepsilon}^{i}(k)-A^{l}(T,k) \tag{4.42}$$

where T_0 is the reference temperature, and $A^l(T,k)$ is a scalar function.

For low frequency fatigue loading, it can be assumed that thermal effects could be ignored, so that $\dot{T}$ and $T\nabla$ equal zero. Thus, Equation 4.38 becomes

$$\frac{\partial G}{\partial k}\dot{k}\geq 0 \tag{4.43}$$

and the form of the Gibbs free energy is then

$$G(\boldsymbol{\sigma},k,T)=\frac{1}{2}\boldsymbol{\sigma}:\mathbf{C}:\boldsymbol{\sigma}+\boldsymbol{\sigma}:\boldsymbol{\varepsilon}^{i}(k)-A^{l}(T,k) \tag{4.44}$$

4.3.1.2. Stress strain relation

With Equation 4.37 and 4.39, the stress strain relation corresponding to the Equation 4.44 is given as follows:

$$\boldsymbol{\varepsilon}=\frac{\partial G}{\partial \boldsymbol{\sigma}}=\mathbf{C}(k):\boldsymbol{\sigma}+\boldsymbol{\varepsilon}^{i}(k) \tag{4.45}$$

Ortiz (1985) proposed a novel idea that the values of the elastic compliances themselves be taken as a characterization of the state of damage of the material and assumed that the elastic compliances have an addictive structure:

$$\mathbf{C}(k)=\mathbf{C}^{0}+\mathbf{C}^{c}(k) \tag{4.46}$$

where C_0 is the initial elasticity tensor of the material and C_c is the added flexibility caused by active microcracks. This formulation allows the induced elastic anisotropy.

With Equation 4.46, the total strain of Equation 4.45 is identified as follows:

$$\boldsymbol{\varepsilon} = \mathbf{C}^0 : \boldsymbol{\sigma} + \mathbf{C}^c(k) : \boldsymbol{\sigma} + \boldsymbol{\varepsilon}^i(k) = \boldsymbol{\varepsilon}^0 + \boldsymbol{\varepsilon}^D(k) + \boldsymbol{\varepsilon}^i(k) \tag{4.47}$$

where $\boldsymbol{\varepsilon}^0 = \mathbf{C}^0 : \boldsymbol{\sigma}$ is the elastic strain tensor for uncracked material; $\boldsymbol{\varepsilon}^D = \mathbf{C}^c : \boldsymbol{\sigma}$ is the additional recoverable strain caused by elastic damage.

4.3.1.3. Damage flow rule and damage criteria

Based on observations on the opening and closing of microcracks, Ortiz (1985) suggested decomposing the added flexibility

$$\mathbf{C}^c = \mathbf{C}^c_I + \mathbf{C}^c_{II} \tag{4.48}$$

where $\mathbf{C}^c_I$ is due to the response of microcracks in Mode I on Figure 4.1 (a); $\mathbf{C}^c_{II}$ is due to the response of microcracks in Mode II on Figure 4.1 (b).

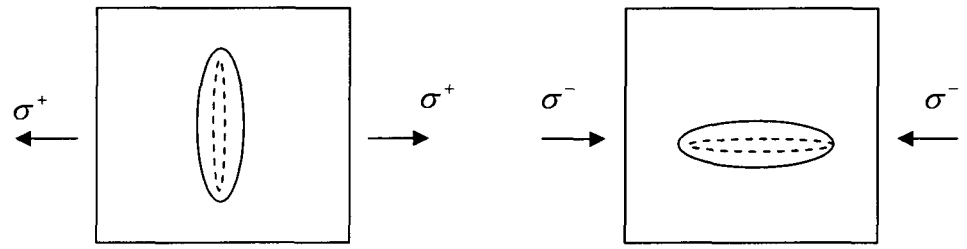

(a) (b)

Figure 4.1. Crack opening in mode I and II.

Ortiz (1985) also suggested a rate independent damage rule:

$$\dot{\mathbf{C}}_{\mathbf{I}}^{c} = \dot{k}\mathbf{R}_{\mathbf{I}}, \qquad \dot{\mathbf{C}}_{\mathbf{II}}^{c} = \dot{k}\mathbf{R}_{\mathbf{II}} \tag{4.49}$$

where $\mathbf{R_I}$ and $\mathbf{R_{II}}$ are response tensors of the material, which determine the direction in which damage takes place; k is a scalar parameter, which may be regarded as a measure of accumulated damage. Usually, the damage is irreversible, which necessitates the following:

$$\dot{k} \geq 0 \tag{4.50}$$

Similar to Equation 4.49, Yazdani and Karnawat (1996) suggested the following:

$$\dot{\varepsilon}^{i} = \dot{k}\mathbf{M} \tag{4.51}$$

For further deduction, it is assumed that the following is true:

$$t(k)^2 = 2\frac{dA^i}{dk} \tag{4.52}$$

where t(k) is termed the softening law.

With the form of Gibbs Free energy, Equation 4.44, and Equation 4.49, 4.51, and 4.52, the dissipation inequality is as follows:

$$\Phi(\boldsymbol{\sigma}, k) = \frac{1}{2}\boldsymbol{\sigma}^{+} : \mathbf{R}_{\mathbf{I}} : \boldsymbol{\sigma}^{+} + \frac{1}{2}\boldsymbol{\sigma}^{-} : \mathbf{R}_{\mathbf{II}} : \boldsymbol{\sigma}^{-} + \boldsymbol{\sigma} : \mathbf{M} - \frac{1}{2}t(k)^2 \geq 0 \tag{4.53}$$

where $\Phi(\boldsymbol{\sigma}, k)$ is termed the damage function; $\boldsymbol{\sigma}$+ and $\boldsymbol{\sigma}$- are termed the positive and negative cones of the stress tensor, $\boldsymbol{\sigma}$, respectively. For further damage to occur, this equation must be satisfied. Otherwise, the material must behave elastically.

Therefore, this equation can be regarded as a damage criterion, which signals the onset of damage. Without viscosity, the following state of stress is unattainable:

$$\Phi(\boldsymbol{\sigma}, k) = \frac{1}{2}\boldsymbol{\sigma}^{+} : \mathbf{R}_{I} : \boldsymbol{\sigma}^{+} + \frac{1}{2}\boldsymbol{\sigma}^{-} : \mathbf{R}_{II} : \boldsymbol{\sigma}^{-} + \boldsymbol{\sigma} : \mathbf{M} - \frac{1}{2}t(k)^{2} > 0 \tag{4.54}$$

Therefore, the onset of damage is characterized by the following criteria:

$$\begin{aligned} &\Phi(\boldsymbol{\sigma}, k) = 0 \\ &\frac{\partial \Phi}{\partial \boldsymbol{\sigma}} : \dot{\boldsymbol{\sigma}} > 0 \end{aligned} \tag{4.55}$$

These two equations are amenable to a revealing geometric interpretation. The locus of points in stress space that satisfy the first equation may be viewed as a damage surface enclosing an elastic domain in which the material behaves elastically. In another words, no new damage occurs. For damage to progress, two conditions must be satisfied. One condition is that the stress point must be on the surface; another condition is that the stress increment must point outside of the elastic domain.

4.3.1.4. Response tensors

The response tensors $\mathbf{R}_{I}$ and $\mathbf{R}_{II}$ are derived from the classical conjugacy arguments of kinetic theory. From the dissipation inequality Equation 4.53, the thermodynamic fluxes conjugate to the variables $\mathbf{C}_{I}^{c}$ and $\mathbf{C}_{II}^{c}$ are as follows:

$$\mathbf{J}_{I} = \boldsymbol{\sigma}^{+} \otimes \boldsymbol{\sigma}^{+}, \quad \mathbf{J}_{II} = \boldsymbol{\sigma}^{-} \otimes \boldsymbol{\sigma}^{-}, \tag{4.56}$$

respectively. Therefore, it is appropriate to postulate that the response tensors depend on the state of stress through the conjugate thermodynamic fluxes. The simplest forms of the response tensors are given as follows:

$$\mathbf{R}_{I} = \frac{\mathbf{J}_{I}}{\mathrm{Tr}\mathbf{J}_{I}} = \frac{\boldsymbol{\sigma}^{+} \otimes \boldsymbol{\sigma}^{+}}{\boldsymbol{\sigma}^{+} : \boldsymbol{\sigma}^{+}}, \qquad \mathbf{R}_{II} = c\frac{\mathbf{J}_{II}}{\mathrm{Tr}\mathbf{J}_{II}} = c\frac{\boldsymbol{\sigma}^{-} \otimes \boldsymbol{\sigma}^{-}}{\boldsymbol{\sigma}^{-} : \boldsymbol{\sigma}^{-}} \tag{4.57}$$

where Tr denotes the trace operation; c is a coefficient that governs the extent of Mode II damage.

4.3.1.5. Softening law

With Equation 4.57, and ignoring the effect of the inelastic strain, the damage function reads as follows:

$$\Phi(\boldsymbol{\sigma}, k) = \frac{1}{2}\boldsymbol{\sigma}^{+} : \boldsymbol{\sigma}^{+} + \frac{1}{2}c\boldsymbol{\sigma}^{-} : \boldsymbol{\sigma}^{-} - \frac{1}{2}t(k)^{2} \tag{4.58}$$

For a uniaxial tension loading condition, the damage criterion reduces to $\sigma = t(k)$. Therefore, the softening law t(k) is considered the critical stress for the extent of damage.

For the damage model defined by Equation 4.58, the relationship between the softening law, t(k), and the cumulative damage parameter, k, can be determined solely on the basis of the uniaxial tensile test as follows:

$$\sigma_{1} = \frac{\varepsilon_{1}}{(1/E_{0}) + k} \tag{4.59}$$

where E_0 is the initial Young's modulus.

For computational purpose, Ortiz (1985) recommended a convenient expression for the stress-strain relation of mortar, which was proposed by Smith and Young (1955).

5. ANISOTROPIC DAMAGE MODEL FOR WOVEN FABRIC COMPOSITES

5.1. Introduction

Inelastic deformation of woven fabric composites is attributed to the formation of a multitude of cracks that develop in the material in the fatigue environment. Cracks destroy material bonds and render composites more compliant. Under tension-tension fatigue, cracks in the plane whose normal is perpendicular to the loading direction tend to close and stop propagating as shown on Figure 5.1; and cracks in the plane whose normal is not perpendicular to the loading direction tend to develop as shown on Figure 5.2. These phenomena show that the crack development in woven fabric composites is a highly directional behavior. The capability of a model to describe the damage anisotropy is very important.

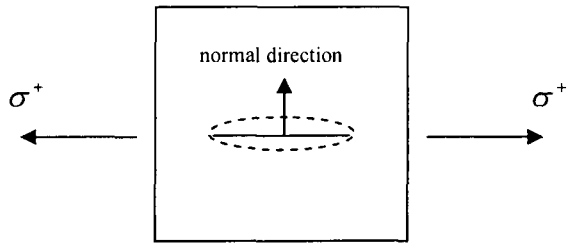

Figure 5.1. Schematic representation of crack closing under tension-tension loading.

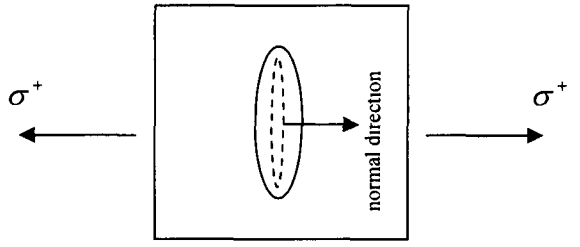

Figure 5.2. Schematic representation of crack opening under tension-tension loading.

As discussed in Chapter 4, continuum damage mechanics is a very suitable theory to describe the fatigue process of composite materials which are saturated with cracks. Some researchers have described this process with the continuum damage mechanics. Hansen (1999) investigated damage nucleation and growth in glass-reinforced woven composites in both quasi-static and fatigue environments. He proposed a continuum damage mechanics model for the fatigue damage relation and growth in tensile stress load paths. His model considered the material compliance tensor as an internal variable evolving with damage. The approach of reflecting damage through the fourth-order compliance tensor has gained wide acceptance and popularity and has also been applied to other materials such as ceramics (Ortiz and Giannakopoulos, 1990 a; Ortiz and Giannakopoulos, 1990 b) and concrete (Yazdani, 1993; Karnawat and Yazdani, 2001). However, the proposed model was isotropic and therefore could not capture the induced anisotropy effects of cracking. The predicted results did not capture the characteristics of the fatigue process very well. Also

lacking was the model's capability to capture permanent deformation during fatigue damage.

This chapter aims at overcoming the perceived shortcomings of Hansen's model by proposing a mathematical framework of damage mechanics whereby anisotropic behavior is modeled. Damage is reflected through the material compliance tensor involving a damage parameter whose increment is obtained from the second invariant of the stress tensor. The formulation is also capable of predicting permanent deformation that may arise due to imperfect fracturing processes.

5.2. Formulation

With the assumption of small deformations which is valid for brittle materials and for low frequency fatigue where thermal effects could be ignored, we consider the state of composite material to be given as that shown in Equation 4.44. For convenience, Equation 4.44 is listed as below.

$$G(\boldsymbol{\sigma},k,T)=\frac{1}{2}\boldsymbol{\sigma}:\mathbf{C}:\boldsymbol{\sigma}+\boldsymbol{\sigma}:\boldsymbol{\varepsilon}^{i}(k)-A^{i}(T,k) \tag{4.44}$$

By differentiating Equation 4.44 to the stress tensor, $\boldsymbol{\sigma}$, we obtain the strain tensor as

$$\varepsilon=\frac{\partial G}{\partial \boldsymbol{\sigma}}=\mathbf{C}(k):\boldsymbol{\sigma}+\boldsymbol{\varepsilon}^{i}(k) \tag{5.1}$$

where the strain and average stress tensors are given by $\boldsymbol{\varepsilon}$, and $\boldsymbol{\sigma}$, respectively, G denotes the Gibbs free energy, $\mathbf{C}$ designates the material compliance tensor, and k is the cumulative fatigue damage parameter. The tensor contraction operation is denoted

by ":", and the inelastic component of deformation due to damage processes is given by ε^{I}. Implied in the constitutive form of Equation 5.1 is that damage is recorded in the fourth-order material compliance tensor and the second-order inelastic strain tensor.

To account for induced anisotropy, we adopt an additive decomposition of the compliance tensor as

$$\mathbf{C}(k) = \mathbf{C}^{0} + \mathbf{C}^{c}(k) \tag{5.2}$$

where $\mathbf{C}^{c}(k)$ denotes the added flexibility due to damage and $\mathbf{C}^{0}$ corresponds to the initial undamaged state of the material.

With this decomposition, Equation 5.1 becomes

$$\varepsilon = \frac{\partial G}{\partial \sigma} = \mathbf{C}^{0} : \sigma + \mathbf{C}^{c}(k) : \sigma + \varepsilon^{I}(k) = \varepsilon^{0} + \varepsilon^{D}(k) + \varepsilon^{I}(k) \tag{5.3}$$

where $\mathbf{C}^{0} : \sigma = \varepsilon^{0}$ is the initial elastic strain corresponding to the undamaged condition; $\mathbf{C}^{c}(k) : \sigma = \varepsilon^{D}(k)$ is the added elastic strain caused by the damage. The relation in Equation 5.3 can be shown on Figure 5.3. E_0 is the initial Young's modulus; E_I is the final Young's modulus after a fatigue loading. The accumulated damage renders the material to be more compliant so that $E_0 > E_I$ and causes inelastic strain. Two extreme conditions are considered for better understanding on the physical meaning of Equation 5.3. For a perfect brittle behavior where no inelastic strain exists, the material returns to the origin after unloading as shown on Figure 5.4. The damage in this process is elastic damage that does not cause any inelastic strain. On the other hand, for an idea inelastic behavior where no damage records in the

compliance, the final Young's modulus equals the initial Young's modulus as shown on Figure 5.5.

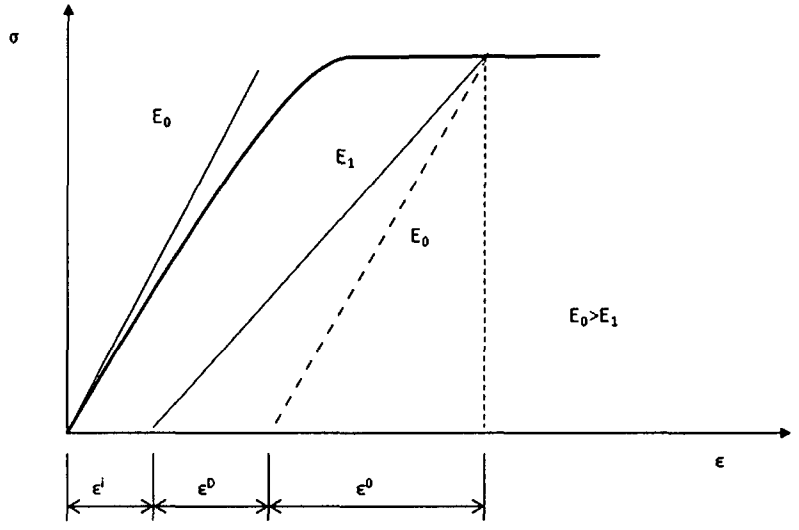

Figure 5.3. Schematic illustration of strains in fatigue process of general condition.

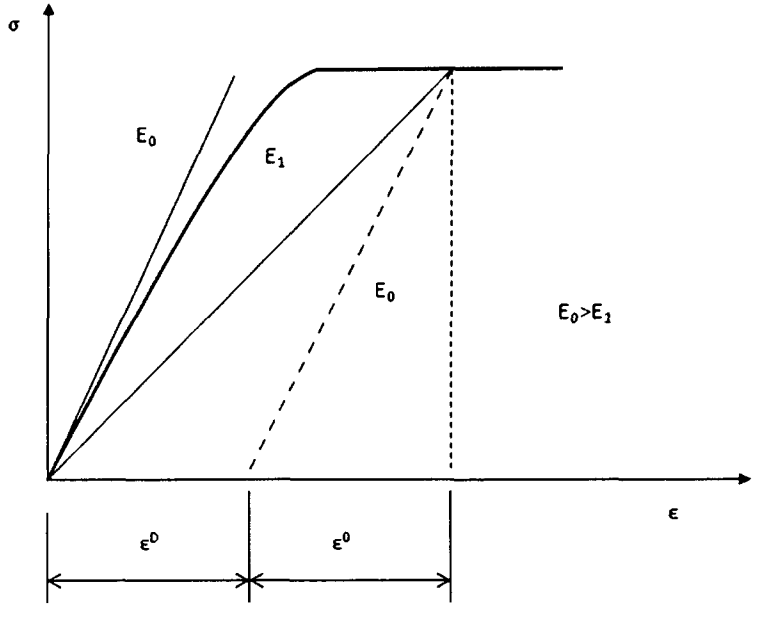

Figure 5.4. Schematic illustration of strains in fatigue process of perfect brittle condition.

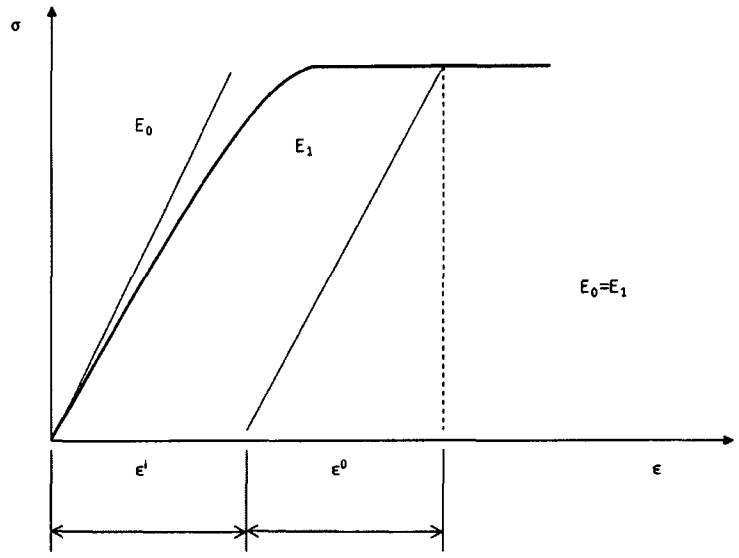

Figure 5.5. Schematic illustration of strains in fatigue process of ideal inelastic condition.

Therefore, the rate form of the total strain tensor is given below:

$$\dot{\boldsymbol{\varepsilon}} = \dot{\mathbf{C}}^0 : \boldsymbol{\sigma} + \mathbf{C}^0 : \dot{\boldsymbol{\sigma}} + \dot{\mathbf{C}}^c(k) : \boldsymbol{\sigma} + \mathbf{C}^c(k) : \dot{\boldsymbol{\sigma}} + \dot{\boldsymbol{\varepsilon}}^I(k) \tag{5.4}$$

We may notice that $\dot{\mathbf{C}}^0$ equals zero, because the initial compliance tensor does not change with the increase of fatigue loading cycles. Then, Equation 5.4 becomes

$$\dot{\boldsymbol{\varepsilon}} = \mathbf{C}(k) : \dot{\boldsymbol{\sigma}} + \dot{\mathbf{C}}^c(k) : \boldsymbol{\sigma} + \dot{\boldsymbol{\varepsilon}}^I(k) = \dot{\boldsymbol{\varepsilon}}^e(k) + \dot{\boldsymbol{\varepsilon}}^d(k) + \dot{\boldsymbol{\varepsilon}}^I(k) \tag{5.5}$$

where $\mathbf{C}(k) : \dot{\boldsymbol{\sigma}} = \dot{\boldsymbol{\varepsilon}}^e(k)$ is the rate form of the elastic strain tensor in one cycle without any further micro-cracking; $\dot{\mathbf{C}}^c(k) : \boldsymbol{\sigma} = \dot{\boldsymbol{\varepsilon}}^d(k)$ is the rate form of the strain tensor due to elastic damage. Components of rate form of total strain tensor of Equation 5.5 are shown on Figure 5.6 for better understanding. E_1 is the Young's modulus after n_1 cycles of fatigue loading; E_2 is the Young's modulus after n+1 cycles of fatigue loading; E_0 is the initial Young's modulus.

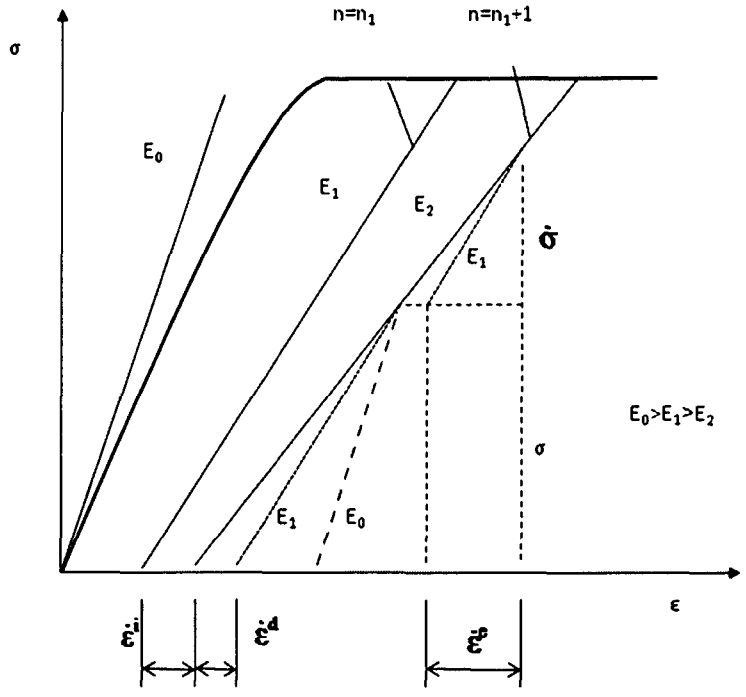

Figure 5.6. Schematic illustration of components of rate of total strain.

The rates of the added flexibility and the inelastic strain tensors are regarded as fluxes in the thermodynamic state sense and are given below with respect to response tensors **R** and **M**:

$$\dot{\mathbf{C}}^c = \dot{k}\,\mathbf{R} \quad \textbf{and} \quad \dot{\varepsilon}^I = \dot{k}\,\mathbf{M} \tag{5.6}$$

To progress further specific forms of the response tensors **R** and **M** must be specified. One should note that if **R** is chosen to be an isotropic tensor, such as the formulation implied in Hansen's work (1999), the model will be isotropic. To predict anisotropic behavior due to damage, **R** should be formulated such that anisotropy is achieved. To do this, we assume that damage takes place in directions of applied stresses and in tension regimes only. To expand this to other situations is feasible and

has been reported elsewhere (Ortiz and Giannakopoulos, 1990 a; Ortiz and Giannakopoulos, 1990 b; Yazdani, 1993; Karnawat and Yazdani, 2001). An elegant mathematical way is to decompose the stress tensor into its positive and negative cones. The mathematical formulation to achieve this has been published in (Ortiz and Giannakopoulos, 1990). Let the positive cone of the stress tensor be given as $\boldsymbol{\sigma}^+$ whereby all the negative eigen-stresses are removed from the stress tensor $\boldsymbol{\sigma}$. Similarly, let $\boldsymbol{\sigma}^-$ represent the negative cone of the stress tensor. Note that $\boldsymbol{\sigma}^+ + \boldsymbol{\sigma}^- = \boldsymbol{\sigma}$.

As it was stated, damage is assumed to occur in the cleavage mode of cracking which is shown schematically on Figure 5.2. To generalize this and with a further assumption of no coupling between cleavage type cracks in orthogonal directions, the following response tensors are postulated for **R** and **M**:

$$\mathbf{R} = \frac{\left(\boldsymbol{\sigma}^+ \otimes \boldsymbol{\sigma}^+\right)}{\left(\boldsymbol{\sigma}^+ : \boldsymbol{\sigma}^+\right)} \tag{5.7}$$

$$\mathbf{M} = \frac{\alpha \boldsymbol{\sigma}^+}{\left(\boldsymbol{\sigma}^+ : \boldsymbol{\sigma}^+\right)^{1/2}} \tag{5.8}$$

where the symbol "$\otimes$" signifies the tensor product operation.

The next step is to establish an evolutionary expression for damage. One particular form proposed by Hansen (1999) is given below which represents the damage rate in terms of second invariant of strain tensor.

$$\dot{k} = A\left(\frac{\varepsilon_e}{\varepsilon_0}\right)^n \tag{5.9}$$

with ε_0 being the reference strain level, and ε_e being an effective strain measure given as $\varepsilon_e = \sqrt{\boldsymbol{\varepsilon} : \boldsymbol{\varepsilon}}$. Although, this form is simple to use, the results predicted were not quite satisfactory as shown on Figure 5.7. In this chapter, an alternate and new damage evolution law is proposed based on the second invariant of the stress tensor. Let

$$k = A\int_0^N \left(\frac{\boldsymbol{\sigma}^+ : \boldsymbol{\sigma}^+}{\sigma_0^2}\right)^m N^B dN \qquad k \le k_{lim} \tag{5.10}$$

where A, B, and m are material constants, N is the cyclic number, and σ_0 is a reference stress.

By differentiating Equation 5.10 with respect to N, the increment of damage in one cycle is given as

$$\dot{k} = A\left(\frac{\boldsymbol{\sigma}^+ : \boldsymbol{\sigma}^+}{\sigma_0^2}\right)^m N^B \tag{5.11}$$

Including Equation (5.7), (5.8) and (5.11) into Eq. (5.6) and then including Equation (5.6) into Equation (5.5) yields:

$$\dot{\boldsymbol{\varepsilon}} = \mathbf{C} : \dot{\boldsymbol{\sigma}} + A\left(\frac{\boldsymbol{\sigma}^+ : \boldsymbol{\sigma}^+}{\sigma_0^2}\right)^m N^B \frac{\left(\boldsymbol{\sigma}^+ \otimes \boldsymbol{\sigma}^+\right)}{\left(\boldsymbol{\sigma}^+ : \boldsymbol{\sigma}^+\right)} : \boldsymbol{\sigma} + \alpha A\left(\frac{\boldsymbol{\sigma}^+ : \boldsymbol{\sigma}^+}{\sigma_0^2}\right)^m N^B \frac{\boldsymbol{\sigma}^+}{\left(\boldsymbol{\sigma}^+ : \boldsymbol{\sigma}^+\right)^{1/2}} \tag{5.12}$$

For computational purposes, the rate of stress tensor is needed and can be described as:

$$\dot{\boldsymbol{\sigma}} = \mathbf{E} : \left[\dot{\boldsymbol{\varepsilon}} - A\left(\frac{\boldsymbol{\sigma}^+ : \boldsymbol{\sigma}^+}{\sigma_0^2}\right)^m N^B \frac{\left(\boldsymbol{\sigma}^+ \otimes \boldsymbol{\sigma}^+\right)}{\left(\boldsymbol{\sigma}^+ : \boldsymbol{\sigma}^+\right)} : \boldsymbol{\sigma} - \alpha A\left(\frac{\boldsymbol{\sigma}^+ : \boldsymbol{\sigma}^+}{\sigma_0^2}\right)^m N^B \frac{\boldsymbol{\sigma}^+}{\left(\boldsymbol{\sigma}^+ : \boldsymbol{\sigma}^+\right)^{1/2}}\right] \tag{5.13}$$

5.3. Numerical Simulation

To demonstrate the advantages of the model, the model prediction is compared with Hansen's work (1999). Hansen performed static and fatigue tests in a servo hydraulic Instron 1333 with hydraulic grips and a 250 KN load cell. The testing laminates are made up of plain woven glass/epoxy prepreg fabrics with the lay-up sequence $[(+45^{o}\#-45^{o})/(90^{o}\#0^{o})]$. The symbol "#" indicates the bi-directional reinforcement of each prepreg. The tensile fatigue testing was in load control mode with a frequency of 5 Hz. He used a thermal imaging system to estimate the surface temperature of the specimen during tests. The records showed that for the first two phases of the fatigue process as described in Section 1.3, the thermal effects under the testing frequency can be ignored.

The comparison of model prediction and experimental data of Hansen's work of longitudinal stiffness reduction is shown on Figure 5.7. For the numerical simulation the following constants were used. $A=0.9 \times 10^{-6}$, B=-0.7, m=1.4, $\boldsymbol{\sigma}^{+} = [155 \quad 0 \quad 0]$ MPa, and σ_0 =330 MPa. Parameters A, B, α, and m are estimated by comparing predicted results and experimental results over a range of applied stresses. As shown on Figure 5.7, the initial damage due to knee effect is captured by the proposed theory quite well. The model also shows its usefulness in the prediction of Phases II of fatigue damage processes.

The predicted S-N curve of the barely visible impact damaged (BVID) composite is compared with the experimental S-N curve on Figure 5.8. The effect of material parameter, m, on the S-N curve is also shown on the same figure. It is seen

that the general trends of the S-N curve are replicated satisfactorily by the proposed model.

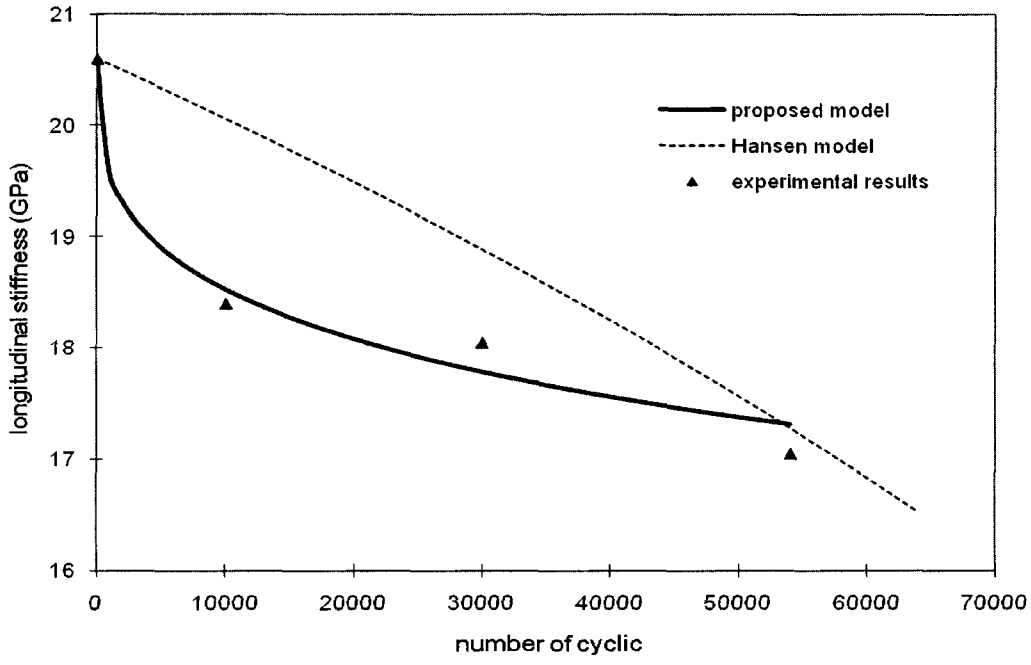

Figure. 5.7. Comparison of longitudinal stiffness reduction prediction between models and experimental results from Hansen's work (1999).

The stress-strain cyclical behavior for the composite material is further illustrated on Figures 5.9 for perfect brittle behavior and Figure 5.10 for general behavior. The first one corresponds to an idealized case whereby crack faces close perfectly upon unloading and is achieved in the model by letting **M**=0. In most heterogeneous materials, such as glass-fiber composites, permanent deformations do take place. The versatility of the model is shown on Figure 5.10 where the process of elastic degradation and permanent deformation is illustrated.

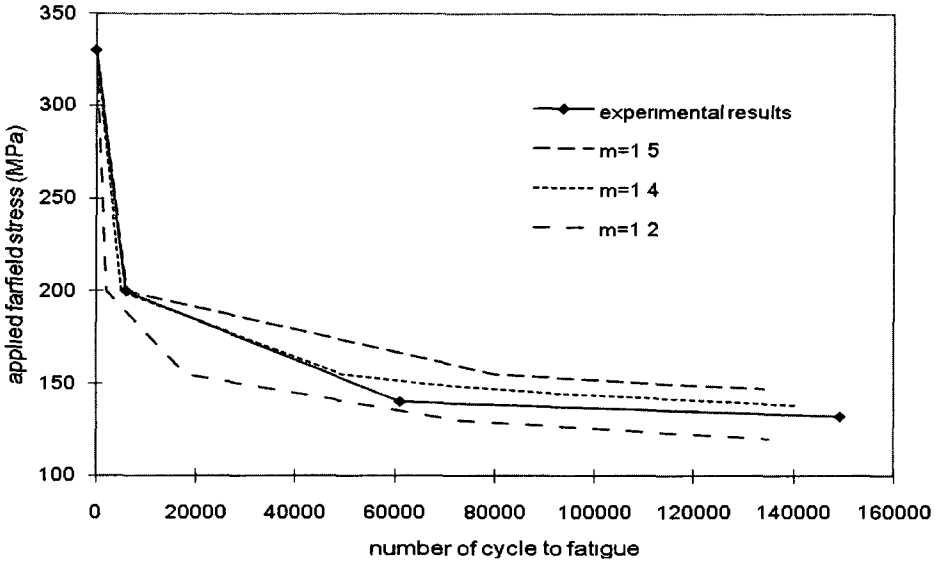

Figure 5.8. Comparison between experimental S-N curve with predicted S-N curves for different values of m.

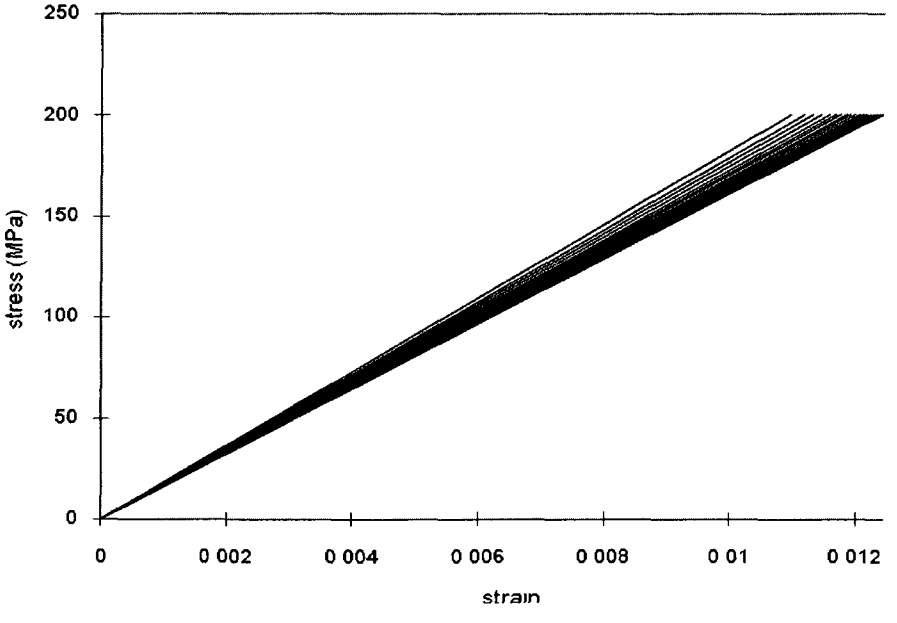

Figure 5.9. Model prediction of stress strain relation for perfect brittle fatigue process with stiffness deduction but no inelastic strain accumulation.

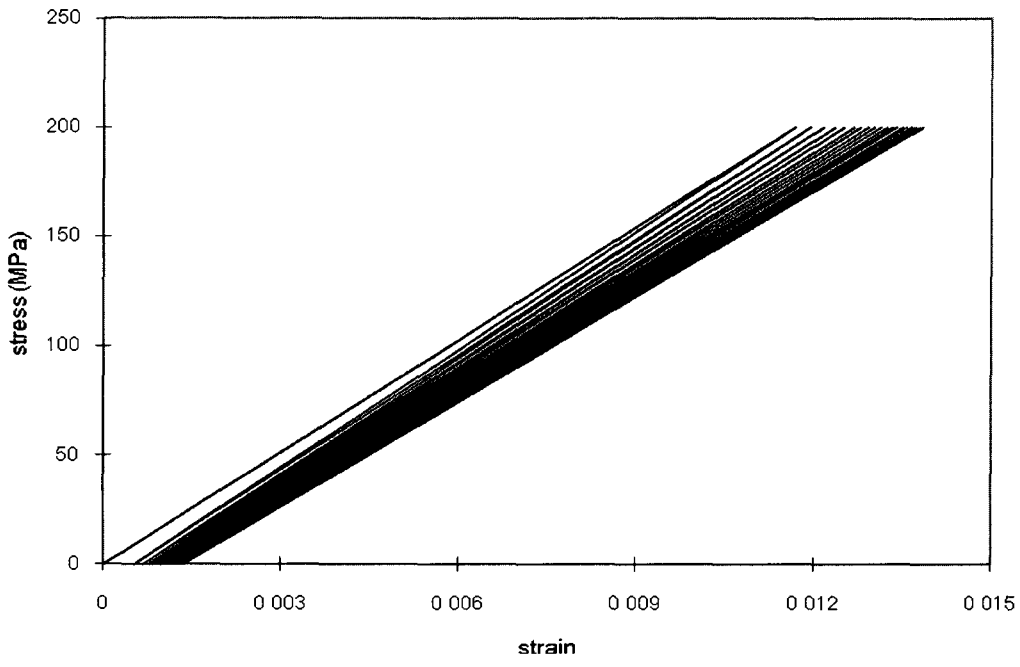

Figure 5.10. Model prediction of stress strain relation for general behavior of fatigue process with stiffness deduction and inelastic strain accumulation.

5.4. Conclusion

An anisotropic inelastic damage model for woven fabric composites during a low frequency tension-tension fatigue is established. Since the fatigue damage in most fatigue life is mainly due to the development of a multitude of matrix cracking and interfacial debonding, a class of damage mechanics theories is used for modeling fatigue processes. Two response tensors are proposed to capture the strong directionality of the multitude of matrix cracking and interfacial debonding in general cases. An expression for the evolution of fatigue damage is proposed based on the second invariant of the stress tensor. The comparison with experimental data is shown

in the chapter to demonstrate the model's capability in capturing the essential features of composite material inelasticity subjected to fatigue loading environment.

6. ANISOTROPIC FATIGUE DAMAGE MODELING OF WOVEN FABRIC COMPOSITE WITH BOUNDING SURFACE APPROACH

6.1. Introduction

Fatigue life is an important factor in the description of the fatigue process; many in the industry are more concerned with fatigue life than with other factors of the process. As discussed in Chapter 2, many models have been proposed to calculate the fatigue life of materials; these models, such as the famous S-N curve, are widely used in industry. Although the model in Chapter 5 captures many aspects of the fatigue process of composite materials, it does not provide the failure criterion, which determines the fatigue life of the material.

A large number of scientific papers have been published on the modeling, simulation, and/or experimental investigation of quasi-brittle materials under fatigue loading. The majority of the published research has addressed various topics associated with the uniaxial stress path loading. By comparison, the amount of research on the multiaxial modeling has been small. The experimental testing under a multiaxial stress state is rather difficult to conduct; it requires special instrumentation and apparatus. This lack of research means that only a small amount of experimental data are available for developing and validating constitutive and failure models. However, the increasing use of woven fabric composites in structures subjected to

complex loadings has required engineers to enhance the modeling and predictive tools for a more reliable design. Therefore, it is plausible to establish a model that is able to predict the fatigue processes under multiaxial fatigue loading paths with the experimental testing under uniaxial fatigue loading paths.

In this chapter, a unified approach to the damage mechanics modeling of woven composites is proposed that utilizes the bounding surface theory, which is explained in the next section. With this theory, a failure criterion for general biaxial or triaxial loading paths can be established. Many complex fatigue loading paths can be modeled and addressed conveniently within the framework proposed. In addition, the effects of the complex multiaxial fatigue loadings can be predicted easily with this theory.

In most cases, the strength requirements of the woven fabric composites differ in different directions. Using same fibers in different directions is a waste of materials. This waste can be eliminated by tailoring different fibers or different densities of the same fibers in different directions, but this modification causes strength anisotropy of the material. Therefore, a successful model should be able to capture the strength anisotropy of the woven fabric materials. However, the model developed in Chapter 5 is unable to describe the effect of the strength anisotropy. In the approach developed in this chapter, a direction function is used to capture the strength anisotropic property of the material. The static damage occurring in the first loading cycle is predicted with a shape function. Comparisons between results from

literature and results of the proposed model show the strong capability of the model to predict the behavior of composite materials in fatigue loading environments.

6.2. Bounding surface theory

Bounding surface theory is the general designation of a class of theories used to describe the change of material properties under some loading paths. This theory has several advantages. One advantage is that it can provide a failure criterion for materials under general loading paths, such as biaxial or triaxial (Seow and Swaddiwudhipong, 2005). In addition, the material behaviors under many complex biaxial or triaxial loading paths can be predicted by a simple experimental test, such as a uniaxial loading test. Also, many researchers in the mechanics community are familiar with the non-linear modeling of materials (plasticity and/or damage mechanics), and the extension of this theory to fatigue modeling would be regarded as natural. These inherent advantages make the bounding surface theory widely accepted and applied in material modeling.

These theories have some common basic features (Dafalias, 1986; Pandolfi and Taliercio, 1998); the theories usually assume that a "bounding surface" exists that encloses or contacts the current stress point at any time of the loading process. The surface is usually defined in the stress space. It can be fixed or evolve according to the loading history and model constitution. The evolution of the material properties is related to the position of the surface. The loading path can be quasi-static (Yazdani and Schreyer, 1990) or cyclic (Smith and Pascoe, 1989; Al-Gadhib and etc., 2000).

However, these theories differ in terms of the surface equation, flowing rule of the surface, constitutive law, etc.

Fardis and etc. (1983) propsed a model in the stress space with the horizontal axis along the direction of the hydrostatic pressure and the vertical axis on the deviatoric plane. They proposed an outer bounding surface which is fixed in the stress space and represents the locus of stress points corresponding to ultimate strength under monotonic loadings. They also proposed a bounding surface which will shrink with the increase of the maximum principal strain, ε_{max} , after ε_{max} exceeds the failure strain, ε_f, which corresponds to the ultimate strength in monotonic, nearly proportional loading. The value of ε_{max} is determined through a proposed stress-strain relation with which the effects of hydrostatic pressure and deviatoric stresses are represented separately. This model gives the failure criteria, but the material strength and damage development have to be isotropic, and lots of parameters need to be determined.

Fardis and Chen (1986) developed the model described above. Instead of using two bounding surfaces, they gave a unified bounding surface. They also proposed an expression of the failure strain, ε_f, as a function of the peak strain of the monotonic uniaxial stress-strain curve. However, the material strength and damage development are still isotropic, and lots of parameters need to be determined.

Yang and etc. (1985) proposed a model in a space similar to the previous two models. They proposed one bounding surface and two loading surfaces to determine the occurrences of the deviatoric plastic strain and the volumetric plastic strain, and

gave the stress strain relation based on the evolutions of the two plastic strains. However, this model also has the shortcomings of the previous two models.

Suaris and etc. (1990) represented the damage by three components along the principal stress directions and proposed a damage mechanical model in the space of thermodynamic force conjugates, strain energy release rate, of the damage components. Then they proposed three surfaces, bounding surface, loading surface, and limit fracture surface, and the damage-growth rate to describe the damage evolution. The damage-growth rate is determined from the loading surface by an associated flow rule. Finally, the authors directly proposed one compliance matrix for tensile and one for compression, respectively, based on the experimental observations. With the model, the damage anisotropy is predicted. However, strength anisotropy is not involved, and the positions of the bounding surface and limit fracture surface need to be determined empirically.

Al-Gadhib and etc. (2000) developed the model of Suaris and etc. (1990) and extended into fatigue loadings. They proposed a new form of the size of the limit fracture surface. Different from the model of Suaris and etc. (1990), they proposed a form of the damage effect tensor which relates the effective Cauchy stress tensor to the usual Cauchy stress tensor. With the damage effect tensor, they obtained the effective compliance matrix. However, other shortcomings of previous model still exist.

These models are able to predict the stress strain relation of isotropic materials in monotonic and in several cycles of cyclic loadings by using lots of parameters.

However, the extension of these models in fatigue loadings is restrained, although they can be developed into fatigue loadings as mentioned by Pandolfi and Taliercio (1998) and fulfilled by Al-Gadhib and etc. (2000). This is because these models use lots of parameters to describe the stress strain relation in one or several loading cycles, which is not necessary in fatigue loadings where overall behaviors of lots of loading cycles are more important and increases the difficulties to calibrate the models with experimental data.

In this chapter a new bounding surface theory with limited parameters is developed for fatigue loadings. The concept of this bounding surface theory is presented below. If one considers a material element, shown on Figure 6.1, where numbers "1" and "2" indicate loading directions, and the biaxial strength envelop (i.e., the limit surface representation in 2-D) of the material is represented by "LS," corresponding to the quasi-static loadings of the material point (Figure 6.2). The LS surface represents the limit (ultimate) strength of the material under a variety of loading paths in a non-fatigue environment. From another perspective, the LS also represents a set of load combinations under which the material will fail statically.

As understood in the fatigue loading, as the number of loading cycles increases, the ultimate strength of the material decreases because of the presence and activation of inherent and new flaws and damage in the material. In a two dimensional representation scheme, as is used here, it is then plausible to consider that the LS would collapse inwardly as represented by the residual strength (RS) family of curved surfaces (the terminology used in fatigue literature). In the same

manner as the LS, the RS also represents a set of load combinations under which the material will fail for the same number of cyclic loadings. As the number of cycles increases, the LS surface shrinks further, as shown for $n_2 > n_1$. At some point, the failure point is reached and the material fails because of the applied stress level at cycle "N." In fatigue literature, "N" is also referred to as the life of the material. Therefore, the fatigue life can be determined through this theory.

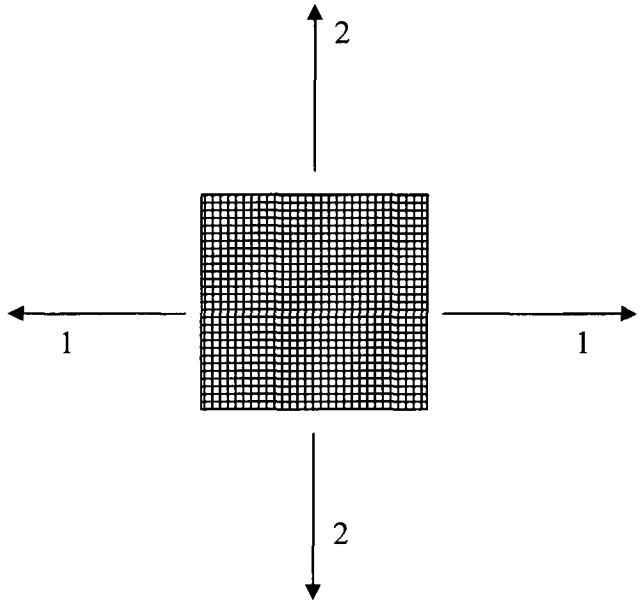

Figure 6.1. Material element with loading directions 1 and 2.

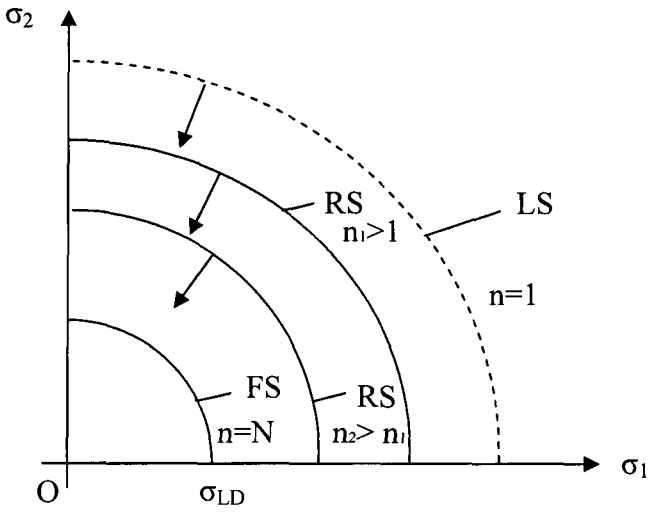

Figure 6.2. Schematic representation of boundary surfaces in two-dimensions.

For a clearer understanding of the process, the bounding surface theory may be explained as a simple loading path, such as a uniaxial loading path. For a given loading stress, σ_0, when the cyclic loading number, n, equals "1," the limit strength is designated as f_{t1}. With the increase of the cyclic number, the residual strength decreases. For example, as shown on Figure 6.3, when $n= n_1$, the residual strength equals σ_1. When the cyclic loading number reaches the fatigue life, which is represented by "n=N," the residual strength equals the applied tensile stress σ_0, and material fails.

The tasks at hand are to develop a realistic and reasonable LS that is based on the principles of mechanics and to propose an evolutionary law that would provide the position of intermediate RS surfaces loading to the failure surface (FS) when n=N. The limit surface and evolutionary law are different for different materials. In the next

section, the limit surface and evolutionary law will be established for the woven fabric composite material under fatigue loading.

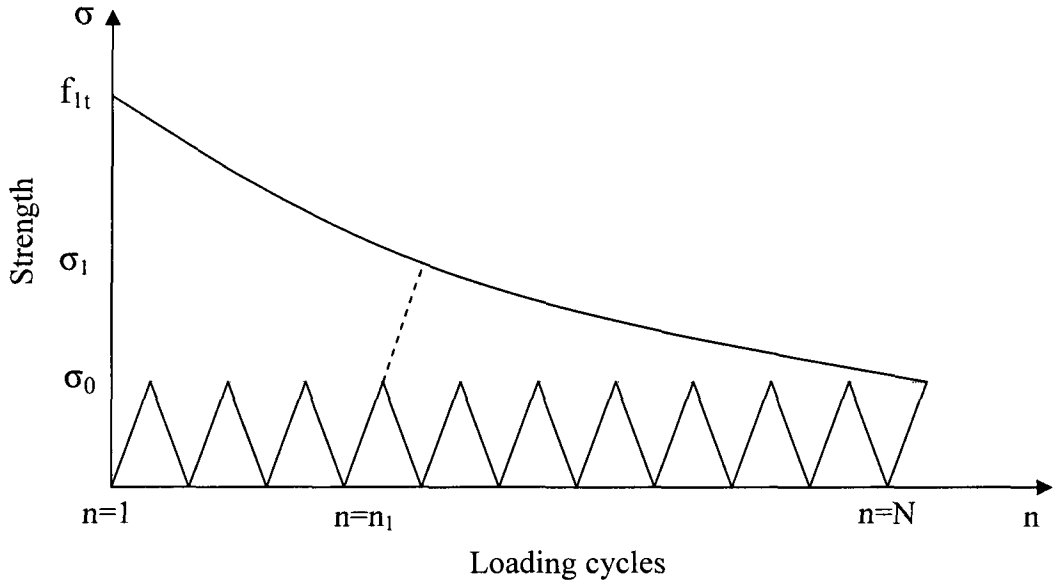

Figure 6.3. Illustration of the development of residual strength surface in uniaxial fatigue loading condition.

6.3. Formulation

In this chapter it is still assumed that the fatigue loading is of low frequency so that thermal effects could be ignored with the further assumption of small deformation. The form of Gibbs Free Energy (GFE) is given as Equation 4.44 and shown as follows.

$$G = \frac{1}{2}\boldsymbol{\sigma} : \mathbf{C} : \boldsymbol{\sigma} + \boldsymbol{\sigma} : \boldsymbol{\varepsilon}^{i} - A^{1}(k) \tag{6.1}$$

where **C** represents the compliance tensor, $\boldsymbol{\varepsilon}^i$ designates the inelastic strain tensor, $\boldsymbol{\sigma}$ is the applied stress tensor, $A^i(k)$ is a scalar function, and k is the cumulative fatigue damage parameter. The symbol ":" denotes the tensor contraction operation.

Following the standard thermodynamics arguments and assuming that the unloading is an elastic process, the dissipation inequality can be stated in terms of the GFE as follows:

$$\frac{\partial G}{\partial k}\dot{k} \geq 0 \tag{6.2}$$

where, $\dot{k}$ is the rate of damage. Introducing Eq. (6.1) into Eq. (6.2), and assuming that damage is irreversible (i.e., $\dot{k} \geq 0$), the dissipation inequality takes the following form:

$$\frac{1}{2}\boldsymbol{\sigma} : \frac{\partial \mathbf{C}}{\partial k} : \boldsymbol{\sigma} + \boldsymbol{\sigma} : \frac{\partial \boldsymbol{\varepsilon}^i}{\partial k} - \frac{\partial A^i}{\partial k} \geq 0 \tag{6.3}$$

To progress further, one can decompose the current compliance tensor into an initial undamaged component plus added flexibility caused by damage during fatigue loadings as discussed in Chapter 5.

$$\mathbf{C}(k) = \mathbf{C}^0 + \mathbf{C}^c(k) \tag{6.4}$$

Where, $\mathbf{C}^0$ is the initial undamaged fourth-order compliance tensor and $\mathbf{C}^c(k)$ denotes the added flexibility tensor due to damage. Also, the changes in the fourth-order compliance tensor and the inelastic strain tensor are regarded as fluxes in the thermodynamic state sense and are expressed below with respect to a set of response tensors **R** and **M** as discussed in Chapter 5:

$$\dot{\mathbf{C}}^c = \dot{k}\mathbf{R} \quad \text{and} \quad \dot{\boldsymbol{\varepsilon}}^i = \dot{k}\mathbf{M} \tag{6.5}$$

The response tensors determine the directions of the fatigue damage and the inelastic deformation processes. Including Equation (6.4) and (6.5) into Equation (6.3) yields the following form of the dissipation inequality:

$$\frac{1}{2}\boldsymbol{\sigma} : \mathbf{R} : \boldsymbol{\sigma} + \boldsymbol{\sigma} : \mathbf{M} - \frac{\partial A^{i}}{\partial k} \geq 0 \tag{6.6}$$

The onset of damage is determined by defining a potential function ψ ($\boldsymbol{\sigma}$, k) that is derived from Equation (6.6) so that

$$\psi(\boldsymbol{\sigma}, k) = \frac{1}{2}\boldsymbol{\sigma} : \mathbf{R} : \boldsymbol{\sigma} + \boldsymbol{\sigma} : \mathbf{M} - \frac{1}{2}t^{2}(\boldsymbol{\sigma}, k) = 0 \tag{6.7}$$

where t($\boldsymbol{\sigma}$, k) is interpreted as the damage function given below as

$$t^{2}(\boldsymbol{\sigma}, k) = 2[\frac{\partial A^{i}}{\partial k} + g^{2}(\boldsymbol{\sigma}, k)] \tag{6.8}$$

for some scalar-valued function $g^{2}(\boldsymbol{\sigma}, k)$. We note that as long the function "t" could be obtained experimentally, the identification of the components shown on the right hand side of the Equation (6.8) is not necessary.

To progress further, specific forms of the response tensors **R** and **M** must be provided. Guided by the experimental data from literature (Smith and Pascoe 1989), the following response tensors are postulated for **R** and **M**:

$$\mathbf{R} = \frac{\boldsymbol{\sigma} \otimes \boldsymbol{\sigma}}{\boldsymbol{\sigma} : \boldsymbol{\sigma}} + \alpha(\mathbf{I} - \mathbf{i} \otimes \mathbf{i}) \tag{6.9}$$

$$\mathbf{M} = \beta\boldsymbol{\sigma} \tag{6.10}$$

where the symbol "$\otimes$" signifies the tensor product operation, **I** represents the fourth-order identity tensor, **i** represents the second-order identity tensor, and α and β are material parameters.

The response tensor **R** is composed of two parts as follows.

$$\mathbf{R}_{\mathrm{I}} = \frac{\boldsymbol{\sigma} \otimes \boldsymbol{\sigma}}{\boldsymbol{\sigma} : \boldsymbol{\sigma}} \tag{6.11}$$

$$\mathbf{R}_{\mathrm{II}} = \alpha(\mathbf{I} - \mathbf{i} \otimes \mathbf{i}) \tag{6.12}$$

The first part, $\mathbf{R}_{\mathrm{I}}$, indicates that damage occurs in the loading directions. This is in concurrence with observed experimental data (Smith and Pascoe 1989). However with $\mathbf{R}_{\mathrm{I}}$ alone, the limit surface that is predicted by the model cannot match the experimental data as shown in Figure 6.4. Also, with $\mathbf{R}_{\mathrm{I}}$ alone any change in the Poisson's ratio could not be predicted by the proposed theory. Thus, the second part, $\mathbf{R}_{\mathrm{II}}$, is included. With an experimentally determined value of parameter α, the limit surface prediction is shown as the solid curve in Figure 6.4. The role of $\mathbf{R}_{\mathrm{II}}$ is thus two fold. One, the form enables the model to predict enhancement in strength under proportional loading, and two enables the model to address changes in the apparent poison's ratio.

The damage function, t ($\boldsymbol{\sigma}$, k), is further represented as the product of two functions L($\boldsymbol{\sigma}$) and q(k) such that

$$t(\boldsymbol{\sigma}, k) = L(\boldsymbol{\sigma})q(k) \tag{6.13}$$

where L($\boldsymbol{\sigma}$) and q(k) are interpreted as the strength and the shape functions of the damage function, t, with a condition that $q_{max}(k) = 1$, that is the maximum value of the

function q(k) and is set to be one. Considering a class of woven composites (0-90), we identify a strength tensor, **S**, as,

$$\mathbf{S} = F_{t1}\mathbf{q}_1 \otimes \mathbf{q}_1 + F_{t2}\mathbf{q}_2 \otimes \mathbf{q}_2 \tag{6.14}$$

where F_{t1} and F_{t2} are scalar parameters, and q_1 and q_2 are Eigen vectors of fiber directions, respectively. It will be shown below that F_{t1} and F_{t2} are related to the material strengths f_{t1} and f_{t2} in direction "1" and "2", respectively. With these backgrounds in place, a particular form for the strength function $L(\boldsymbol{\sigma})$ of Equation (6.13) is proposed as

$$L(\boldsymbol{\sigma}) = \frac{\boldsymbol{\sigma} : \mathbf{S}}{\mathrm{Tr}(\boldsymbol{\sigma})} \tag{6.15}$$

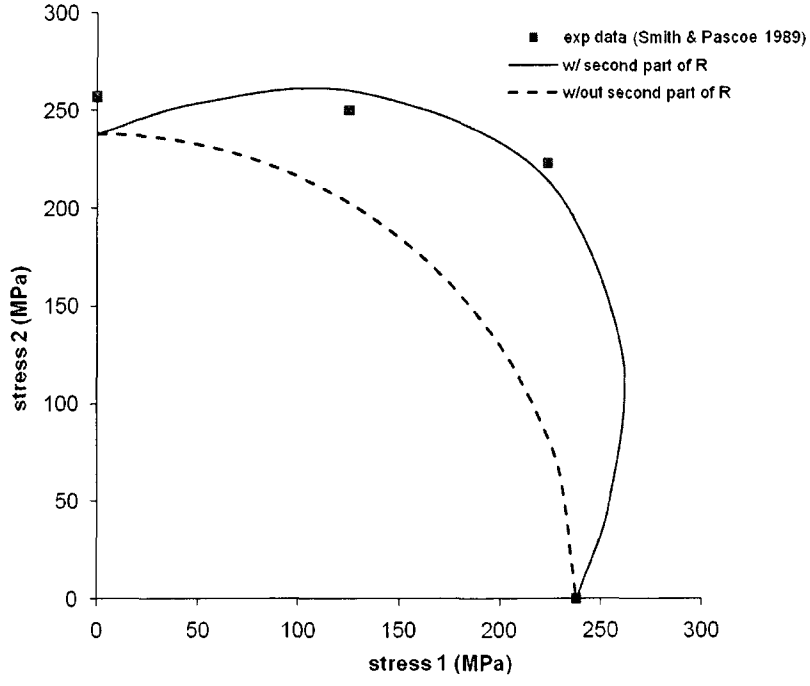

Figure 6.4. Effect of the two parts of response tensor **R**. Experimental data are of the biaxial ultimate strengths of specimen of Smith and Pascoe's work (1989).

By substituting Equations (6.9), (6.10), (6.13), and (6.15) into Equation (6.7), the potential function can be written as

$$\psi(\boldsymbol{\sigma},k)=\frac{1}{2}(1+\alpha+2\beta)\boldsymbol{\sigma}:\boldsymbol{\sigma}-\frac{1}{2}\alpha[Tr(\boldsymbol{\sigma})]^2-\frac{1}{2}[\frac{\boldsymbol{\sigma}:\mathbf{S}}{Tr(\boldsymbol{\sigma})}q(k)]^2=0 \tag{6.16}$$

To obtain the forms of scalar parameters F_{t1} and F_{t2}, two uniaxial loading paths in fiber direction "1" and "2" at the limit state are considered, respectively. In direction "1" Equation (6.16) is simplified to be as

$$\frac{1}{2}(1+2\beta)\sigma_1^{\,2}-\frac{1}{2}F_{t1}^{\,2}q^2(k)=0 \tag{6.17}$$

Since at the limit state the function q(k)=1, and $\sigma_1=f_{t1}$, where f_{t1} is the tensile strength in direction "1," it follows that

$$F_{t1}^{\,2}=f_{t1}^{\,2}(1+2\beta) \tag{6.18}$$

Similarly, in direction "2" Equation (6.16) is simplified to be as

$$\frac{1}{2}(1+2\beta)\sigma_2^{\,2}-\frac{1}{2}F_{t2}^{\,2}q^2(k)=0 \tag{6.19}$$

and since at the limit state the function q(k)=1, and $\sigma_2=f_{t2}$, where f_{t2} is the tensile strength in direction "2," we get the following relation that

$$F_{t2}^{\,2}=f_{t2}^{\,2}(1+2\beta) \tag{6.20}$$

It is observed that if f_{t1} and f_{t2} are the same, the model will predict strength isotropy; with f_{t1} and f_{t2} being unequal, the model will predict strength anisotropy as one expects in most composites.

An example is provided here to illustrate the capability of the model to predict strength isotropy and anisotropy. The predicted limit surfaces of two materials are

shown in Figure 6.5. The dashed curve represents a material with strength anisotropic with strength f_{t1} = 80 MPa in direction "1" and f_{t2} = 50 MPa in direction "2." The solid curve represent a material with a strength isotropy with strength $f_{t1} = f_{t2}$ = 80 MPa in both directions.

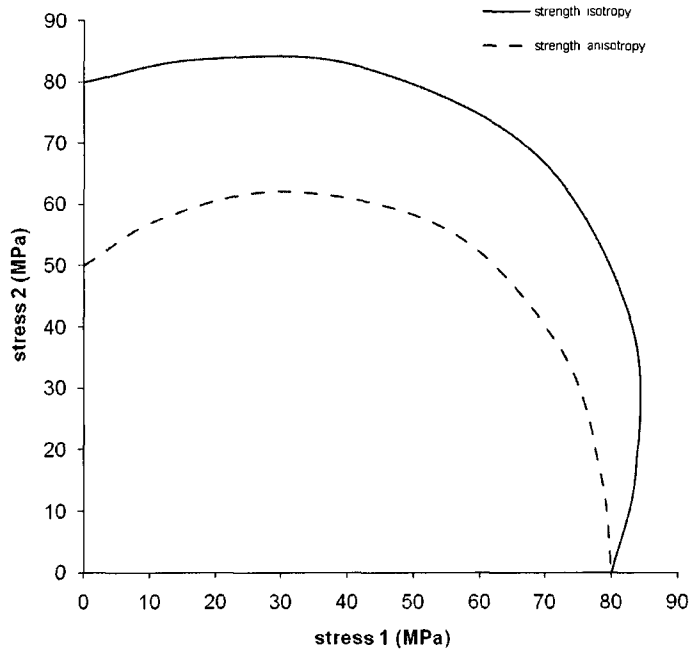

Figure 6.5. Schematic illustration of model predicted limit surface for strength isotropic and anisotropic materials.

As the number of loading cycles starts to increase, the strength of the material is affected and reduced. The limit surface representing the foci of all strength points associated with n=1 is therefore affected and should be modeled to soften to failure surface. To achieve this, the strength function $L(\boldsymbol{\sigma})$ should be modified to predict

lower limit strength of the material with increasing number of cycles. Therefore, we propose a new strength function, $L(\boldsymbol{\sigma},n)$ as

$$L(\boldsymbol{\sigma},n) = \frac{\boldsymbol{\sigma}:\mathbf{S}}{Tr(\boldsymbol{\sigma})} F(n) \tag{6.21}$$

where F(n) acts as a the softening function.

Incorporating the damage softening function back into the general formulation yields

$$\psi(\boldsymbol{\sigma},k) = \frac{1}{2}(1+\alpha+2\beta)\boldsymbol{\sigma}:\boldsymbol{\sigma} - \frac{1}{2}\alpha[Tr(\boldsymbol{\sigma})]^2 - \frac{1}{2}[\frac{\boldsymbol{\sigma}:\mathbf{S}}{Tr(\boldsymbol{\sigma})} F(n)q(k)]^2 = 0 \tag{6.22}$$

6.3.1 Interpretation and identification of F(n)

To interpret the softening function F(n) we consider a uniaxial fatigue loading path in the fiber direction "1" with $q_{max}=1$ as follows.

$$\psi(\boldsymbol{\sigma},k) = \frac{1}{2}(1+\alpha+2\beta)\sigma_1^2 - \frac{1}{2}\alpha(\sigma_1)^2 - \frac{1}{2}[F_{t1}F(n)]^2 = 0 \tag{6.23}$$

With the previously obtained result that $F_{t1}^{\ 2} = f_{t1}^{\ 2}(1+2\beta)$, we obtains the relation for F(n) as

$$F(n) = \frac{\sigma_1}{f_{t1}} \tag{6.24}$$

The relation (6.24) represents the ratio of the residual strength over the ultimate strength. This is also referred to the classical S-N curve in fatigue literature terminologies. To determine a proper form for F(n), we therefore refer to the experimental S-N curve for uniaxial tension in the literature. The two most fundamental classical S-N curves are the power function and logarithm function as

discussed in Section 2.2.1. Based on the comparison in Appendix 4 between power function and logarithm function with experimental work of Smith & Pascoe (1989), the power function is used as follows.

$$F(n) = n^A \tag{6.25}$$

where n is the number of cyclic loading, and A is a material parameter.

For the experimental work of Smith and Pascoe (1989) that is used here, the model predictions are shown in Figure 6.6, 6.7, and 6.8 for various stress ratios.

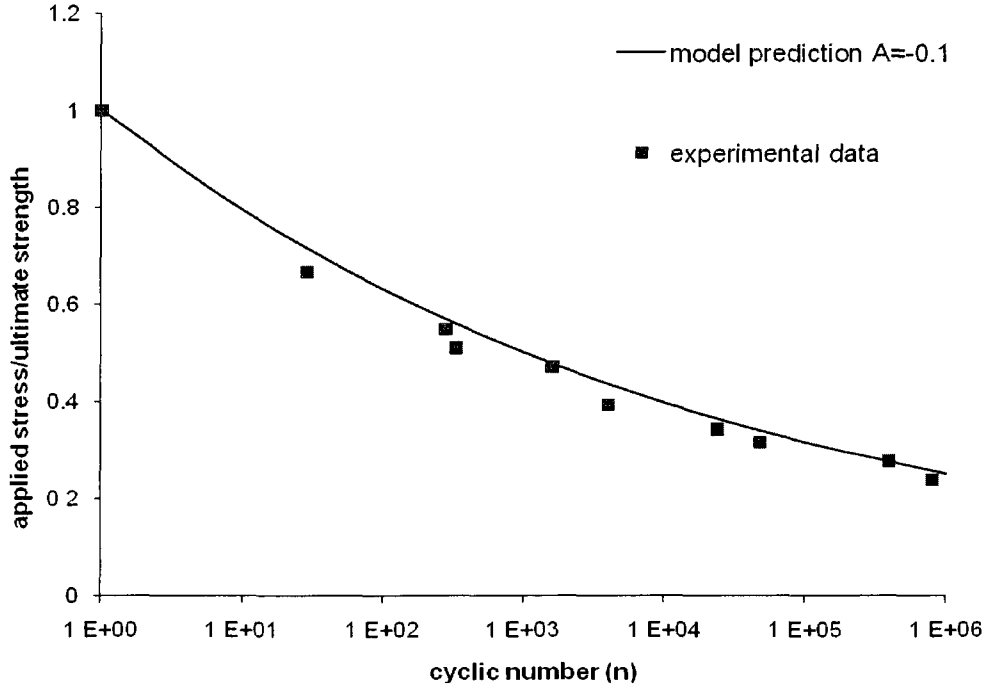

Figure 6.6. Comparison between softening function and experimental data (Smith & Pascoe, 1989) with stress ratio 1:0.

To obtain the constant material parameter "A", we utilize Equations (6.18) and (6.25) to get

$$A = \ln\left(\frac{\sigma_1}{f_{t1}}\right)/\ln(n) \tag{6.26}$$

Finally, the rate of the damage parameter, k, must be obtained from the constitutive relations used and the strength degradation forms proposed due to fatigue cycles. For the simple constitutive relation of the form shown as $\varepsilon=\mathbf{C}(k):\sigma+\varepsilon^{I}$, the rate of damage parameter, dk/dn, for the uniaxial path can be shown to be as

$$\frac{dk}{dn} = \frac{1}{E_0(1+\beta)}(-A)(n^{-A-1}) \tag{6.27}$$

where E_0 is the initial Young's modulus in the absence of any damage.

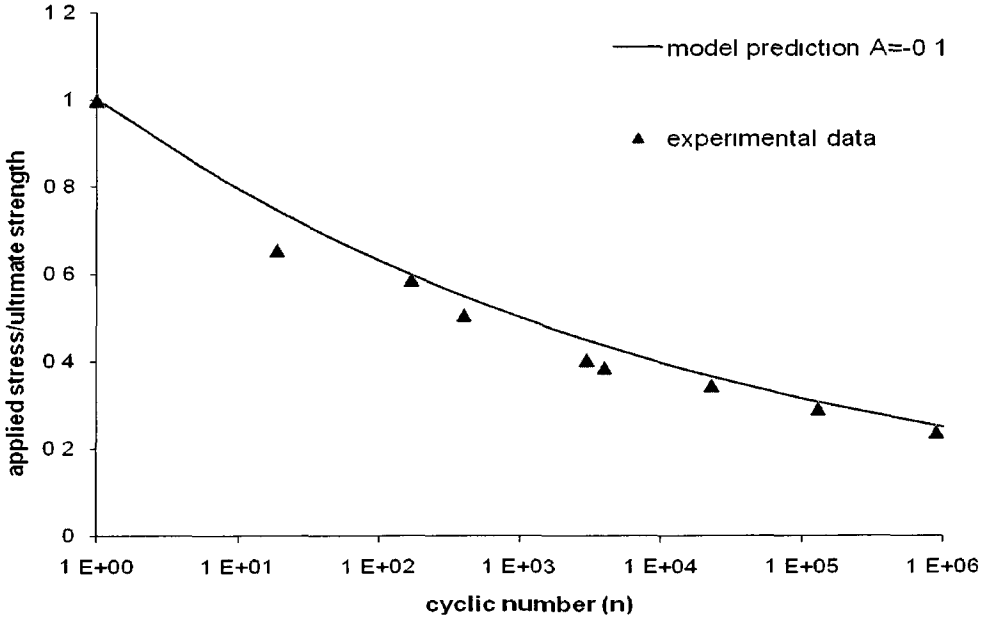

Figure 6.7. Comparison between softening function and experimental data (Smith & Pascoe, 1989) with stress ratio 1:0.5.

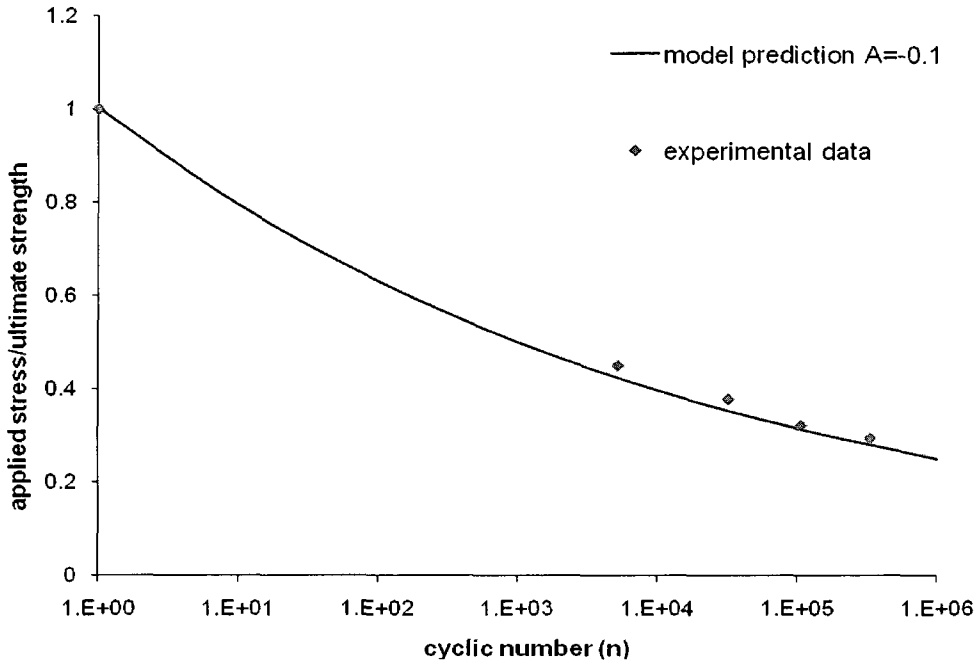

Figure 6.8. Comparison between softening function and experimental data (Smith & Pascoe, 1989) with stress ratio 1:1.

6.4. One-dimensional illustration

This section illustrates the procedures for the model through a uniaxial cyclic loading process. The cyclic load with the maximum loading stress, σ_0, is added in direction "1," as shown on Figure 6.1. In the two-dimension condition, the load is expressed in the matrix form as follows:

$$\boldsymbol{\sigma} \equiv [\sigma_0 \quad 0] \tag{6.28}$$

The response tensors, **R** and **M**, of Equations 6.9 and 6.10 are expressed in the following matrix forms:

$$\mathbf{R} \equiv \begin{bmatrix} 1 & \alpha \\ \alpha & 0 \end{bmatrix} \tag{6.29}$$

$$\mathbf{M} \equiv \begin{bmatrix} \beta\sigma_0 \\ 0 \end{bmatrix} \tag{6.30}$$

The strength tensor, **S**, of Equation 6.14 is also shown in the matrix form as follows:

$$\mathbf{S} \equiv \begin{bmatrix} f_{t1}\sqrt{1+2\beta} & f_{t2}\sqrt{1+2\beta} \end{bmatrix} \tag{6.31}$$

Therefore, the strength function, L ($\boldsymbol{\sigma}$, n), of Equation 6.21 is as follows:

$$L(\boldsymbol{\sigma}, n) = f_{t1}\sqrt{1+2\beta}F(n) \tag{6.32}$$

And the damage surface in a fatigue environment, is as follows:

$$\psi(\boldsymbol{\sigma}, k) = \frac{1}{2}(1+2\beta)\sigma_1^{\,2} - \frac{1}{2}(f_{t1}\sqrt{1+2\beta}n^A)^2 = 0 \tag{6.33}$$

Then the following relationship is obtained for a uniaxial loading condition:

$$\sigma_1 = f_{t1}n^A \tag{6.34}$$

When the residual strength σ_1 equals f_{t1}, the material fails in the first loading cycle, which means that the fatigue life of the material is "1." When the residual strength σ_1 equals σ_0, the fatigue life is "N." With Equations 6.5 and 6.27, the added flexibility tensor, $C^c(k)$, and inelastic strain tensor, $\boldsymbol{\varepsilon}^i$ are obtained.

6.5. Numerical Simulation

In this section, the predictions of the proposed model are compared with the experimental data of Smith & Pascoe (1989). Smith & Pascoe used a biaxial hydraulic servo-controlled rig developed at the Cambridge University Engineering Department. Nine biaxial and three uniaxial stress states were tested. All tests were load control. Fatigue test frequencies were generally kept in the range 0.1-0.6 Hz to prevent excessive cyclic induced heating. The specimens were cruciform for biaxial

tests and parallel-sided for uniaxial tests. All specimens were from one batch of laminate which was laid up from reinforcement of glass fiber woven roving (0-90) and isophthalic polyester resin. Each laminate contains 13 laminas. Warp and weft fibers of different lamina are aligned in the same directions, respectively.

Three material parameters, A, α, and β are used in the model. To determine the parameters, the following tests can be used. With one uniaxial fatigue test and knowing the uniaxial strength of the material, the residual strength, σ_1, and cyclic number, n, can be obtained. The constant A can then be determined by Equation 6.26. The parameter β is a kinematic parameter and is identified by measuring the inelastic deformation after unloading. With one biaxial quasi-static test and parameter β, α can be determined by Equation 6.16.

Figure 6.9 shows the prediction results of biaxial limit surface and residual strength surface against the experimental work of Smith and Pascoe (1989), for the monotonic loading when n=1 and the fatigue loading when $n=10^5$ cycles. The theoretical results for predictions are good considering the simplicity of the forms that were used. The following material parameters were used: α=0.46, β=0.1, A=-0.1.

Figure 6.10 shows the comparison of the model prediction of the increment of compliance with the experimental data of Smith and Pascoe (1989). The experimental data are of an equal biaxial fatigue test. The values of parameters α, β, and A are the same as those of Figure 6.9. Lastly, the predicted stress-strain relations are shown on Figure 6.11, 6.12, and 6.13 where the strength and ductility reductions are demonstrated due to effect of fatigue loading. Figure 6.11 shows the predicted stress-

strain relations of uniaxial monotonic and fatigue loadings; Figure 6.12 shows those of monotonic and fatigue loadings with stress ratio 1:0.5; Figure 6.13 shows those of monotonic and fatigue loadings with stress ratio 1:1. The experimental data are from the work of Smith and Pascoe (1989).

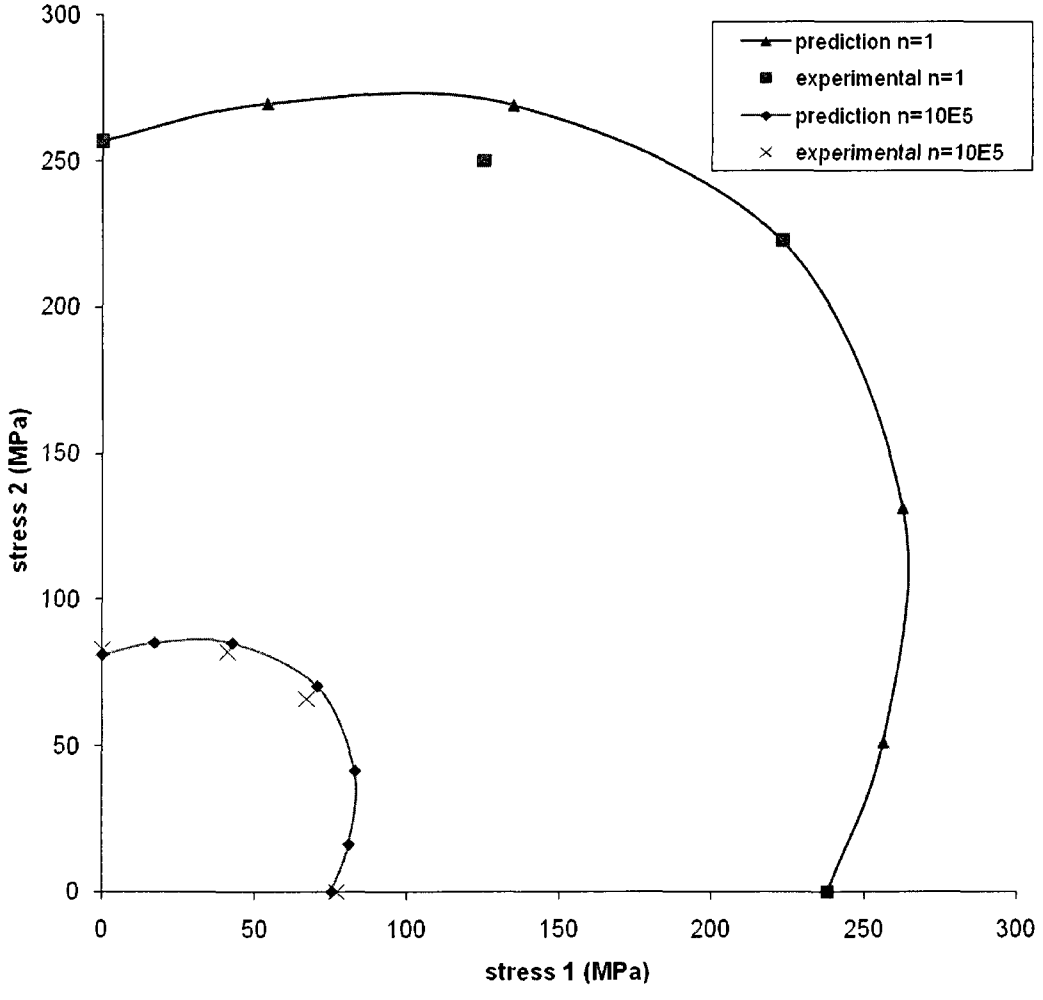

Figure 6.9. Comparison between experimental data (Smith & Pascoe, 1989) and theory predictions of limit surface and residual strength surface of 10^5 loading cycles.

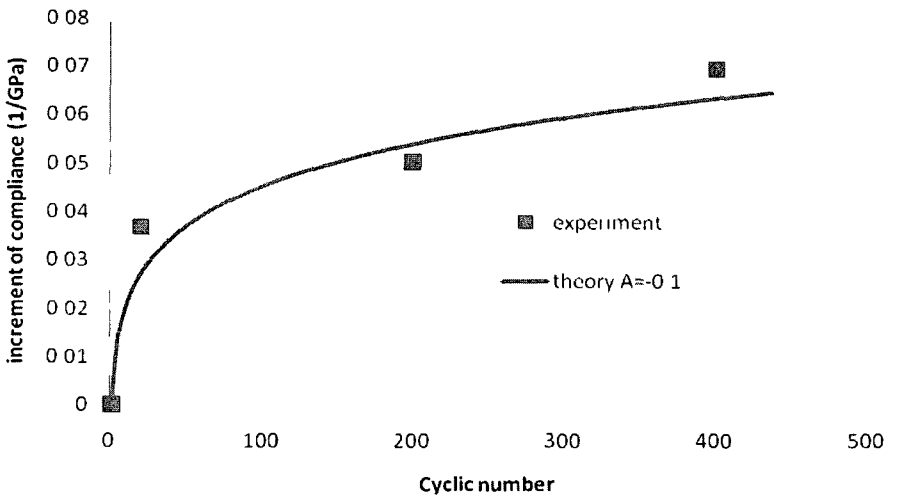

Figure 6.10. Comparison of increment of compliance of equal biaxial fatigue between experimental data (Smith & Pascoe, 1989) and model prediction.

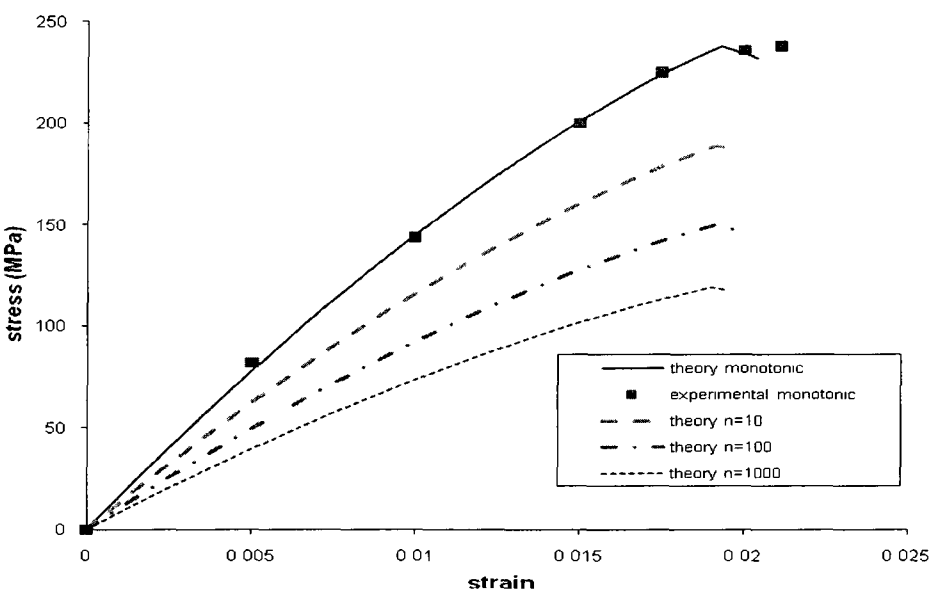

Figure 6.11. Predictions of the stress strain relationship of uniaxial monotonic failure loading and uniaxial fatigue loadings. The experimental data are from the work of Smith & Pascoe (1989).

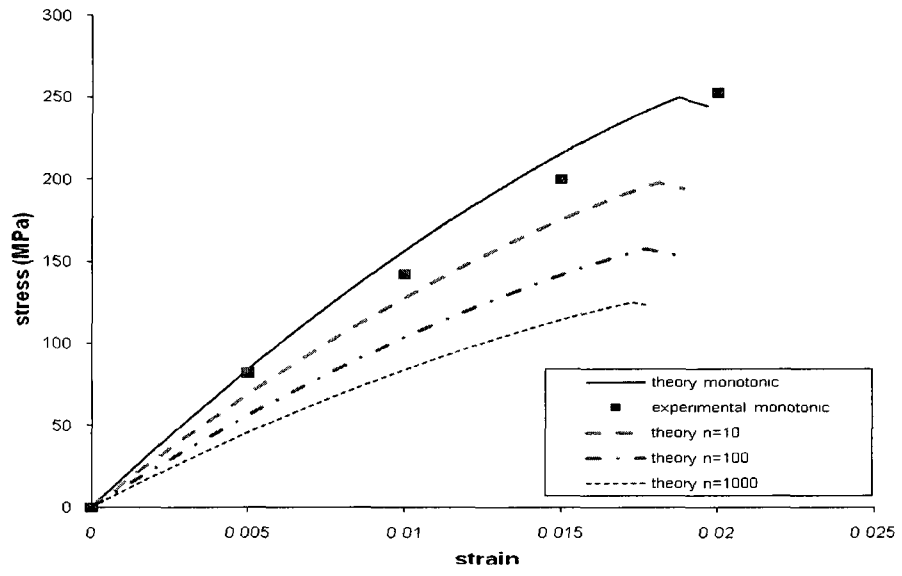

Figure 6.12. Predictions of the stress strain relationship of monotonic failure loading and fatigue loadings with stress ratio 1:0.5. The experimental data are from the work of Smith & Pascoe (1989).

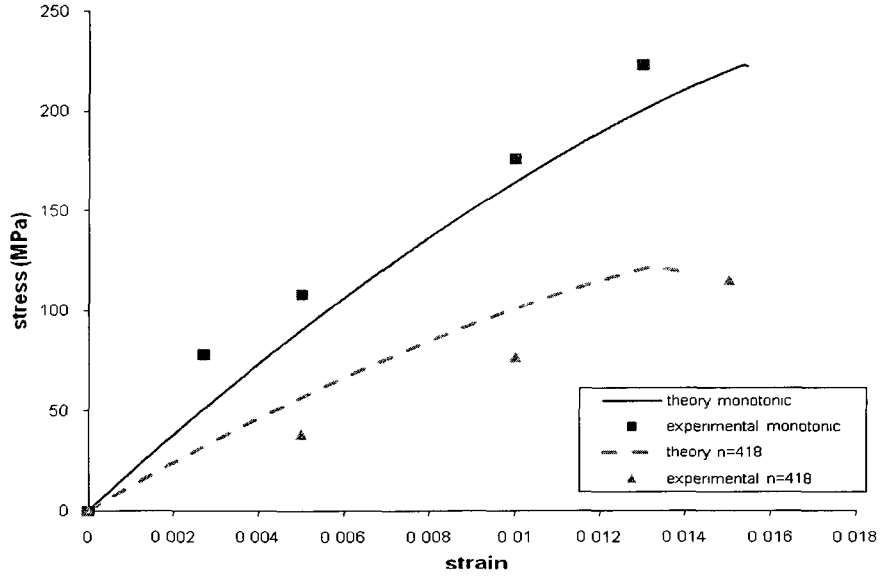

Figure 6.13. Predictions of the stress strain relationship of monotonic failure loading and fatigue loadings with stress ratio 1:1. The experimental data are from the work of Smith & Pascoe (1989).

The effects of parameters α, β and A on the model are shown in the following figures. The effects of parameters α and β on the limit surface, Equation 6.16, are shown in Figures 6.14 and 6.15. The effects of parameter A on the softening function, Equation 6.25, are shown in Figures 6.16, 6.17, and 6.18 for stress ratios of 1:0, 1:1, and 1:0.5, respectively. Finally, the effects of parameters β and A on the damage increment, Equation 6.27, are shown in Figure 6.19, and 6.20. From these figures, it can be observed that the predicted results stably change with the changes of the parameters.

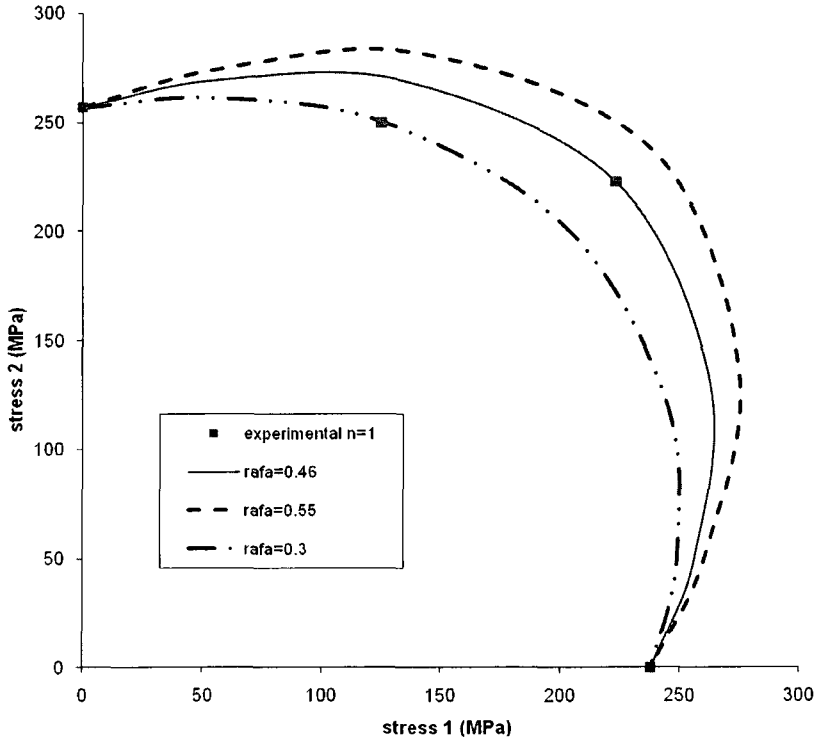

Figure 6.14. Comparison between the experimental data of limit surface and predicted limit surfaces for different values of α and constant value of β equal to 0.1.

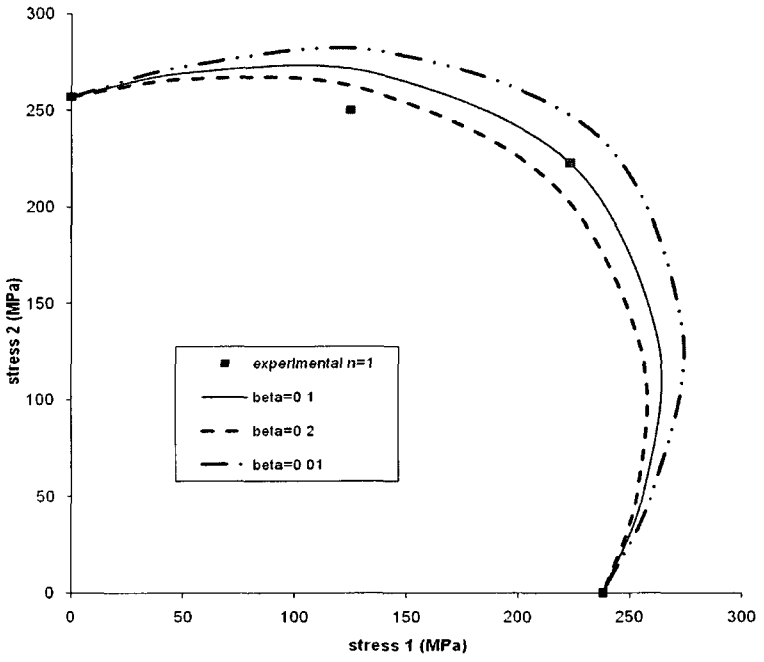

Figure 6.15. Comparison between the experimental data of limit surface and predicted limit surfaces for different values of β and constant value of α equal to 0.46.

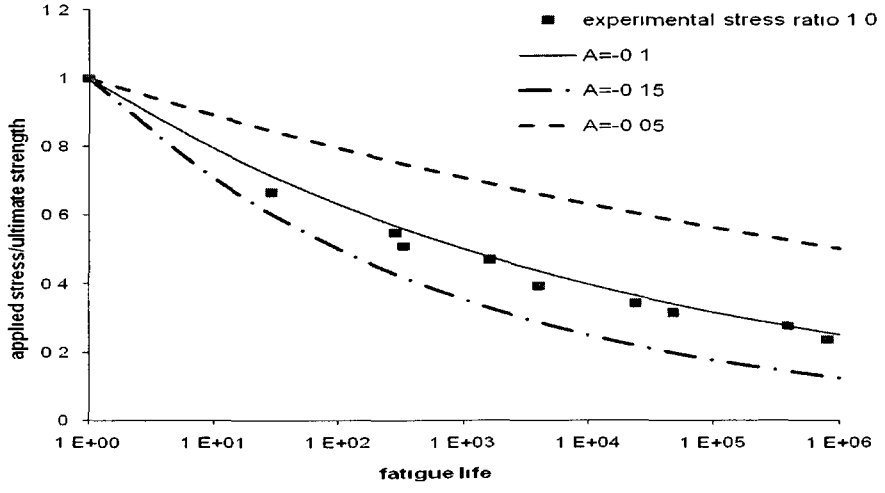

Figure 6.16. Comparison between the experimental data of softening function and predicted results for different values of A for stress ratio 1:0.

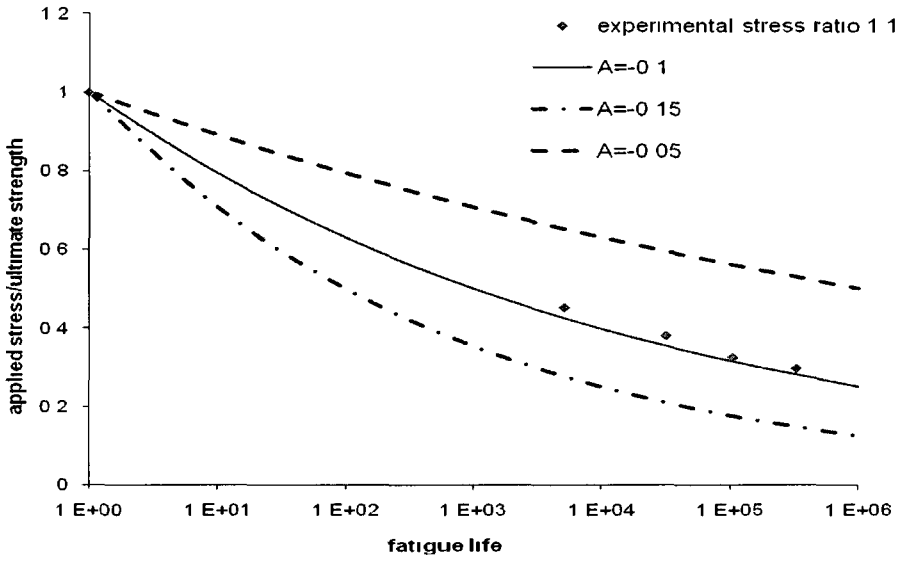

Figure 6.17. Comparison between the experimental data of softening function and predicted results for different values of A for stress ratio 1:1.

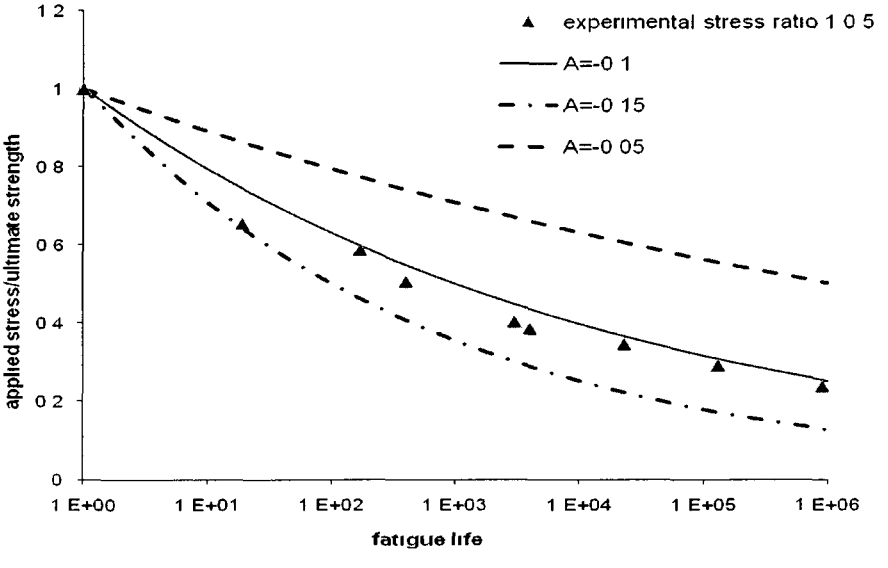

Figure 6.18. Comparison between the experimental data of softening function and predicted results for different values of A for stress ratio 1:0.5.

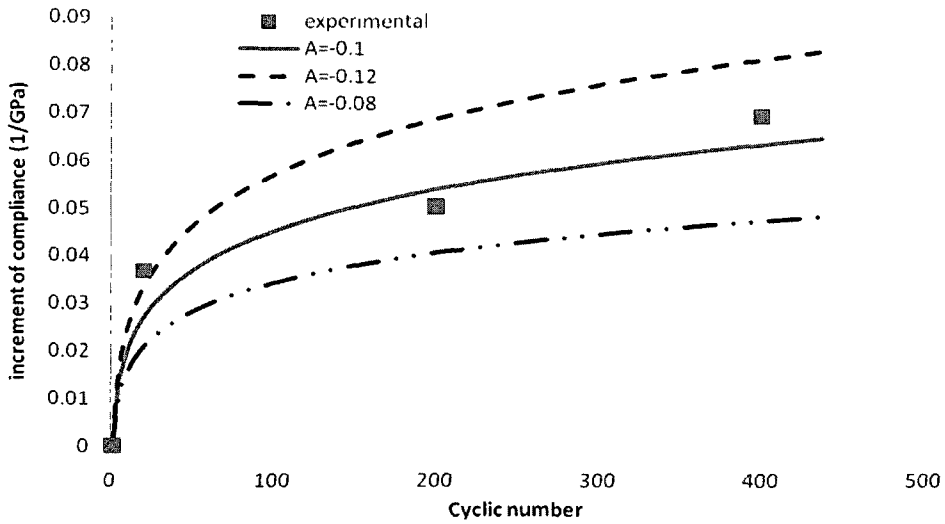

Figure 6.19. Comparison between the experimental data of the damage rate function and predicted results for different values of A and constant value of β equal to 0.1.

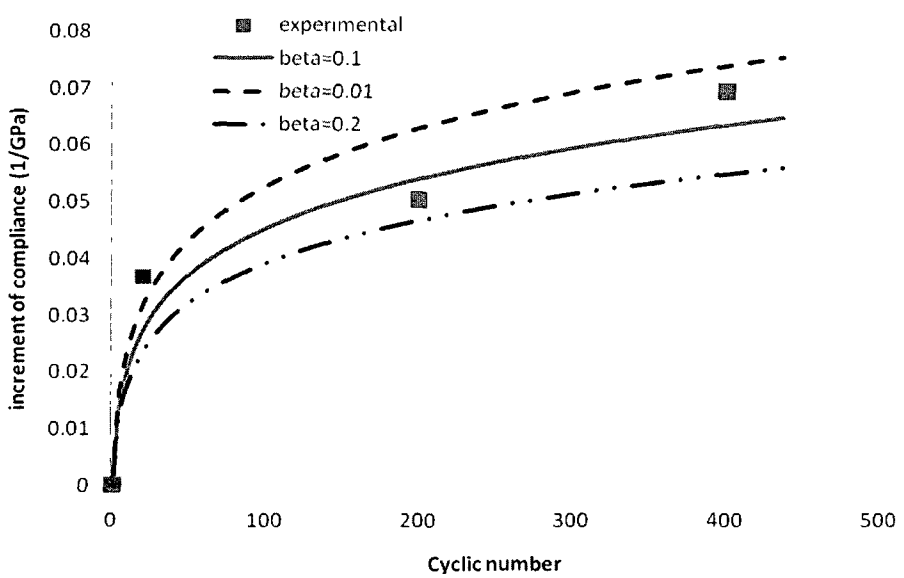

Figure 6.20. Comparison between the experimental data of the damage rate function and predicted results for different values of β and constant value of A equal to -0.1.

6.6. Conclusion

An anisotropic damage model is established to predict the fatigue behaviors of woven composite materials under low frequency fatigue loading. A class of damage mechanics is applied since cracking is the main type of damage and dominates most of the fatigue life. A bounding surface theory is developed to predict the fatigue behavior of material under biaxial loadings. A direction function that is involved in the damage function captures the strength anisotropic of materials. The damage rate is established and shows good prediction capability of the increment of compliance. By comparison with experimental data, the model shows good capability to describe the essential properties of woven composite materials under fatigue loading.

7. BOUNDING SURFACE DAMAGE MODEL FOR FATIGUE RESPONSE OF STEEL FIBER REINFORCED CONCRETE

7.1. Introduction

Concrete contains several defects, such as microcracks and micro-voids (Yazdani and Karnawat, 1996). Under static and fatigue compression loadings, damage in plain concrete, primarily in the form of cracks, nucleates at these defects and develops rapidly along the loading direction because of the low tensile strength of the plain concrete. Therefore, the introduction of closely spaced steel fibers in the plain concrete is a reasonable and effective method of increasing the tensile strength of the material. These fibers arrest the nucleation and development of the cracks and give concrete better resistance to fatigue loading, impact loading, thermal loading, and cracking (Xie, 2004; Ochi, 2005; Hou, 2006).

With these advantages, steel fiber-reinforced concrete is more widely used in civil engineering structures, such as highway pavements, bridges, pipes, walls, shell roofs, offshore platforms, submerged storage tanks, etc. These structures could be subjected to uniaxial or biaxial compression fatigue loadings that are caused by vehicles, wind, machine vibrations, and earthquakes (Yin and Hsu, 1995).

The introduction of the steel fibers changes the failure mode of plain concrete. In plain concrete, the failure mode is a splitting type as shown on Figure 7.1. Under

uniaxial loading, splitting occurs in the loading direction; under biaxial loading, splitting occurs in the plane parallel to the loading plane (Su and Hsu, 1988). However, in steel fiber-reinforced concrete, the failure mode is the faulting mode, as shown on Figure 7.2. In uniaxial compression, the failure occurs along two planes that have an angle with the loading direction; in biaxial compression, the failure occurs along one or two planes that have an angle with the loading plane (Yin and Hsu, 1995).

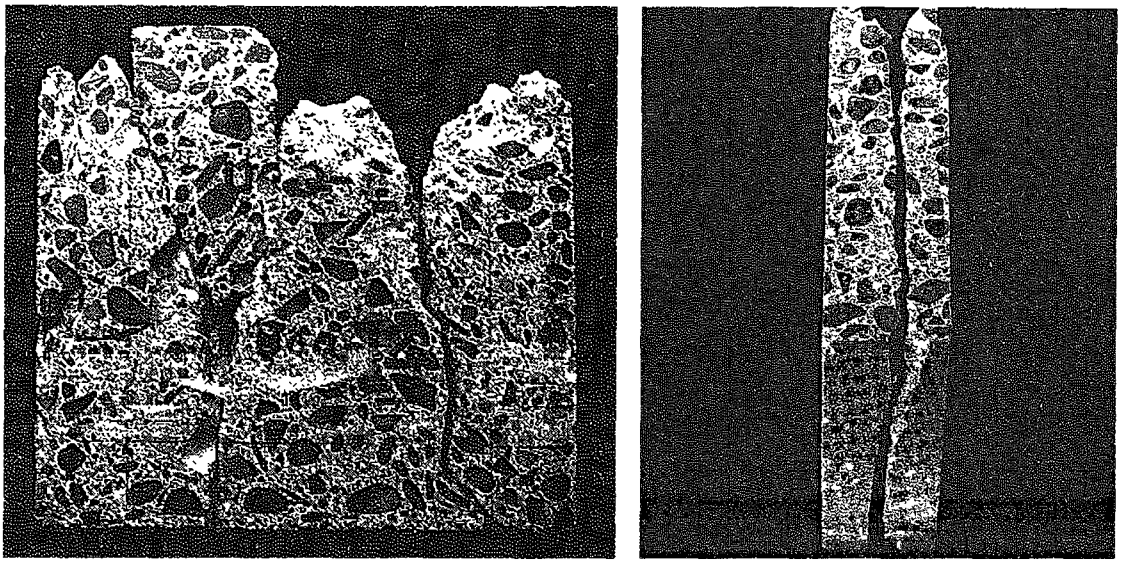

(a) (b)

Figure 7.1. Failure mode of plain concrete. (a) Uniaxial compression fatigue (front view of speciman; loading in vertical direction); (b) Biaxial compression fatigue (side view of speciman; loading in vertical and normal to picture directions). (Yin, W. and Hsu T.C., 1995)

It has been addressed that steel fiber-reinforced concrete shows different mechanical properties from plain concrete. However, most of the research has been

focused on the mechanical behavior of fiber-reinforced concrete under monotonic loading, and only relatively few studies have addressed the material behavior under fatigue loading. Yin and Hsu (1995) compared the fatigue behaviors of plain concrete and fiber-reinforced concrete, where they proposed several equations for S-N curves, and reported data for the biaxial fatigue strength envelopes. Singh and Kaushik (2000) presented a probabilistic analysis of the fatigue life of fiber-reinforced concrete. Hou et al. (2006) investigated the change of the elastic modulus of the steel fiber-reinforced concrete with different steel fiber contents and under different stress levels. Chang et al. (1998) studied the effect of initial crack depth to the fatigue strength of steel fiber-reinforced concrete. Extensive experimental data are presented in these research papers, but, theoretically, most of these studies focused only on proposing new S-N curves for uniaxial stress path, and few of them developed a unified approach capable of describing the fatigue behavior of steel fiber-reinforced concrete under different loading patterns.

In this chapter, a unified approach based on bounding surface theory that was introduced in the previous chapter, is proposed for the damage mechanics modeling of steel fiber-reinforced concrete. The high directionality of the damage development is reflected through a new fourth-order response tensor, and the evolution of inelastic deformation caused by damage is described by a new second-order response tensor. The foundation of the theory is the same as in Chapters 5 and 6 and will therefore be presented in a more compact fashion than the previous chapters.

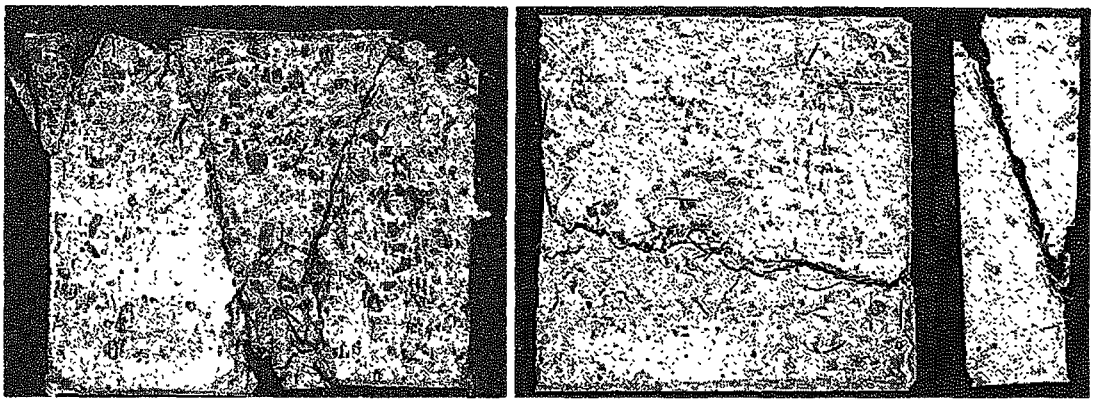

(a) (b) (c)

Figure 7.2. Failure mode of steel fiber reinforced concrete. (a) Uniaxial compression fatigue (front view of speciman; loading in vertical direction); (b) Biaxial compression fatigue (front view of speciman; loading in vertical and horizontal directions); (c) Biaxial compression fatigue (side view of speciman; loading in vertical and normal to picture directions). (Yin, W. and Hsu T.C., 1995)

7.2. Formulation

It is assumed that the fatigue loading is of low frequency so that thermal effects could be ignored with the further assumption of small deformation. The form of Gibbs Free Energy (GFE) is Equation 4.44 and shows as follows

$$G = \frac{1}{2}\boldsymbol{\sigma} : \mathbf{C} : \boldsymbol{\sigma} + \boldsymbol{\sigma} : \boldsymbol{\varepsilon}^{i} - A^{l}(k) \tag{7.1}$$

where $\mathbf{C}$ represents the compliance tensor, $\boldsymbol{\varepsilon}_i$ designates the inelastic strain tensor, $\boldsymbol{\sigma}$ is the applied compression stress tensor, and the signs for compression components are positive, $A^l(k)$ is a scalar function, and k is the cumulative fatigue damage parameter. The symbol ":" denotes the tensor contraction operation.

Following the standard thermodynamics arguments and assuming that the unloading is an elastic process, the dissipation inequality can be stated in terms of GFE as follows:

$$\frac{\partial G}{\partial k}\dot{k} \geq 0 \tag{7.2}$$

where, $\dot{\mathbf{k}}$ is the rate of fatigue damage. Introducing Equation (7.1) into Equation (7.2), and assuming that damage is irreversible (i.e., $\dot{k} \geq 0$), the dissipation inequality takes the following form:

$$\frac{1}{2}\boldsymbol{\sigma} : \frac{\partial \mathbf{C}}{\partial k} : \boldsymbol{\sigma} + \boldsymbol{\sigma} : \frac{\partial \boldsymbol{\varepsilon}^{i}}{\partial k} - \frac{\partial A'}{\partial k} \geq 0 \tag{7.3}$$

To progress further, one can decompose the current compliance tensor into an initial undamaged component plus added flexibility caused by damage during fatigue loadings as discussed in Chapter 5.

$$\mathbf{C}(k) = \mathbf{C}^{0} + \mathbf{C}^{c}(k) \tag{7.4}$$

Where, $\mathbf{C}^{0}$ is the initial undamaged fourth-order compliance tensor and $\mathbf{C}^{c}(k)$ denotes the added flexibility tensor due to damage. Also, the changes in the fourth-order compliance tensor and the inelastic strain tensor are regarded as fluxes in the thermodynamic state sense and are expressed below with respect to a set of response tensors **R** and **M** as discussed in Chapter 5:

$$\dot{\mathbf{C}}^{c} = \dot{k}\mathbf{R} \quad \text{and} \quad \dot{\boldsymbol{\varepsilon}}' = \dot{k}\mathbf{M} \tag{7.5}$$

The response tensors determine the directions of the fatigue damage and the inelastic deformation processes. Including Equation (7.4) and (7.5) into Equation (7.3) yields the following form of the dissipation inequality

$$\frac{1}{2}\boldsymbol{\sigma} : \mathbf{R} : \boldsymbol{\sigma} + \boldsymbol{\sigma} : \mathbf{M} - \frac{\partial A'}{\partial k} \geq 0 \tag{7.6}$$

The onset of damage is determined by defining a potential function ψ ($\boldsymbol{\sigma}$, k) that is derived from Equation (7.6) so that

$$\psi(\boldsymbol{\sigma},k)=\frac{1}{2}\boldsymbol{\sigma}:\mathbf{R}:\boldsymbol{\sigma}+\boldsymbol{\sigma}:\mathbf{M}-\frac{1}{2}t^2(\boldsymbol{\sigma},k)=0 \tag{7.7}$$

where t($\boldsymbol{\sigma}$, k) is interpreted as the damage function given below as

$$t^2(\boldsymbol{\sigma},k)=2[\frac{\partial A^i}{\partial k}+g^2(\boldsymbol{\sigma},k)] \tag{7.8}$$

for some scalar-valued function $g^2(\boldsymbol{\sigma}, k)$. We note that as long as the function "t" could be obtained experimentally or specified guided by experimental records, the identification of the components shown on the right hand side of the Equation (7.8) is not necessary.

To progress further, forms of the response tensors **R** and **M** must be specified. To predict anisotropic behavior due to damage, **R** should be formulated such that damage anisotropy is achieved. Not like the composite material in the previous chapter, concrete is mainly used in the compression loading conditions as shown on Figure 7.3. It is feasible to expand this to other situations and other damage modes (Ortiz and Giannakopoulos, 1990 a, b; Yazdani, 1993; Karnawat and Yazdani, 2001). To generalize this and with a further assumption of no coupling between orthogonal cracks, the following response tensors are postulated for **R** and **M**:

$$\mathbf{R}=\frac{\tilde{\boldsymbol{\sigma}}\otimes\tilde{\boldsymbol{\sigma}}}{\tilde{\boldsymbol{\sigma}}:\tilde{\boldsymbol{\sigma}}}+\alpha H(\bar{\lambda})(\mathbf{I}-\mathbf{i}\otimes\mathbf{i})+\gamma H(\bar{\lambda})[h(-\tilde{\sigma}_1)q_1\otimes q_1+h(-\tilde{\sigma}_2)q_2\otimes q_2+h(-\tilde{\sigma}_3)q_3\otimes q_3] \tag{7.9}$$

$$\mathbf{M}=\mathbf{S}^{-}+\beta\mathbf{S}^{+} \tag{7.10}$$

where

$$\tilde{\boldsymbol{\sigma}} = \boldsymbol{\sigma} - \lambda \mathbf{i} \tag{7.11}$$

λ is the minimum eigen value of $\boldsymbol{\sigma}$. $\bar{\lambda}$ is the maximum eigenvalue of $\tilde{\boldsymbol{\sigma}}$. $\tilde{\sigma}_i$ are the eigenvalues of $\tilde{\boldsymbol{\sigma}}$. α, β and γ are material parameters. qi are defined in Chapter 6. H(.) and h(.) are Heaviside functions that are defined as follows.

$$H(x) = \begin{cases} 0 & x \le 0 \\ 1 & x > 0 \end{cases} \tag{7.12}$$

$$h(x) = \begin{cases} 0 & x < 0 \\ 1 & x \ge 0 \end{cases} \tag{7.13}$$

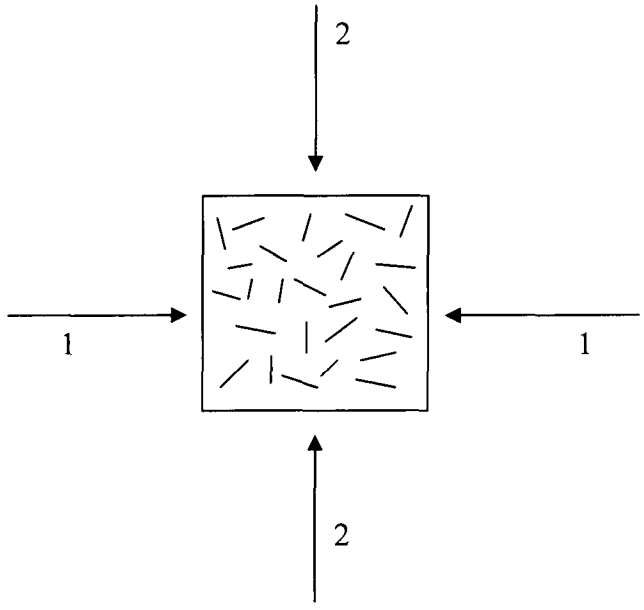

Figure 7.3. Material element with loading directions 1 & 2.

The response tensor **R** is composed of three parts,

$$\mathbf{R}_{\mathrm{I}} = \frac{\tilde{\boldsymbol{\sigma}} \otimes \tilde{\boldsymbol{\sigma}}}{\tilde{\boldsymbol{\sigma}} : \tilde{\boldsymbol{\sigma}}}, \tag{7.14}$$

$$\mathbf{R}_{\mathrm{II}} = \alpha \mathrm{H}(\bar{\tilde{\lambda}})(\mathbf{I} - \mathbf{i} \otimes \mathbf{i}) \quad \text{and} \tag{7.15}$$

$$\mathbf{R}_{\mathrm{III}} = \gamma \mathrm{H}(\bar{\tilde{\lambda}})[\mathrm{h}(-\tilde{\sigma}_1)\mathbf{q}_1 \otimes \mathbf{q}_1 + \mathrm{h}(-\tilde{\sigma}_2)\mathbf{q}_2 \otimes \mathbf{q}_2 + \mathrm{h}(-\tilde{\sigma}_3)\mathbf{q}_3 \otimes \mathbf{q}_3] \tag{7.16}$$

$\mathbf{R}_{\mathrm{I}}$ ensures that damage occurs in the loading directions (Figure 7.4) but does not occur in the direction of the minimum stress and ensures that there is no damage in the case of hydrostatic pressure. Similar to the discussion in Chapter 6, $\mathbf{R}_{\mathrm{II}}$ is used to adjust the limit surface so that the model prediction can match the experimental data and include the change in the Poisson's ratio. However, only with $\mathbf{R}_{\mathrm{I}}$ and $\mathbf{R}_{\mathrm{II}}$ the model will predict the damage only occurs in the loading directions where $\tilde{\sigma}_1$ does not equal to zero. This does not match the experimental observation described in section 7.1 that the damage occurs also in the loading directions where $\tilde{\sigma}_1$ equals zero, except the hydrostatic loading. Therefore, $\mathbf{R}_{\mathrm{III}}$ is introduced to capture this phenomenon. α includes the effect of the lateral pressures into the stress strain relation. H(.) implies if $\tilde{\boldsymbol{\sigma}}$ is a null tensor, the lateral pressures have no effect to the compliance of the material and no damage occurs in the loading directions where $\tilde{\sigma}_1$ equals zero. h(.) ensures that the damage occurs also in the loading directions where $\tilde{\sigma}_1$ equals zero. **I** is the fourth order identity tensor, and **i** is the second order identity tensor. $\mathbf{S}^-$ and $\mathbf{S}^+$ are the negative cones and positive cones of the deviatory part of $\boldsymbol{\sigma}$. The symbol "$\otimes$" signifies the tensor product operation; β is determined from experimental data and greater than one so that inelastic volumetric deformation will be predicted.

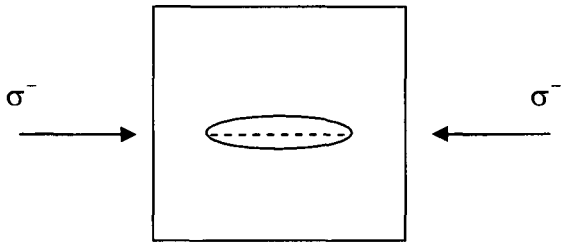

Figure 7.4. Schematic representation of crack opening under compression loading.

The damage function, t(k), is further represented as

$$t(k)=F_c q(k_s) \tag{7.17}$$

where F_c is a scalar parameter and related to the material strength f_c. $q(k_s)$ is the shape function of the damage function, t and used to capture the quasi-static damage, k_s, occurs in the first loading cycle. At limit state the function $q(k_s)=1$.

By substituting Equations (7.9), (7.10), and (7.17) into Equation (7.7), the potential function can be written as

$$\begin{aligned}\psi(\boldsymbol{\sigma},k) &= \frac{1}{2}\boldsymbol{\sigma}:\frac{\tilde{\boldsymbol{\sigma}}\otimes\tilde{\boldsymbol{\sigma}}}{\tilde{\boldsymbol{\sigma}}:\tilde{\boldsymbol{\sigma}}}:\boldsymbol{\sigma}+\left(\mathbf{S}^{-}+\beta\mathbf{S}^{+}\right):\boldsymbol{\sigma}+\frac{1}{2}\alpha H(\bar{\lambda})\boldsymbol{\sigma}:\boldsymbol{\sigma}-\frac{9}{2}\alpha H(\bar{\lambda})p^2 \\ &+\frac{1}{2}\gamma H(\bar{\lambda})\boldsymbol{\sigma}:\left[h(-\tilde{\sigma}_1)q_1\otimes q_1+h(-\tilde{\sigma}_2)q_2\otimes q_2+h(-\tilde{\sigma}_3)q_3\otimes q_3\right]:\boldsymbol{\sigma}-\frac{1}{2}\left[F_c q(k_s)\right]^2=0\end{aligned} \tag{7.18}$$

where p is the hydrostatic pressure.

To obtain the form of parameter F_c, one may consider a state at the limit surface and in loading direction "1" where Equation (7.18) is simplified to

$$\psi(\sigma,k)=\frac{1}{2}\left(1+\frac{4}{3}\beta\right)\sigma_1^{\,2}-\frac{1}{2}\left[F_c q(k_s)\right]^2=0 \tag{7.19}$$

At limit surface, the function $q(k_s)=1$, and $\sigma_1=f_c$. Thus, the result is

$$F_c = f_c\sqrt{1+\frac{4}{3}\beta} \tag{7.20}$$

As the number of loading cycles starts to increase, the strength of the material is affected and is reduced. The limit surface representing the foci of all strength points associated with n=1 is therefore affected and should be modeled to soften to failure surface. To achieve this, a new softening function F(n) is included into the damage function to predict lower limit strength of the material with increasing number of cycles. Therefore, the new damage function is

$$t(n, k)=F_cF(n)q(k_s) \tag{7.21}$$

Incorporating the new damage function into the general form of the potential function yields

$$\begin{aligned}\psi(\boldsymbol{\sigma}, k) &= \frac{1}{2}\boldsymbol{\sigma}:\frac{\tilde{\boldsymbol{\sigma}}\otimes\tilde{\boldsymbol{\sigma}}}{\tilde{\boldsymbol{\sigma}}:\tilde{\boldsymbol{\sigma}}}:\boldsymbol{\sigma}+\left(\mathbf{S}^{-}+\beta\mathbf{S}^{+}\right):\boldsymbol{\sigma}+\frac{1}{2}\alpha H(\bar{\lambda})\boldsymbol{\sigma}:\boldsymbol{\sigma}-\frac{9}{2}\alpha H(\bar{\lambda})p^2 \\ &+\frac{1}{2}\gamma H(\bar{\lambda})\boldsymbol{\sigma}:\left[h(-\tilde{\sigma}_1)q_1\otimes q_1+h(-\tilde{\sigma}_2)q_2\otimes q_2+h(-\tilde{\sigma}_3)q_3\otimes q_3\right]:\boldsymbol{\sigma}-\frac{1}{2}\left[F_cF(n)q(k_s)\right]^2=0\end{aligned} \tag{7.22}$$

With the examination in Chapter 6 and the experimental data from Yin and Hsu's work (1995) which are shown in Figures 7.5, 7.6, and 7.7, the softening function is proposed to be

$$F(n)=n^A \tag{7.23}$$

where n is the number of cyclic loading, and A is a material constant.

This is regarded as one of the simplest form one could use. The simplicity of the form proposed by Equation (7.23) is appealing and will be retained in the sequel.

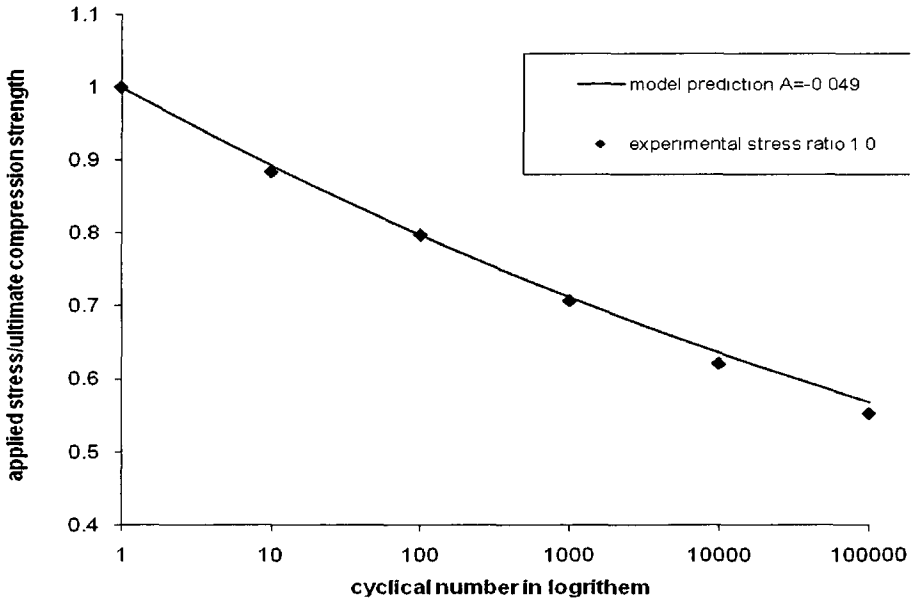

Figure 7.5. Comparison between softening function and experimental data (Yin and Hsu, 1995) with stress ratio 1:0.

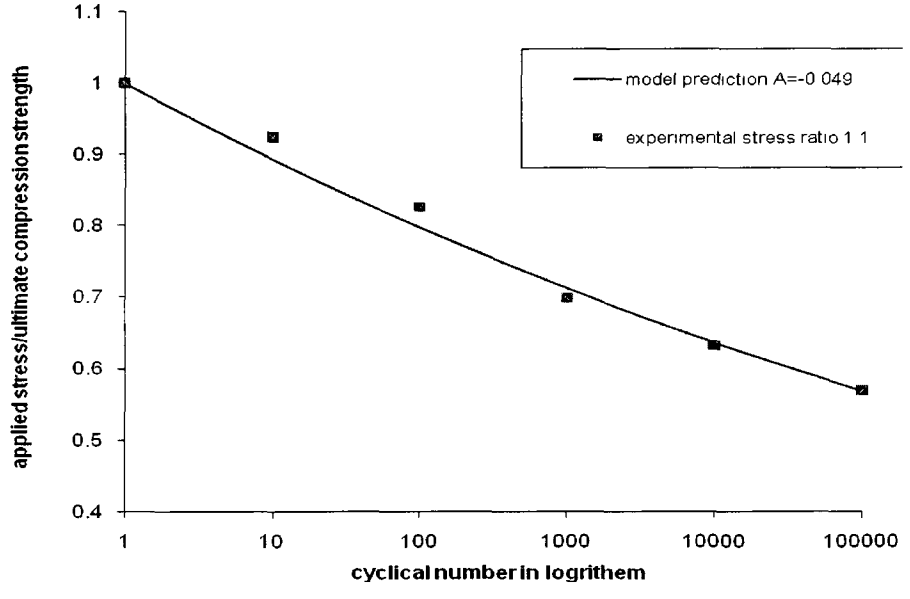

Figure 7.6. Comparison between softening function and experimental data (Yin and Hsu, 1995) with stress ratio 1:1.

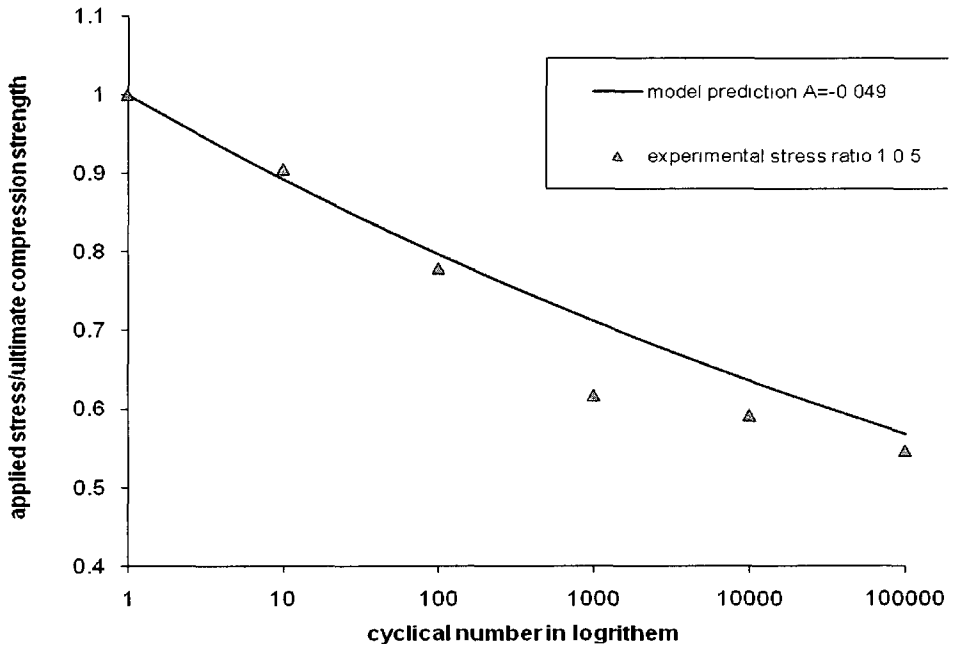

Figure 7.7. Comparison between softening function and experimental data (Yin and Hsu, 1995) with stress ratio 1:0.5.

To determine the value of "A", one may rewrite the potential function at a limit state when the fatigue life $n=n_l\neq 1$ and $q(k_s)=1$ and under uniaxial fatigue loading

$$\left(1+\frac{4}{3}\beta\right)\sigma_1^{\,2}=[F_c F(n)]^2 \tag{7.24}$$

With Equation (7.20) and (7.23), the value of "A" can be obtained as

$$A=\ln\left(\frac{\sigma_1}{f_c}\right)\Big/\ln(n) \tag{7.25}$$

The form of $q(k_s)$ can be established with the suggestion of Yazdani and Schreyer (1988). The static damage, k_s, can be interpreted as the added flexibility under uniaxial loading as follows

$$\sigma_1 = \frac{\varepsilon_1}{(1/E_0)+k_s} \tag{7.26}$$

where σ_1 is the uniaxial stress, and ε_1 is the corresponding strain. E_0 is the initial value of Young's modulus. Therefore, the form of $q(k_s)$ can be proposed as

$$q(k_s) = \frac{\sigma_1}{f_1} = \frac{\varepsilon_1/f_1}{(1/E_0)+k_s} \tag{7.27}$$

where f_1 is the compression strength of the concrete.

The particular form of the stress strain relation is proposed as

$$\sigma_1 = f_1 \frac{\varepsilon_1}{\varepsilon_u} \exp\left(1-\frac{\varepsilon_1}{\varepsilon_u}\right) \tag{7.28}$$

where ε_u is the strain corresponding to f_1.

Finally, the rate of the damage parameter, k, must be obtained from the constitutive relations used and the strength degradation forms proposed due to fatigue cycles (Equation 7.23). For the simple constitutive relation of the form shown as $\boldsymbol{\varepsilon}=\mathbf{C}(k):\boldsymbol{\sigma}+\boldsymbol{\varepsilon}^i$, the rate of damage parameter, dk/dn, can be shown to be

$$\frac{dk}{dn} = \frac{1}{E_1(1+2\beta/3)}(-A)(n^{-A-1}) \tag{7.29}$$

where E_1 is the material Young's modulus after the first cycle.

7.3. Numerical Simulation

In this section, the predictions of the proposed model are compared with the experimental work of Yin and Hsu, 1995. Yin and Hsu used a specially designed biaxial test machine. The load was supplied by a 220-kip-capacity hydraulic actuator and then resolved into a pair of forces by a load bifurcation mechanism. The specimens are 6X6X1.5 inch steel fiber reinforced concrete plates. The fiber size is 0.01X0.022X1 inch. The volume percentage of steel fiber is 1 percent. Four principal compressive stress ratios were included, 1:0, 5:1, 2:1, and 1:1. The loading rate is 1 cycle per second.

Four material parameters, A, α, β, and γ are used in the model. The first three parameters can be determined with the similar methods introduced in Chapter 6. The parameter γ can be determined with one uniaxial fatigue test. Measuring the ratio between the damage accumulated in the loading direction and one other direction, one can determine the value of parameter γ.

As shown on Figure 7.8, with experimental data of monotonic loading, the values of parameters α and β of the response tensors are determined as 0.7 and 0.01, respectively. With the experimental data shown in Figures 7.5, 7.6, and 7.7, the value of the parameter A is determined as -0.049. With the value, the residual strength surface after 10^4 cyclic loading is predicted by the model and compared with the experimental data (Yin and Hsu, 1995) in the same figure. Here, the "PCS" is the uniaxial ultimate compression strength of plain concrete. The comparison shows that the surface form of the model matches the experimental data well.

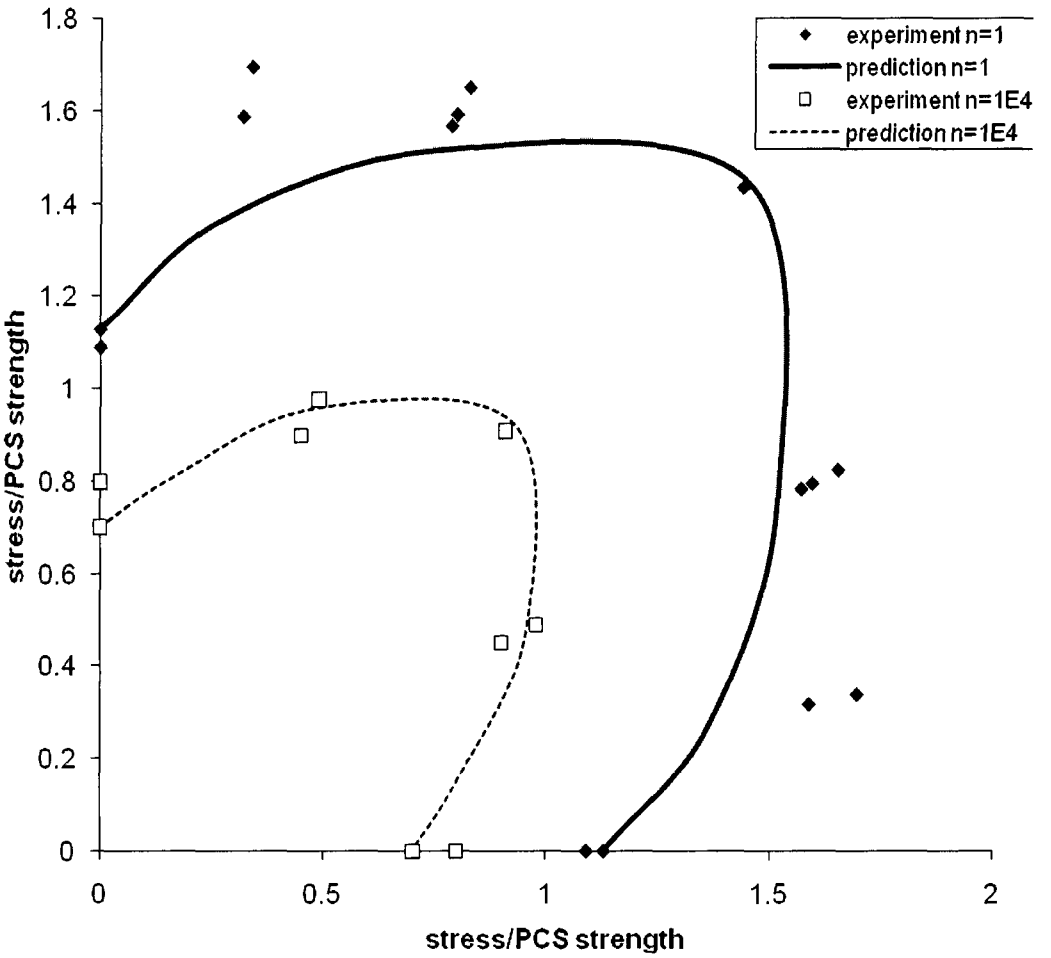

Figure 7.8. Comparison of strength surfaces between experimental data (Yin and Hsu, 1995) and theory predictions of 10^4 loading cycles and monotonic loading.

Lastly, the stress-strain relations of stress ratio 1:0, 1:1, and 1:0.5 are shown on Figure 7.9, 7.10, and 7.11 respectively where the strength and ductility reductions due to the effect of fatigue loading are shown.

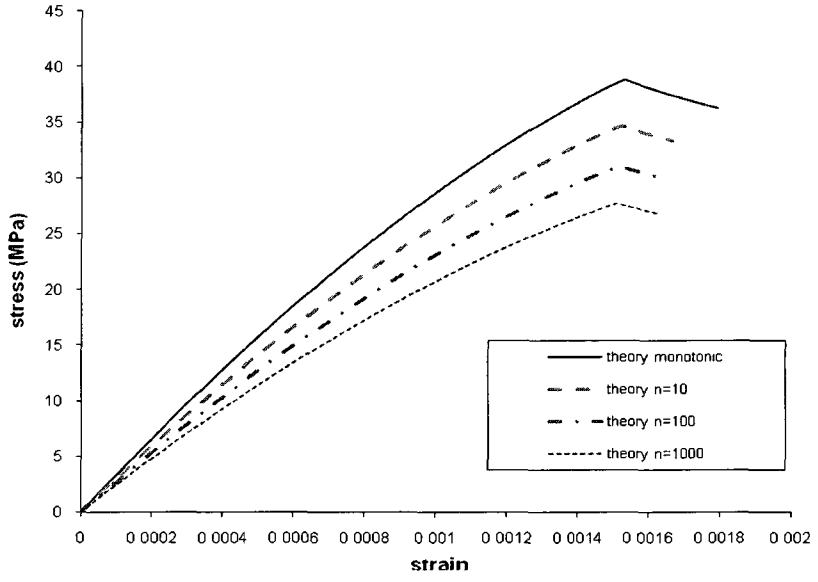

Figure 7.9. Predictions of the stress strain relationship of uniaxial monotonic failure loading and uniaxial fatigue loadings.

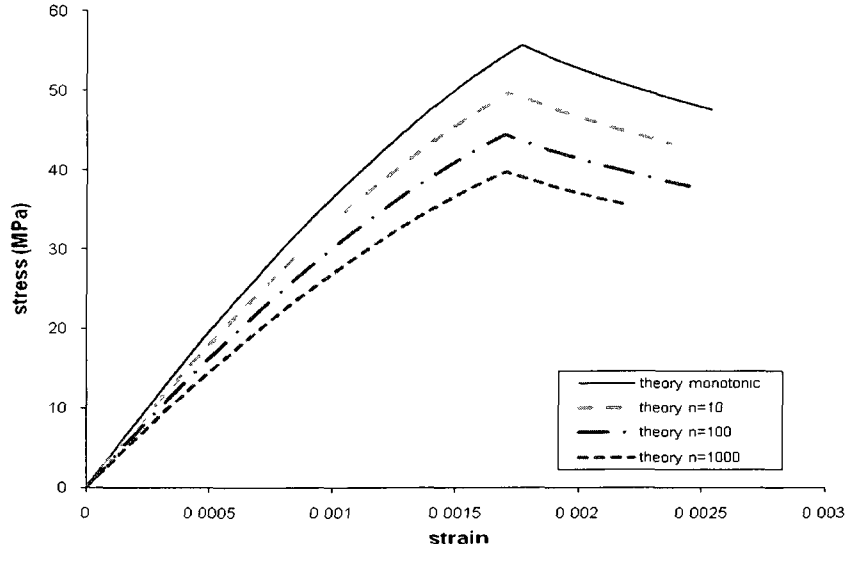

Figure 7.10. Predictions of the stress strain relationship of monotonic failure loading and fatigue loadings with stress ratio 1:0.5.

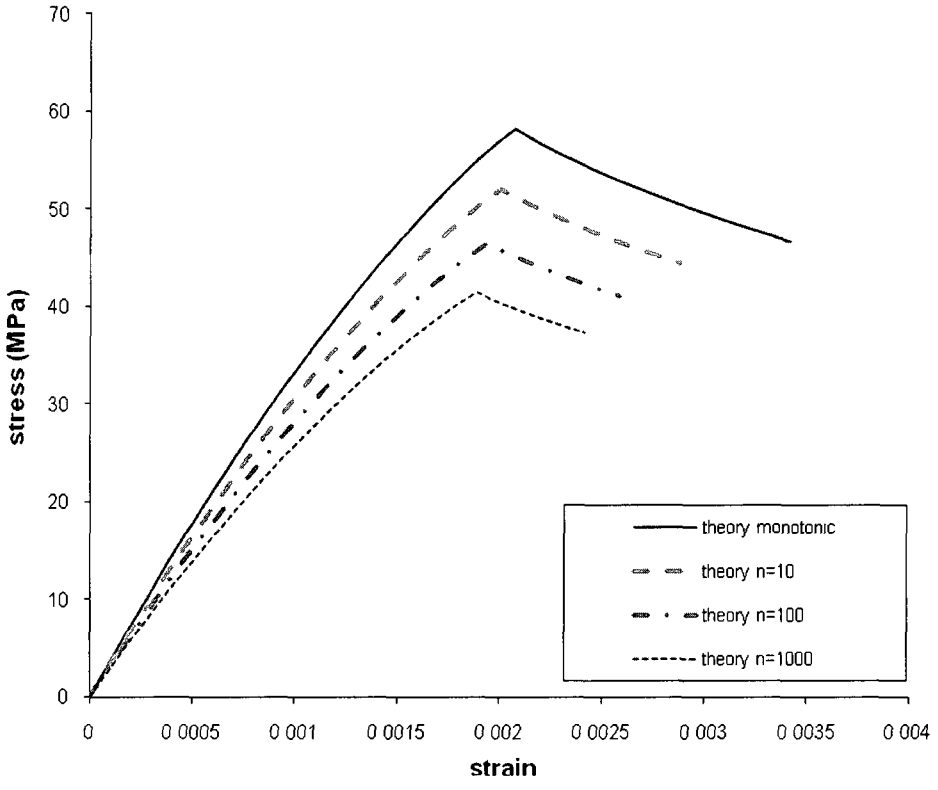

Figure 7.11. Predictions of the stress strain relationship of monotonic failure loading and fatigue loadings with stress ratio 1:1.

The effects of parameters A, α, and β on the model are shown in the following figures. The effects of parameters α and β on the limit surface, Equation 7.18, are shown in Figures 7.12 and 7.13. The effects of parameter A on the softening function, Equation 7.23, are shown in Figures 7.14, 7.15, and 7.16 for stress ratios of 1:0, 1:1, and 1:0.5, respectively. From these figures, it can be observed that the predicted results stably change with the changes of the parameters.

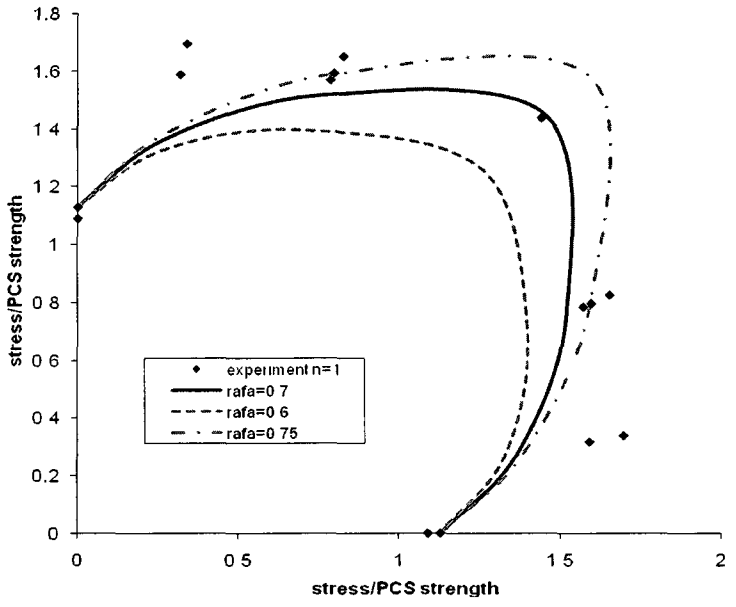

Figure 7.12. Comparison between the experimental data of limit surface and predicted limit surfaces for different values of α and constant value of β equal to 0.01.

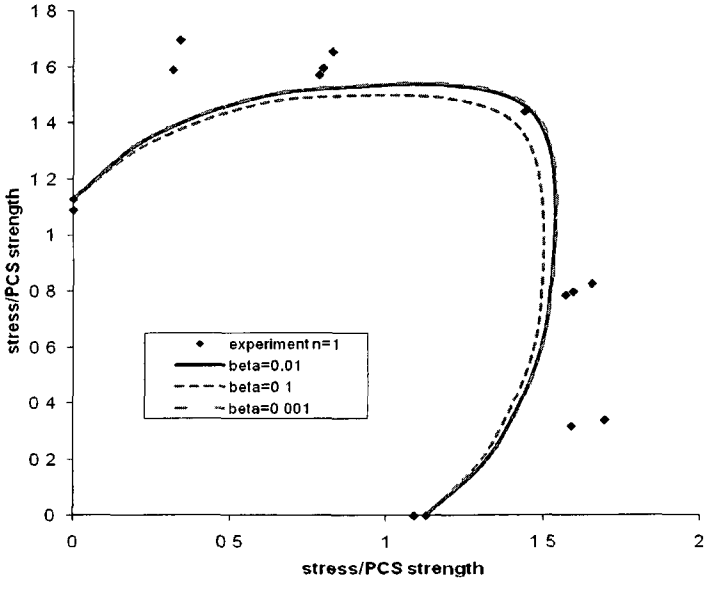

Figure 7.13. Comparison between the experimental data of limit surface and predicted limit surfaces for different values of β and constant value of α equal to 0.7.

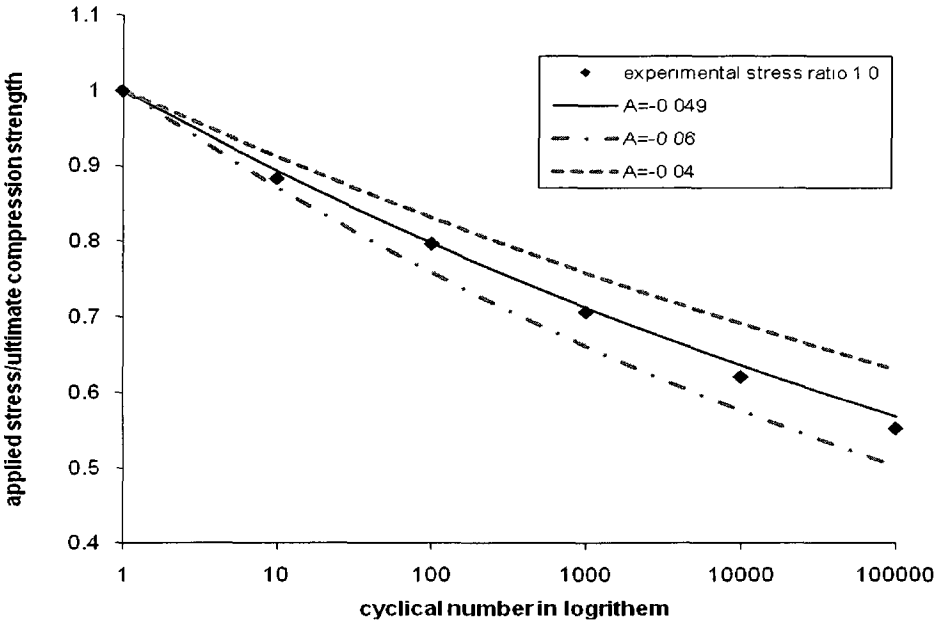

Figure 7.14. Comparison between the experimental data of softening function and predicted results for different values of A for stress ratio 1:0.

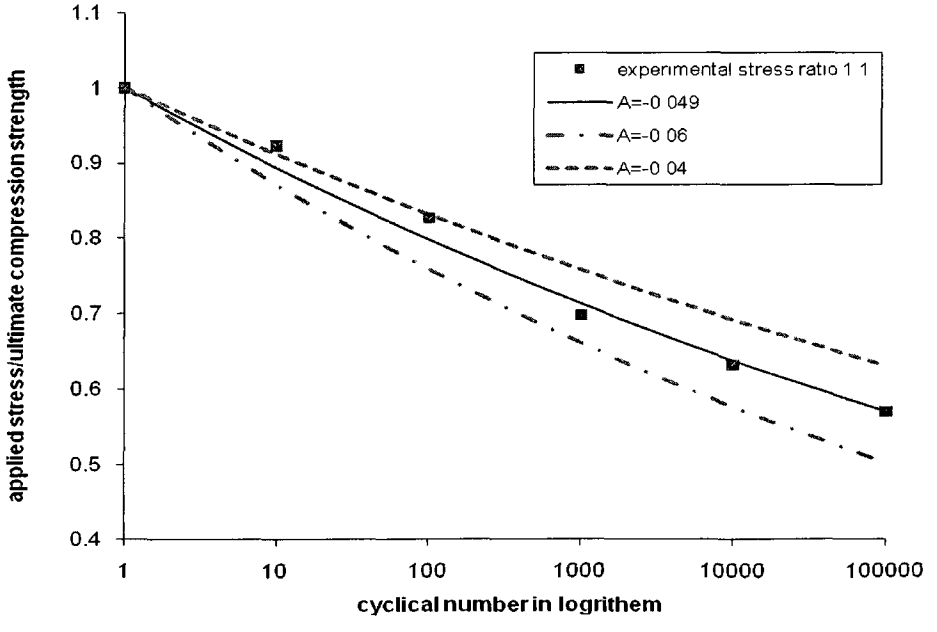

Figure 7.15. Comparison between the experimental data of softening function and predicted results for different values of A for stress ratio 1:1.

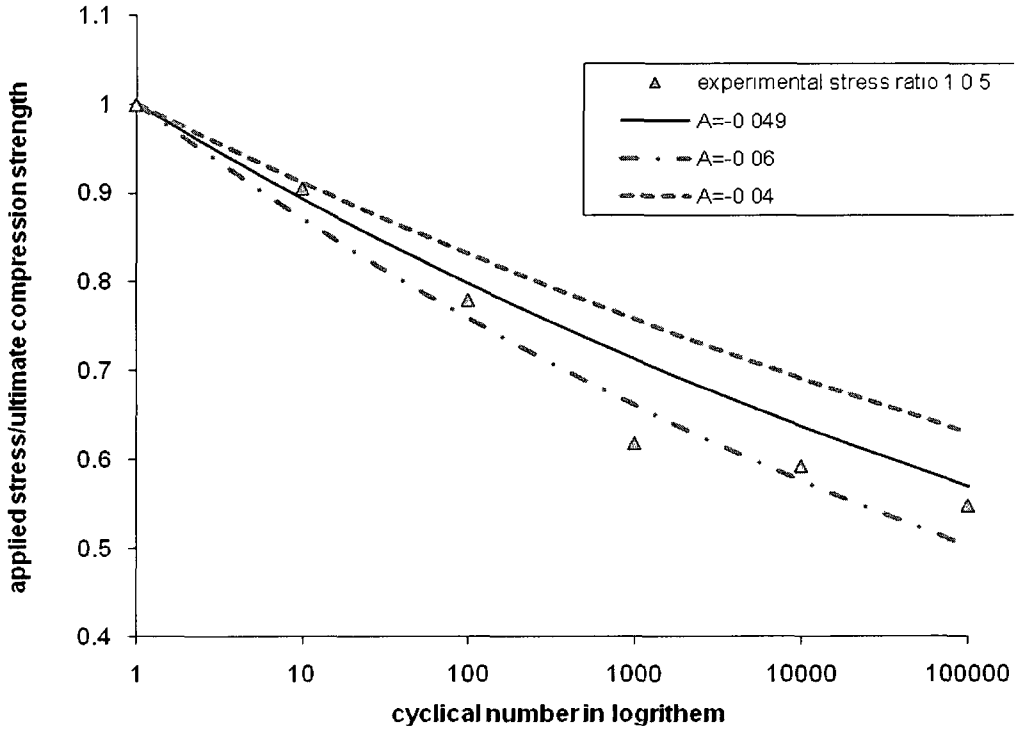

Figure 7.16. Comparison between the experimental data of softening function and predicted results for different values of A for stress ratio 1:0.5.

7.4. Conclusion

A damage model is established to predict the fatigue behaviors of steel fiber reinforced concrete under low frequency fatigue loading. A class of damage mechanics is applied, because cracking is the main type of damage and dominates most of the fatigue life. The relationship between various fatigue loading paths has been established through the surface theory. The static damage and fatigue damage are both captured. The high directionalities of elastic damage and permanent deformation are described through response tensors. By comparison with

experimental data, the model shows good capability to describe the essential properties of woven composite materials under fatigue loading.

8. CONCLUSIONS AND FUTURE WORK

8.1. Conclusions

Material fatigue is one major reason for failure of engineering materials. For better understanding of material behaviors under fatigue loadings, many fatigue tests have been performed, and many fatigue models have been proposed to direct the engineering design. However, these tests and models were mainly for uniaxial fatigue loadings. Only a few multi-axial fatigue tests have been conducted and models have been developed.

To model multi-axial fatigue, the approach taken in this thesis was to base the foundation on the first principle of mechanics and thermodynamics. The theories of thermodynamics provide a solid theoretical framework for the modeling and guide the selections of variables used in the approach. Continuum damage mechanics was also utilized because it is suitable for describing the behaviors of materials when the crack size is smaller than the size of the volume element of a specific material, and it remains distributed for a significant range of load history. For brittle or quasi-brittle materials, the main part of the fatigue life occurs in the first and second stages of the fatigue process as evidenced by experimental work cited in the body of this thesis.

In the first attempt, Hansen's model (1999) on woven fabric composites was improved by using the internal variable theory of thermodynamics. The following contributions were obtained. First, the damage anisotropy was captured through properly postulated fourth-order and second-order response tensors. Second, the

"knee effect" that shows the character of the longitudinal stiffness degradation was predicted with the application of a stress invariant instead of the strain invariant. Lastly, the permanent deformation was modeled.

The above approach involved some postulates that were not general enough for multi-axial modeling. The main contribution was then brought in by proposing an evolution of a bounding surface potential. With this approach a general formulation was developed to predict the behaviors of brittle or quasi-brittle materials under proportional multi-axial fatigue loadings. This approach was then applied to woven fabric composites and steel fiber reinforced concretes to capture the material characteristics under proportional multi-axial tensile and compression fatigue loadings, respectively.

The incorporation of the bounding surface theory enabled the present approach to predict the fatigue life and the material behaviors under complex proportional multi-axial fatigue loading conditions. The form of the limit surface was determined by postulating response tensors **R** and **M** with the associated strength parameters determined from experimental data for ultimate strengths of those materials under uniaxial and biaxial monotonic loadings. The positions of the residual strength surfaces were then obtained by using a softening function that described the decrease of the ultimate tensile strength of woven fabric composites and the ultimate compression strength of fiber reinforced concretes. The specific forms of the softening function were obtained with reference to classic S-N curves. When the

residual strength surface contacted the loading point in the loading condition, the fatigue life of the material was determined.

To capture induced damage and inelastic deformation, two damage flow rules were proposed. In postulating tensor **R**, the micro-mechanics of crack growth was considered. In the woven fabric composite the strength enhances under biaxial loadings, and damage only occurs in the loading directions. In the steel fiber reinforced concrete the strength enhances under biaxial loadings, no damage occurs under the hydrostatic loading, and the damage occurs not only in the loading directions, but in the non-loading directions as well.

The model was shown also to predict the "knee effect" showing the compliance increase or stiffness decrease. This was achieved by obtaining damage evolutionary relation from the constitutive relation and the softening function. Another significant contribution presented in this work is the ability to address the "strength anisotropy" that is present in some materials such as composites.

The presented approach, however, has some limitations. First, only small strain was considered. Second, the thermal effects occurring during the fatigue loadings should be negligible, which is usually the case for low frequency fatigue. Also, only proportional loading paths were used in the formulation. Although this is restrictive, yet it encompasses a great majority of loading cases. The first limitation is valid for the first two stages of the fatigue process. Since most part of the fatigue life of brittle or quasi-brittle materials occurs in the first two stages, the predictions of the approach are precise enough for engineering design and analysis. The second

limitation can be verified with different ways, such as monitoring the surface temperature of the specimen during fatigue loadings, or limiting the loading frequency.

In this thesis, the endurance limit is not considered as explained below. The endurance limit exists for some engineering materials because below that limit, damage is shown not to occur, or if damage occurs and propagates, it will effectively be stopped by some arresting mechanism. However, many recent researches (Donald and Pradeep, 2003; Ramakrishnan, Malhotra and Langley, 2005) suggested that the endurance limit does not actually exist for quasi-brittle solids such as concrete and woven fabric composite. If enough stress cycles are performed, materials will eventually fail even for very small stresses. On the other hand, many other factors may cause the material to fail below the endurance limit, such as corrosion and occasional overloads (Donald and Pradeep, 2003), so one should be cautious in considering the endurance limit in the engineering design. Therefore, the predictions of the proposed approach were conservative without the consideration of the endurance limit.

Finally, the approach predictions were compared with experimental data from literatures. Good correlation between the predictions and experimental data showed that the approach was able to capture the behaviors of brittle or quasi-brittle materials under proportional multi-axial fatigue loadings.

8.2. Recommendation for future work

Although the models developed in this dissertation have several advantages over previous models, there are still several aspects that can be improved. First, an assumption that the frequency of the fatigue loading is low was given in the theory, so that the thermal effect can be ignored. Although this assumption is valid for many engineering conditions, there are still some conditions of high frequency fatigue loadings where the thermal effect cannot be ignored. Therefore, extending the models into the high frequency fatigue loading would greatly improve the capability of the model. Second, the current models only considered the damage. However, many engineering materials also show plasticity under fatigue loadings. Developing the models to capture the behaviors of ductile materials would increase the applicability of the models.

REFERENCES

Al-Gadhib, A. H., Baluch, M. H., Shaalan, A. and Khan, A. R. (2000) Damage model for monotonic and fatigue response of high strength concrete. *International Journal of Damage Mechanics*, 9: 57-78.

Cachim, P. B. et al. (2002) Fatigue behavior of fiber-reinforced concrete in compression. *Cement and Concrete Composites*, Vol. 24, Issue 2, p. 211-217.

Caprino, G. and Giorleo, G. (1999) Fatigue Lifetime of Glass Fabric/Epoxy Composites. *Composites Part A*; 299-304.

Chang, D. I. et al. (1998) An experimental study on the fatigue strength of steel fiber reinforced concrete beams with initial cracks. *Struct. Eng. Cons.: Tradition, Present and Future*, Vol. 3, p. 1737-1742.

Degrieck, J. and Van Paepegem, W. (2001) Fatigue damage modeling of fiber-reinforced composite materials: Review. *Applied Mechanics Review (USA)* 54: 279-300.

Donald, R. A. and Pradeep, P. P. (2003) The Science and Engineering of Materials (4th ed.).

Fardis, M. N. and Chen, E. S. (1986) A cyclic multiaxial model for concrete. *Computational Mechanics*, 1: 301-315.

Fardis, M. N., Alibe, B., and Tassoulas, J. L. (1983) Monotonic and cyclic constitutive law for concrete. *Journal of Engineering Mechanics*, 109: 516-536.

Gan, L. (2005) Experimental Study of the Compression Fatigue Behaviors of the Steel Fiber Reinforced Concrete under Low Temperature, Master Thesis, Anhui University of Science and Technology, China.

Gude, M. et al (2010) Damage evolution of novel 3D textile-reinforced composites under fatigue loading conditions. *Composites Science and Technology*; 70: 186-192.

Hansen, U. (1999) Damage Development in Woven Fabric Composites during Tension-Tension Fatigue. *Journal of Composite Materials* 33: 614-639.

Henaff-Gardin, C. and Lafarie-Frenot, M. C. (2002) The use of a characteristic damage variable in the study of transverse cracking development under fatigue loading in cross ply laminates. *International Journal of Fatigue* 24: 389-395.

Hou, J. et al. (2006) Experimental Study on the Fatigue Elastic Modulus of Steel Fiber Reinforced Prestressed Concrete Slabs, *China Civil Eng. J.*, Vol. 39, p.22-25.

Karnawat, S. and Yazdani, S. (2001) Effects of preloading on brittle solids. *J. Eng. Mech.* Vol. 127, no. 1, p. 11-17

Krajcinovic, D. (1985) Continuous damage Mechanics revisited: basic concepts and definitions. *Journal of Applied Mechanics*; 52:829-834.

Lee, M. K. and Barr, B. I. G. (2004) An overview of the fatigue behaviour of plain and fibre reinforced concrete. *Cement and Concrete Composites*, Vol. 26, Issue 4, p. 299-305.

Lemaitre, J. L. and Chaboche, J. L. (1990) Mechanics of solid materials. *Cambridge University Press.*

Mao, H. and Mahadevan, S. (2002) Fatigue damage modeling of composite materials. *Composite Structures*; 58:405–410.

Natarajan, V., Gangarao, H., and Shekar, V. (2004) Fatigue response of fabric-reinforced polymeric composites. *Journal of Composite Materials* 39: 1541-1559.

Ochi, T. et al. (2005) Characteristics and Development Process of Steel-Fiber Reinforced Concrete, *Journal of the Mining and Materials Processing Institute of Japan*, Vol. 121, no. 12, p. 555-563.

Ortiz, M. (1985) A constitutive theory for the inelastic behavior of concrete. *Mechanics of Materials*; 4(1): 67-93.

Ortiz, M. and Giannakopoulos, A. E. (1990 a) Crack Propagation in Monolithic Ceramics Under Mixed Mode Loading. *International Journal of Fracture*, Vol. 44, no. 4, p. 233-258.

Ortiz, M. and Giannakopoulos, A. E. (1990 b) Mixed mode crack-tip fields in monolithic ceramics. *Int. J. Solids Struct.* 26(7). P.705-723.

Ortiz, M. and Popov, E. P. (1982) Plain concrete as a composite material. *Mechanics of Materials*; 1(2): 139-150.

Pandolfi, A. and Taliercio, A. (1998) Bounding surface models applied to fatigue of plain concrete. *Journal of Engineering Mechanics*, 124: 556-564.

Ramakrishnan, V., Malhotra, V. M., and Langley, W. S. (2005) Comparative Evaluation of Flexural Fatigue Behavior of High-Volume Fly Ash and Plain Concrete. *International concrete research & information portal.* 351-368.

Samborsky, D. D., Agastra, P., and Mandell, J. F. (2008) Effects of Glass Fabric and Laminate Construction on the Fatigue of Resin Infused Blade Materials. *Wind Energy Symposium*, January 2008, Reno, Nevada

Simo, J. C. and Ju, J. W. (1987) Strain and stress based continuum damage models I. formulation. *Int. J. Solids Structures*; 23: 821-840.

Simo, J. C. and Ju, J. W. (1987) Strain and stress based continuum damage models II. Computational aspects. *Int. J. Solids Structures*; 23: 841-869.

Singh, S. P. and Kaushik, S. K. (2000) Probabilistic analysis of fatigue-life of steel fiber reinforced concrete. *Journal of Ferrocement*, Vol. 30, no. 3, p. 237-247, July.

Smith, E. W. and Pascoe, K. J. (1989) Biaxial Fatigue of a Glass-Fiber Reinforced Composite. I. Fatigue and Fracture Behavior. *Mechanical Engineering Publications, Biaxial and Multiaxial Fatigue*; 367-396.

Su, C. M. and Hsu, T. C. (1988) Biaxial Compression Fatigue and Discontinuity of Concrete. *ACI Mater. J.*, May-June, p. 178-188.

Suaris, W., Ouyang, C., and Fernando, V. M. (1990) Damage model for cyclic loading of concrete. *Journal of Engineering Mechanics*, 116: 1020-1035.

Van Paepegem, W. and Degrieck, (2001) J. Fatigue degradation modeling of plain woven glass/epoxy composites. *Composites Part A*; 32:1433-1441.

Van Paepegem, W. and Degrieck, (2002) J. Coupled residual stiffness and strength model for fatigue of fibre-reinforced composite materials. *Composite Science and Technology*; 62:687-696.

Van Paepegem, W. and Degrieck, (2003) J. Modeling damage and permanent strain in fiber-reinforced composites under in-plane fatigue. *Composites Science and Tech*; 63:677-694.

Voyiadjis, G. Z. et al. (2009) Theoretical Formulation of a Coupled Elastica Plastic Anisotropic Damage Model for Concrete using the Strain Energy Equivalence Concept. *International Journal of Damage Mechanics*; 18: 603-638.

Xie, J. B. et al. (2004) Investigation Flexural Fatigue Behavior of Steel Fiber Reinforced Concrete for Pavement Surface Stratum under Cyclic Load, *J. Lanzhou Univ. Tech.*, Vol. 30, p. 104-109.

Yang, B., Dafalias, Y. F., and Herrmann, L. R. (1985) A bounding surface plasticity model for concrete. *Journal of Engineering Mechanics*, 111:359-380.

Yazdani, S. (1993) On a class of continuum damage mechanics theories. *Int. J. Damage Mech.* Vol. 2. p. 162-176.

Yazdani, S. and Karnawat, S. (1996) A Constitutive Theory for Brittle Solids with Application to Concrete. *Inter. J. Damage Mechanics*, Vol. 5, p. 93-110.

Yazdani, S. and Schreyer, H. L. (1988) An anisotropic damage model with dilatation for concrete. *Mechanics of Materials*, Vol. 7, No. 3, p. 231-244.

Yin, W. S. and Hsu, T. C. (1995) Fatigue Behavior of Steel Fiber Reinforced Concrete in Uniaxial and Biaxial Compression. *ACI Mater. J.*, Vol. 92, No.1, p. 71-81.

Yoshioka, K. and Seferis, J. C. (2002) Modeling of tensile fatigue damage in resin transfer molded woven carbon fabric composites. *Composites: Part A*; 33: 1593-1601.

Zhang, J., Stang, H., and Li, V. C. (1999) Fatigue life prediction of fiber reinforced concrete under flexural load. *International Journal of Fatigue,* 21: 1033-1049.

APPENDIX A

Three FORTRAN programs were developed to evaluate the model of Chapter 5 and repeat the results of Hansen's work, respectively. Figures 5.3, 5.4, 5.5, and 5.6 show the results of the programs. The programs are listed as follows.

1. Hansen's work:

```
!       ------------------- commons block -----------------------
      common /stress/ stress,delse
      common /strain/ strain,straine,staref,delsa
      common /modulous/ ee0,ee1,eeout(1000)
      common /poisonratio/ vu0,vu
      common /constant/ aa,nn
      common /calculation/ numb(1000)
      real kk
!
      open(unit=4,file='input.dat',status='old')
      open(unit=3,file='output.dat',status='old')
      open(unit=5,file='stress.dat',status='old')
!
!       ------------------------------------------------------------
!     write(3,*) 'kkk'
      read(4,*) numberc,nmax
      read(4,*) ee0,vu0
      read(4,*) staref,stressapp
      read(4,*) delsa
      read(4,*) aa,nn
      read(4,*) kk
!      write(3,*)numberc,nmax,ee0,vu0,staref,stressapp,delsa,aa,nn,kk
     ee1=ee0
       vu=vu0
!       write(3,*)ee1,vu
       straine=0
       ii=0
       mm=0
      write(3,*) '0',ee0
     do 10 i=1, numberc
       strain=0
       delse=0
```

```
      stress=0
      do 100 j=1, nmax
!     write(3,*)ee1,delsa,aa,ee0,ee1,straine,staref,nn,stress
     delse=(ee1)*(delsa-aa*(ee0/ee1**2)*(straine/staref)**nn*stress)
         stress=stress+delse
         strain=strain+delsa
     if (stress+0.2.gt.stressapp) goto 500
100   continue
500   continue
!     write(3,*)stress,j
!     pause
     straine=strain
      delkk=aa*(straine/staref)**nn
      kk=kk+delkk
      if (kk.ge.0.2) goto 2000
      ee1=ee0*(1-kk)
      vu=vu0*(1-kk)
      mm=mm+1
     if (mm.eq.10000) then
      ii=ii+1
      mm=0
      write(3,*)i,ee1
      write(5,*)stress
      write(*,*)ii
!      numb(ii)=i
!      eeout(ii)=ee1
     else
      continue
     end if
10    continue
2000  continue
!     do 3000 i=1,ii
!      write(3,*) numb(i),eeout(i)
!3000  continue
     end
```

2. My model (inelastic):

```
!       ---------- commons block ----------
     common /stress/ stress,delse
     common /strain/ strain,straine,staref,delsa
     common /modulous/ ee0,ee1,eeout(1000)
     common /poisonratio/ vu0,vu
```

```
      common /constant/ aa,nn
      common /calculation/ numb(1000)
      real kk,nn,mm,istrain,kkk
!
      open(unit=4,file='input.dat',status='old')
      open(unit=3,file='output.dat',status='old')
      open(unit=5,file='stress.dat',status='old')
      open(unit=7,file='lingshi.dat',status='old')
!
!       ------------------------------------------------------------
!     write(3,*) 'kkk'
      read(4,*) numberc,nmax
      read(4,*) ee0,vu0
      read(4,*) staref,stressapp,strength
      read(4,*) delsa
      read(4,*) aa,nn,dd,cc,raf
      read(4,*) kk
!      write(3,*)numberc,nmax,ee0,vu0,staref,stressapp,delsa,aa,nn,kk
     ee1=ee0
       vu=vu0
!       write(3,*)ee1,vu
       straine=0
       istrain=0
       ii=0
       mm=0
      write(3,*) '0',ee0
      write(5,*)'0',' ','0'
     do 10 i=1, numberc
       strain=0
       delse=0
       stress=0
       do 100 j=1, nmax
!     write(3,*)ee1,delsa,aa,ee0,ee1,straine,staref,nn,stress
     delse=(ee1)*(delsa-aa*(stressapp/strength)
    #  **nn*i**dd*stress-raf*aa*(stressapp/strength)**nn*i**cc)
          stress=stress+delse
          strain=strain+delsa
     if (stress+0.002.gt.stressapp) goto 500
100    continue
500    continue
!      write(3,*)stress,j
!      pause
      istrain=istrain+raf*aa*(stressapp/strength)**nn*i**cc
      strainm=strain+istrain
```

```
!      straine=(strain**2+(strain*vu)**2)**0.5
       delkk=aa*(stressapp/strength)**nn*i**dd
       kk=kk+delkk
       ee1=1/(1/ee0+kk)
       kkk=(ee0-ee1)/ee0
!       write(*,*)kk
       if (kkk.ge.0.4) goto 2000
!       vu=vu0*(1-kk)
       mm=mm+1
      if (mm.eq.1000) then
       ii=ii+1
       mm=0
       write(3,*)i,ee1
       write(5,*)strainm,stress
       write(5,*)istrain,' ','0'
       write(7,*)istrain
       write(*,*)ii
!       numb(ii)=i
!       eeout(ii)=ee1
      else
       continue
      end if
10     continue
2000   continue
!      do 3000 i=1,ii
!       write(3,*) numb(i),eeout(i)
!3000   continue
      end
```

3. My model (elastic):

```
!       ---------- commons block -----------
      common /stress/ stress,delse
      common /strain/ strain,straine,staref,delsa
      common /modulous/ ee0,ee1,eeout(1000)
      common /poisonratio/ vu0,vu
      common /constant/ aa,nn
      common /calculation/ numb(1000)
      real kk,nn,mm,kkk
!
      open(unit=4,file='input.dat',status='old')
      open(unit=3,file='output.dat',status='old')
      open(unit=5,file='stress.dat',status='old')
```

```
      open(unit=7,file='lingshi.dat',status='old')
!
!       ------------------------------------------------------------
!     write(3,*) 'kkk'
      read(4,*) numberc,nmax
      read(4,*) ee0,vu0
      read(4,*) staref,stressapp,strength
      read(4,*) delsa
      read(4,*) aa,nn,dd
      read(4,*) kk
!      write(3,*)numberc,nmax,ee0,vu0,staref,stressapp,delsa,aa,nn,kk
     ee1=ee0
       vu=vu0
!       write(3,*)ee1,vu
        kk=0
       straine=0
       ii=0
       mm=0
      write(3,*) '0',ee0
     do 10 i=1, numberc
       bb=i*1.0+1
       strain=0
       delse=0
       stress=0
       do 100 j=1, nmax
!     write(3,*)ee1,delsa,aa,ee0,ee1,straine,staref,nn,stress
     delse=(ee1)*(delsa-aa*
    #  (stressapp/strength)**nn*i**dd*stress)
          stress=stress+delse
          strain=strain+delsa
      if (stress+0.002.gt.stressapp) goto 500
100    continue
500    continue
!      write(3,*)stress,j
!      pause
!      straine=(strain**2+(strain*vu)**2)**0.5
       delkk=aa*(stressapp/strength)**nn*i**dd
       kk=kk+delkk
       ee1=1/(1/ee0+kk)
       kkk=(ee0-ee1)/ee0
!       write(*,*)kkk
       if (kkk.ge.0.17) goto 2000
!       vu=vu0-1/kk
       mm=mm+1
```

```
      if (mm.eq.1000) then
       ii=ii+1
       mm=0
       write(3,*)i,ee1
       write(5,*)'0',' ','0'
       write(5,*)strain,stress
       write(7,*)kk
       write(*,*)ii,ee1
!       numb(ii)=i
!       eeout(ii)=ee1
      else
       continue
      end if
10    continue
2000  continue
!     do 3000 i=1,ii
!       write(3,*) numb(i),eeout(i)
!3000  continue
      end
```

APPENDIX B

Several EXCEL sheets were developed to evaluate the model of Chapter 6 and are shown below.

1. EXCEL sheet for Figure 6.5

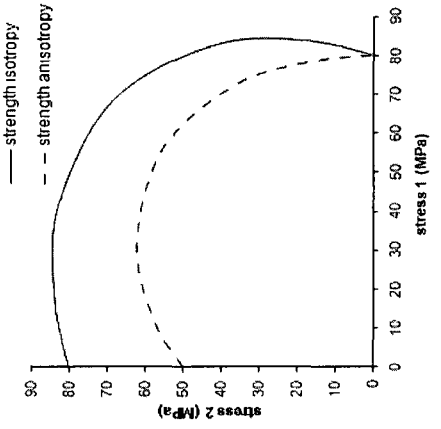

Isotropic					Anisotropic				
			stress					stress	
	stress ratio	rafa	x	y		stress ratio	rafa	x	y
80	0 01	0 24	-49 32	49 32	50	0 01	0 24	-30 82	30 82
	1 05		-31 97	63 93	80	1 05		-19 98	39 96
	1 02		-14 82	74 08		1 02		-9 26	46 30
	1 01		0 00	80 00		1 01		0 00	50 00
			16 74	83 69				11 51	57 54
			41 38	82 77				31 04	62 08
			68 39	68 39				55 57	55 57
			82 77	41 38				72 42	36 21
			83 69	16 74				78 46	15 69
			80 00	0 00				80 00	0 00
			74 08	-14 82				46 30	-9 26
			63 93	-31 97				39 96	-19 98
			49 32	-49 32				30 82	-30 82

2. EXCEL sheet for Figure 6.6

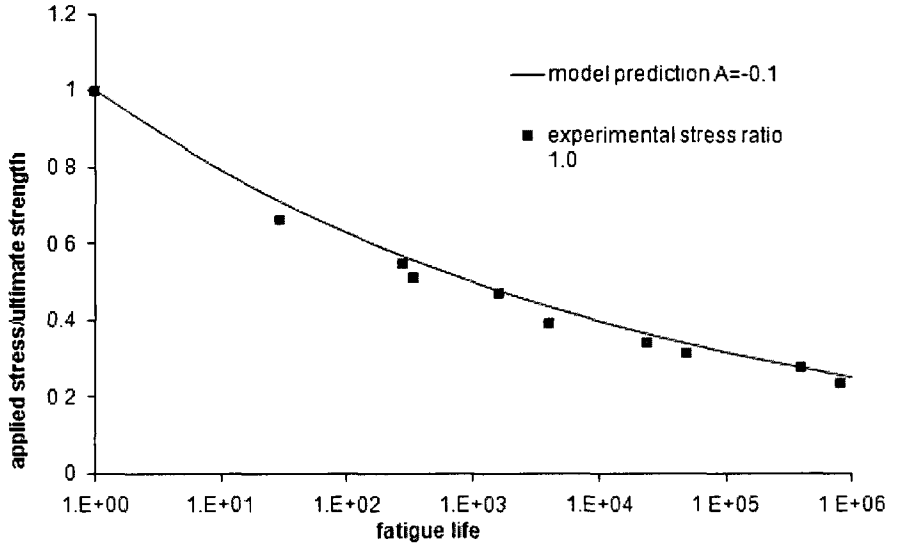

S-N	0			-0.1	
	n	Mpa		n	t=A*n^B
	1	257	1	1	1
	29	171	0.6654	10	0.7943
	280	141	0.5486	100	0.631
	330	131	0.5097	1000	0.5012
	1600	121	0.4708	10000	0.3981
	4000	101	0.393	100000	0.3162
	24000	88	0.3424	1000000	0.2512
	48000	81	0.3152		
	390000	71	0.2763		
	800000	61	0.2374		

3. EXCEL sheet for Figure 6.7

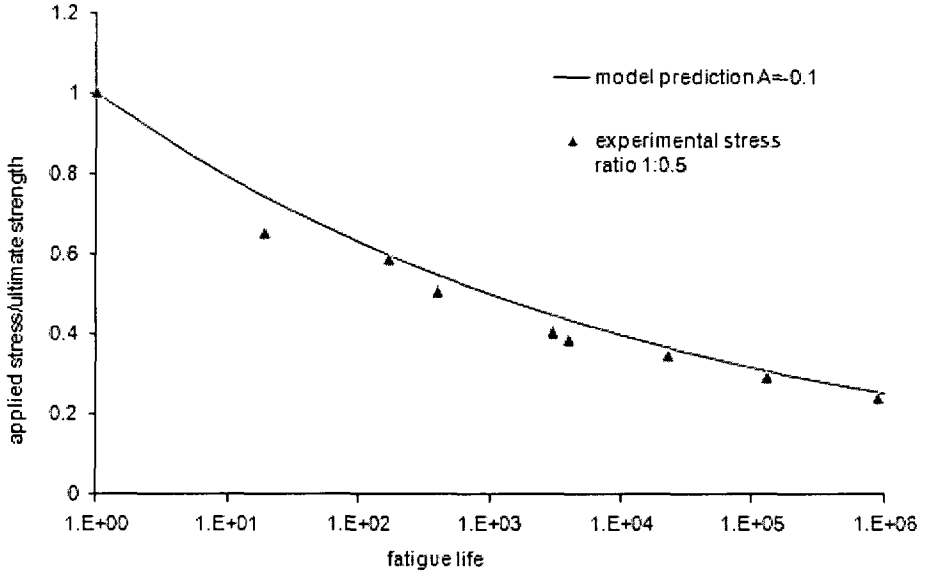

	1				-0.1
n	Mpa			n	t=A*n^B
1	223	1		1	1
19	146	0.6547		10	0.7943
170	131	0.5874		100	0.631
400	113	0.5067		1000	0.5012
3000	90	0.4036		10000	0.3981
4000	86	0.3857		100000	0.3162
23000	77	0.3453		1000000	0.2512
130000	65	0.2915			
900000	53	0.2377			

4. EXCEL sheet for Figure 6.8

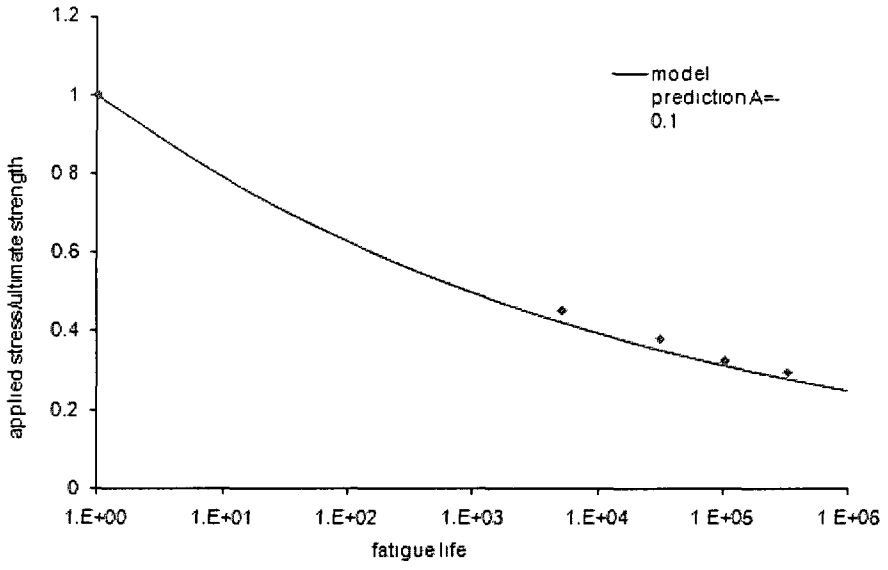

(1/2)

n	Mpa		
1	250	1	
5200	113	0 452	
32000	95	0 38	
105000	81	0.324	
330000	74	0.296	

n	-0 1 t=A*n^B
1	1
10	0 7943
100	0.631
1000	0.5012
10000	0.3981
100000	0.3162
1000000	0 2512

5. EXCEL sheet for Figure 6.9

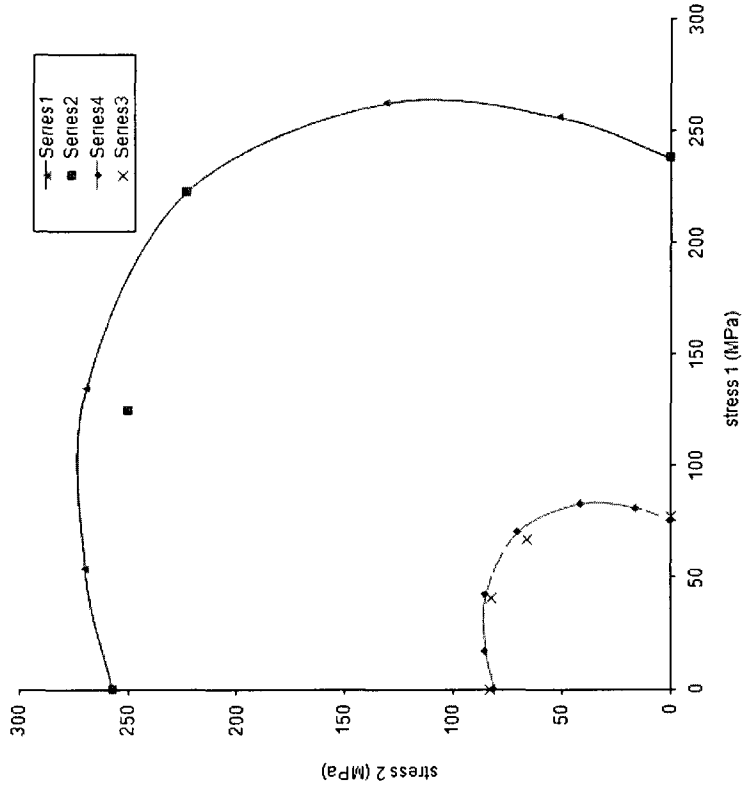

n=1					
experience		theory			
x	y	rafa		x	y
0	257	-0 46		0 00	257 00
125	250			53 91	269 57
223	223	bata		134 63	269 26
238	0	0 1		222 86	222 86
				262 46	131 23
				256 12	51 22
				238 00	0 00

n=100000				
experience		theory		
0	83	rafa	0 00	81 27
41	82	-0 46	17 05	85 24
67	66		42 57	85 15
77	0	bata	70 47	70 47
		0 1	83 00	41 50
			80 99	16 20
			75 26	0 00

Parameters				
fail sta	final sta	A	arfa	E
0.0156	0.013	-0.1	0.24	28.8

Theoritical data		
n	dk/dn	k
1	0.005482	0
2	0.002938	0.005482
3	0.00204	0.00842
4	0.001574	0.01046
5	0.001288	0.012035
6	0.001093	0.013323
7	0.000951	0.014416
8	0.000844	0.015367
9	0.000759	0.016211
10	0.00069	0.01697
11	0.000633	0.01766
12	0.000586	0.018293
13	0.000545	0.018879
14	0.00051	0.019424
15	0.000479	0.019934
16	0.000452	0.020413
17	0.000428	0.020865
18	0.000407	0.021293

Experimental data		
Stress=	113	
n	E (Gpa)	Damage K
0	28.8	
1	15.5	0
20	13.8	0.037742
200	12.6	0.044643
400	10.9	0.057021

7. EXCEL sheet for Figure 6.11

A B C D E F G H I J K L M N O P Q R S T U V W X

E	deltak	ft
17070 00	0 00	238 00

k= 0 00
n= 1 00

E1= 17070 00
stress= 238 00

i	k	t	E	stress	strain
				0 00	0 00
1 00	0 00	30 74	16238 43	30 74	0 00
2 00	0 00	57 22	15484 12	57 22	0 00
3 00	0 00	80 15	14796 77	80 15	0 01
4 00	0 00	100 06	14167 86	100 06	0 01
5 00	0 00	117 42	13590 22	117 42	0 01
6 00	0 00	132 60	13057 85	132 60	0 01
7 00	0 00	145 90	12565 61	145 90	0 01
8 00	0 00	157 58	12109 13	157 58	0 01
9 00	0 00	167 86	11684 66	167 86	0 01
10 00	0 00	176 92	11288 94	176 92	0 01
11 00	0 00	184 90	10919 14	184 90	0 01
12 00	0 00	191 95	10572 80	191 95	0 01
13 00	0 00	198 18	10247 76	198 18	0 01
14 00	0 00	203 68	9942 11	203 68	0 02
15 00	0 00	208 53	9654 16	208 53	0 02
16 00	0 00	212 82	9382 42	212 82	0 02
17 00	0 00	216 59	9125 56	216 59	0 02
18 00	0 00	219 91	8882 39	219 91	0 02
19 00	0 00	222 83	8651 84	222 83	0 02
20 00	0 00	225 38	8432 96	225 38	0 02
21 00	0 00	227 61	8224 88	227 61	0 02
22 00	0 00	229 54	8026 82	229 54	0 02
23 00	0 00	231 21	7838 08	231 21	0 02
24 00	0 00	232 65	7658 01	232 65	0 02
25 00	0 00	233 87	7486 02	233 87	0 02
26 00	0 00	234 89	7321 59	234 89	0 02
27 00	0 00	235 74	7164 23	235 74	0 02
28 00	0 00	236 43	7013 49	236 43	0 02

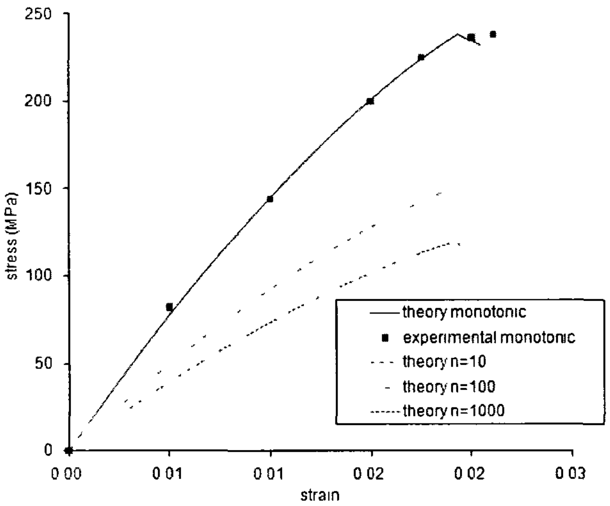

0 01 217.70
0 01 218 80

stress=	119 00	stress=	150 00	stress=	189 00
k=	0 00	k=	0 00	k=	0 00
0 00	0 00	0 00	0 00	0 00	0 00
8 03	0 00	12 60	0 00	19 72	0 00
15 47	0 00	24 06	0 00	37 23	0 00
22 38	0 00	34 50	0 00	52 81	0 00
28 79	0 00	44 02	0 00	66 72	0 01
34 76	0 00	52 72	0 01	79 16	0 01
40 31	0 01	60 69	0 01	90 31	0 01
45 48	0 01	67 98	0 01	100 33	0 01
50 30	0 01	74 68	0 01	109 34	0 01
54 81	0 01	80 83	0 01	117 46	0 01
59 01	0 01	86 48	0 01	124 79	0 01
62 94	0 01	91 69	0 01	131 40	0 01
66 61	0 01	96 48	0 01	137 38	0 01
70 05	0 01	100 90	0 01	142 79	0 01
73 27	0 01	104 97	0 01	147 68	0 01
76 29	0 01	108 73	0 01	152 11	0 01
79 11	0 01	112 20	0 01	156 13	0 01
81 76	0 01	115 41	0 01	159 77	0 01
84 25	0 01	118 38	0 01	163 06	0 02
86 58	0 01	121 11	0 01	166 04	0 02
88 77	0 01	123 64	0 01	168 74	0 02
90 82	0 01	125 98	0 01	171 18	0 02
92 75	0 01	128 15	0 02	173 39	0 02
94 57	0 01	130 15	0 02	175 38	0 02
96 27	0 01	131 99	0 02	177 17	0 02
97 87	0 01	133 70	0 02	178 79	0 02
99 37	0 01	135 27	0 02	180 23	0 02
100 78	0 01	136 73	0 02	181 53	0 02

A	B	C	D	E	F	G	H	I	J	K	L	M	N	O	P	Q	R	S	T	U	V	W	X
E	deltak	ft				k=	0		E1=	18504		beta=	0 01										
18504	3 00E 06		250			n=	1		stress=	250		rapha=	0 39										
i	k	t	E	stress	strain											stress=	125	stress=	158	stress=	198		
				0	0											k=	5E 05	k=	2 8E-05	k=	1 2E-05		
1	3 00E 06	3 48E+01	17530 829	3 48E+01	1 98E-03		0	0		0	0		0	0		0	0	0	0	0	0		
2	6 00E-06	6 44E+01	16654 906	6 44E+01	3 76E-03		0 005	82		0 0012	26 5		0 0025	53		9 7035	0 001	15	0 00127	22 842	0 00158		
3	9 00E-06	8 97E+01	15862 348	8 97E+01	5 36E-03		0 01	142		0 0022	49 6		0 005	89		18 591	0 002	28 463	0 00244	42 853	0 00302		
4	1 20E-05	1 12E+02	15141 795	1 12E+02	6 80E 03		0 015	200		0 0032	69 9		0 0075	114		26 744	0 0028	40 576	0 00354	60 446	0 00434		
5	1 50E-05	1 30E+02	14483 86	1 30E+02	8 09E-03		0 02	253		0 0041	87 6		0 01	140		34 235	0 0037	51 497	0 00456	75 962	0 00556		
6	1 80E-05	1 47E+02	13880 721	1 47E+02	9 27E-03											41 126	0 0045	61 364	0 00551	89 682	0 00667		
7	2 10E-05	1 61E+02	13325 805	1 61E+02	1 03E 02											47 473	0 0052	70 293	0 00639	101 85	0 00769		
8	2 40E-05	1 73E+02	12813 553	1 73E+02	1 13E-02											53 327	0 0059	78 388	0 00722	112 65	0 00863		
9	2 70E-05	1 84E+02	12339 225	1 84E+02	1 21E-02											58 732	0 0066	85 737	0 008	122 27	0 0095		
10	3 00E-05	1 93E+02	11898 76	1 93E+02	1 29E-02											63 727	0 0073	92 417	0 00872	130 85	0 0103		
11	3 30E-05	2 01E+02	11488 658	2 01E+02	1 36E-02											68 348	0 0079	98 497	0 0094	138 5	0 01104		
12	3 60E-05	2 08E+02	11105 883	2 08E+02	1 43E-02											72 625	0 0084	104 04	0 01003	145 34	0 01171		
13	3 90E 05	2 14E+02	10747 792	2 14E+02	1 49E 02											76 588	0 009	109 09	0 01062	151 46	0 01234		
14	4 20E 05	2 20E+02	10412 071	2 20E+02	1 54E-02											80 263	0 0095	113 7	0 01118	156 94	0 01292		
15	4 50E-05	2 25E+02	10096 689	2 25E+02	1 59E-02											83 672	0 01	117 9	0 0117	161 85	0 01345		
16	4 80E-05	2 29E+02	9799 8509	2 29E+02	1 63E-02											86 836	0 0104	121 75	0 01218	166 25	0 01393		
17	5 10E-05	2 32E+02	9519 9681	2 32E+02	1 67E-02											89 775	0 0109	125 26	0 01264	170 18	0 01438		
18	5 40E-05	2 35E+02	9255 6282	2 35E+02	1 70E-02											92 506	0 0113	128 48	0 01306	173 71	0 0148		
19	5 70E-05	2 38E+02	9005 5715	2 38E+02	1 73E-02											95 043	0 0117	131 42	0 01346	176 86	0 01518		
20	6 00E-05	2 40E+02	8768 6709	2 40E+02	1 76E-02											97 403	0 012	134 1	0 01383	179 69	0 01552		
21	6 30E-05	2 42E+02	8543 9145	2 42E+02	1 78E-02											99 597	0 0124	136 56	0 01418	182 2	0 01584		
22	6 60E-05	2 44E+02	8330 3921	2 44E+02	1 80E-02											101 64	0 0127	138 8	0 0145	184 45	0 01613		
23	6 90E 05	2 46E+02	8127 2817	2 46E+02	1 82E 02											103 53	0 013	140 86	0 01481	186 45	0 0164		
24	7 20E-05	2 47E+02	7933 8401	2 47E+02	1 83E-02											105 3	0 0133	142 73	0 01509	188 22	0 01664		
25	7 50E-05	2 48E+02	7749 3927	2 48E+02	1 84E-02											106 94	0 0136	144 44	0 01535	189 79	0 01685		
26	7 80E 05	2 48E+02	7573 3267	2 48E+02	1 85E-02											108 47	0 0139	146	0 01559	191 18	0 01705		
27	8 10E-05	2 49E+02	7405 0834	2 49E+02	1 86E-02											109 89	0 0141	147 42	0 01582	192 39	0 01722		
28	8 40E-05	2 49E+02	7244 1527	2 49E+02	1 87E-02											111 21	0 0144	148 71	0 01603	193 45	0 01738		
29	8 70E-05	2 50E+02	7090 0681	2 50E+02	1 87E 02											112 43	0 0146	149 88	0 01622	194 37	0 01752		
30	9 00E-05	2 50E+02	6942 4018	2 50E+02	1 87E-02											113 57	0 0148	150 94	0 0164	195 16	0 01764		
31	9 30E 05	2 50E+02	6800 7609	2 50E+02	1 87E-02											114 63	0 015	151 9	0 01657	195 84	0 01774		

A	B	C	D	E	F	G	H	I	J	K	L	M	N	O	P	Q	R
E	deltak	ft				k=	0		E1=	20201.2		beta=	0.01				
20201	3.00E-06		223			n=	1		stress=	223		alpha=	3.90E-01				
																stress=	122
i	k	t	E'	stress	strain											k=	2.33451E-05
				0	0												
1	3.00E-06	3.36E+01	19046.712	3.36E+01	1.77E-03		0	0		0	0		0	0		0	0
2	6.00E-06	6.19E+01	18017.206	6.19E+01	3.33E-03		0.0027	78		0.0012	26.5		0.0025	53		11.934	0.000976425
3	9.00E-06	8.57E+01	17093.287	8.57E+01	4.73E-03		0.005	108		0.0022	49.6		0.005	89		22.609	0.001881885
4	1.20E-05	1.06E+02	16259.502	1.06E+02	5.97E-03		0.01	176		0.0032	69.9		0.0075	114		32.182	0.0027226
5	1.50E-05	1.23E+02	15503.275	1.23E+02	7.08E-03		0.013	223		0.0041	87.6		0.01	140		40.786	0.003504075
6	1.80E-05	1.38E+02	14814.266	1.38E+02	8.08E-03											48.536	0.0042312
7	2.10E-05	1.51E+02	14183.894	1.51E+02	8.97E-03											55.53	0.004908334
8	2.40E-05	1.61E+02	13604.979	1.61E+02	9.77E-03											61.852	0.00553938
9	2.70E-05	1.71E+02	13071.468	1.71E+02	1.05E-02											67.575	0.00612784
10	3.00E-05	1.79E+02	12578.221	1.79E+02	1.11E-02											72.763	0.006676868
11	3.30E-05	1.86E+02	12120.845	1.86E+02	1.17E-02											77.472	0.007189314
12	3.60E-05	1.92E+02	11695.564	1.92E+02	1.22E-02											81.751	0.00766776
13	3.90E-05	1.97E+02	11299.116	1.97E+02	1.27E-02											85.642	0.008114548
14	4.20E-05	2.01E+02	10928.663	2.01E+02	1.31E-02											89.184	0.008531813
15	4.50E-05	2.05E+02	10581.731	2.05E+02	1.34E-02											92.409	0.0089215
16	4.80E-05	2.09E+02	10256.147	2.09E+02	1.38E-02											95.348	0.009285391
17	5.10E-05	2.11E+02	9950.0013	2.11E+02	1.41E-02											98.027	0.009625116
18	5.40E-05	2.14E+02	9661.6024	2.14E+02	1.43E-02											100.47	0.009942173
19	5.70E-05	2.16E+02	9389.451	2.16E+02	1.45E-02											102.7	0.010237941
20	6.00E-05	2.18E+02	9132.2116	2.18E+02	1.47E-02											104.73	0.01051369
21	6.30E-05	2.19E+02	8888.6914	2.19E+02	1.49E-02											106.58	0.010770593
22	6.60E-05	2.20E+02	8657.8213	2.20E+02	1.50E-02											108.26	0.011009733
23	6.90E-05	2.21E+02	8438.6405	2.21E+02	1.51E-02											109.8	0.011232115
24	7.20E-05	2.22E+02	8230.2833	2.22E+02	1.52E-02											111.2	0.011438671
25	7.50E-05	2.22E+02	8031.9672	2.22E+02	1.53E-02											112.47	0.011630267
26	7.80E-05	2.23E+02	7842.9835	2.23E+02	1.53E-02											113.62	0.011807707
27	8.10E-05	2.23E+02	7662.6885	2.23E+02	1.53E-02											114.67	0.011971742
28	8.40E-05	2.23E+02	7490.4964	2.23E+02	1.53E-02											115.61	0.012123072
29	8.70E-05	2.23E+02	7325.8732	2.23E+02	1.53E-02											116.47	0.012262348
30	9.00E-05	2.23E+02	7168.3303	2.23E+02	1.54E-02											117.24	0.012390183
31	9.30E-05	2.23E+02	7017.4208	2.23E+02	1.54E-02											117.93	0.012507149

APPENDIX C

Several EXCEL sheets are developed to evaluate the model of Chapter 7 and shown as below.

1. EXCEL sheet for Figure 7.5

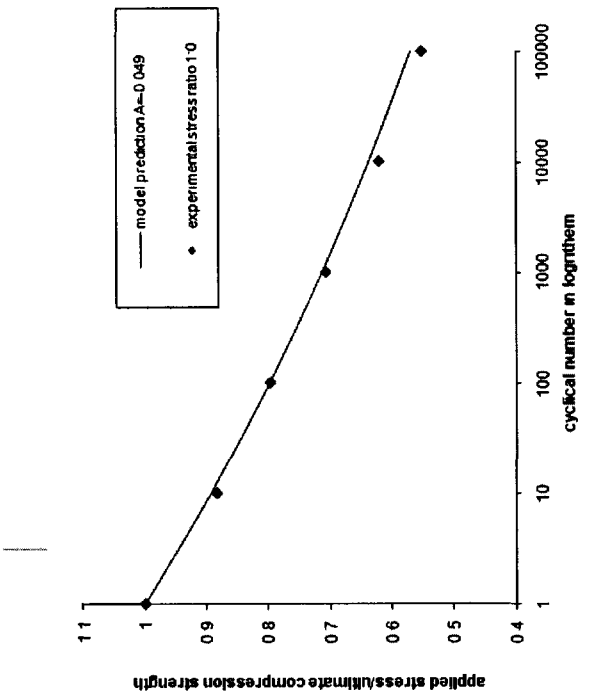

stress/stre n	1	A 1	theory 1
1 1292			
0 9979	10	0 883723	0 893109
0 9007	100	0 797644	-0 0491 0 797644
0 7986	1000	0 707226	0 712384
0 7014	10000	0 621148	0 636237
0 6236	100000	0 552249	0 568229

2. EXCEL sheet for Figure 7.6

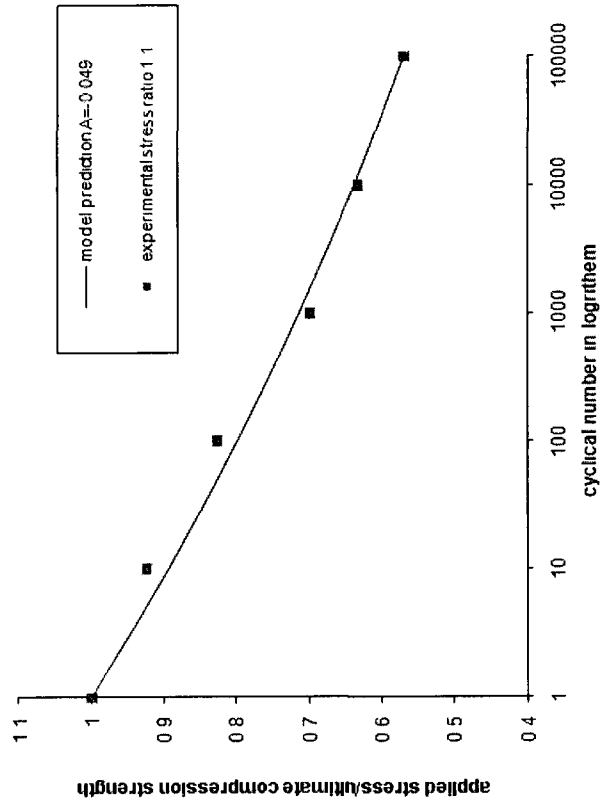

stress/streng	n		A	theory
1 44	1	1		1
1 33	10	0 923611		0 853305
1 19	100	0 826389	0 049	0 797995
1 0055	1000	0 698264		0 712853
0 91	10000	0 631944		0 636796
0 82	100000	0 569444		0 568853

3. EXCEL sheet for Figure 7.7

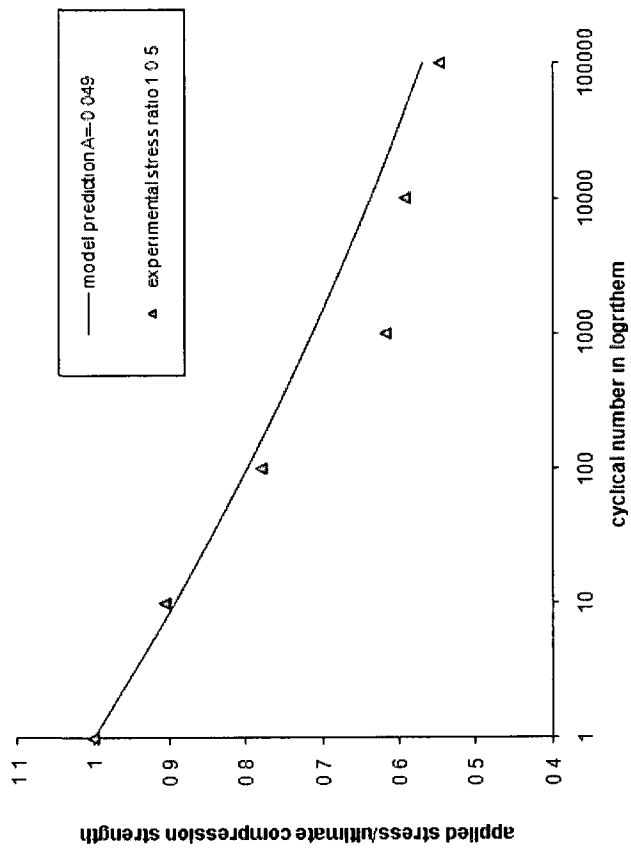

stress:stren		A		theory	
1 6542	1	1			1
1 4986	10	0 905936		0 893305	
1 29	100	0 779833	-0 049	0 797995	
1 0222	1000	0 617942		0 712853	
0 98	10000	0 592431		0 636795	
0 9056	100000	0 547455		0 568853	

N=1

experimental data		theoritical results			
		arfa	mu	beta	
		1	1	1	
x	y	x	y		
1 1292	0	0	1 1292		
1 0903	0	0 260036	1 300178		
1 6976	0 3395	0 77139	1 542781		
1 5902	0 318	1 493791	1 493791		
1 6542	0 8271	1 542781	0 77139		
1 5958	0 7979	1 300178	0 260036		
1 5715	0 7858	1 1292	0		
1 44	1 44				
0	1 1292				
0	1 0903				
0 3395	1 6976				
0 318	1 5902				
0 8271	1 6542				
0 7979	1 5958				
0 7858	1 5715				

N=10000

experimental data		theoritical results			
		arfa	mu	beta	
		1	1	1	
x	y	x	y		
0 7014	0	0	0 7014		
0 7986	0	0 161521	0 807603		
0 9785	0 4893	0 479147	0 958295		
0 9007	0 4504	0 927865	0 927865		
0 91	0 91	0 958295	0 479147		
0	0 7986	0 807603	0 161521		
0	0 7014	0 7014	0		
0 4893	0 9785				
0 4504	0 9007				

5. EXCEL sheet for Figure 7.9

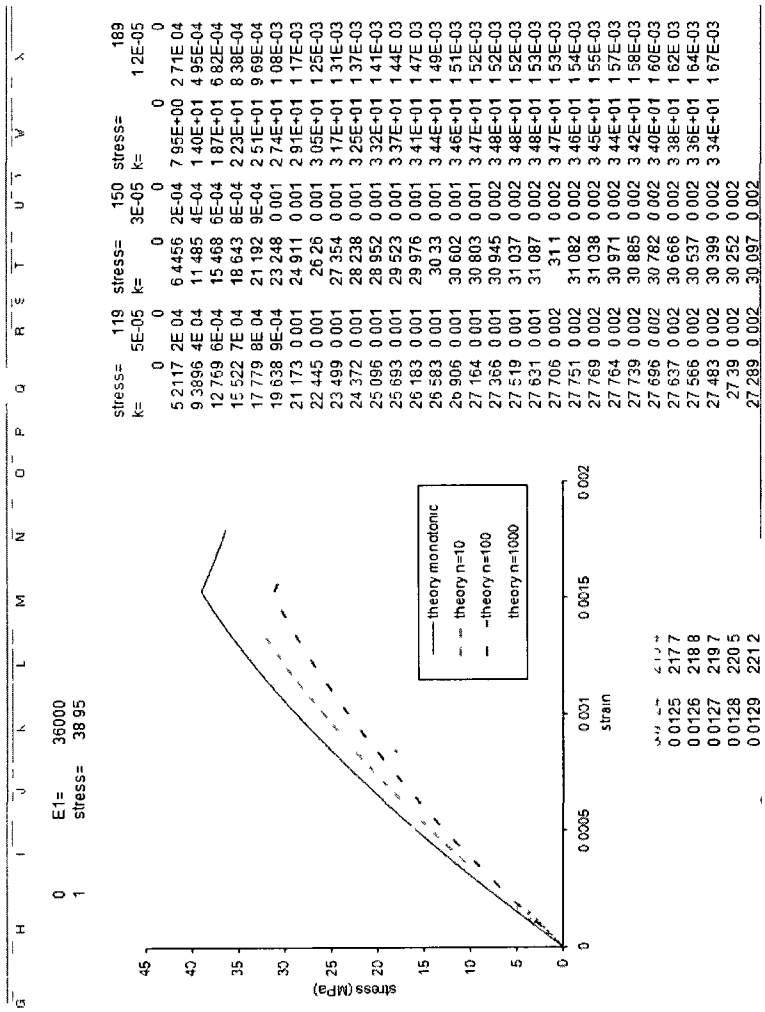

	A	B	C	D	E	F	G	H	I	J	K	L	M	N	O	P	Q	R	S	T	U	V	W	X
	E	deltak	ft				k=		0	E1=	36000													
	36000	3 00E-06	38 95				n=		1	stress=	38 95													
	i	k	t	E	stress	strain											stress=	119	stress=	150	stress=	189		
						0	C										k=	5E-05	k=	3E-05	k=	1 2E-05		
	1	3 00E-06	9 80E+00	32490 975	9 80E+00	3 02E-04											0	0	0	0	0	0		
	2	6 00E-06	1 70E+01	29605 263	1 70E+01	5 46E-04											5 2117	2E 04	6 4456	2E-04	7 95E+00	2 71E 04		
	3	9 00E 06	2 24E+01	27190 332	2 24E+01	7 45E 04											9 3996	4E 04	11 485	4E-04	1 40E+01	4 95E-04		
	4	1 20E 05	2 65E+01	25139 665	2 65E+01	9 08E-04											12 759	6E-04	15 468	6E-04	1 87E+01	6 82E-04		
	5	1 50E-05	2 97E+01	23376 623	2 97E+01	1 04E-0C											15 522	7E 04	18 643	8E-04	2 23E+01	8 38E-04		
	6	1 80E-05	3 21E+01	21844 66	3 21E+01	1 15E-0C											17 779	8E 04	21 192	9E-04	2 51E+01	9 69E-04		
	7	2 10E 05	3 39E+01	20501 139	3 39E+01	1 24E-03											19 638	9E-04	23 248	0 001	2 74E+01	1 08E-03		
	8	2 40E 05	3 54E+01	19313 305	3 54E+01	1 32E-0C											21 173	0 001	24 911	0 001	2 91E+01	1 17E-03		
	9	2 70E-05	3 65E+01	18255 578	3 65E+01	1 38E 0C											22 445	0 001	26 26	0 001	3 05E+01	1 25E-03		
	10	3 00E-05	3 73E+01	17307 692	3 73E+01	1 42E-0C											23 499	0 001	27 354	0 001	3 17E+01	1 31E-03		
	11	3 30E-05	3 79E+01	16453 382	3 79E+01	1 46E-03											24 372	0 001	28 238	0 001	3 25E+01	1 37E-03		
	12	3 60E-05	3 83E+01	15679 443	3 83E+01	1 49E-0C											25 096	0 001	28 952	0 001	3 32E+01	1 41E-03		
	13	3 90E-05	3 86E+01	14975 042	3 86E+01	1 51E-0C											25 693	0 001	29 523	0 001	3 37E+01	1 44E 03		
	14	4 20E-05	3 88E+01	14331 21	3 88E+01	1 52E-0C											26 183	0 001	29 976	0 001	3 41E+01	1 47E 03		
	15	4 50E-05	3 89E+01	13740 458	3 89E+01	1 53E-03											26 583	0 001	30 33	0 001	3 44E+01	1 49E-03		
	16	4 80E-05	3 89E+01	13196 481	3 89E+01	1 53E-0C											26 906	0 001	30 602	0 001	3 46E+01	1 51E-03		
	17	5 10E-05	3 89E+01	12693 935	3 89E+01	1 53E-0C											27 164	0 001	30 803	0 001	3 47E+01	1 52E-03		
	18	5 40E-05	3 88E+01	12228 261	3 88E+01	1 54E-0C											27 366	0 001	30 945	0 002	3 48E+01	1 52E-03		
	19	5 70E-05	3 87E+01	11795 544	3 87E+01	1 55E-0C											27 519	0 001	31 037	0 002	3 48E+01	1 52E-03		
	20	6 00E-05	3 86E+01	11392 405	3 86E+01	1 57E-0C											27 631	0 001	31 087	0 002	3 48E+01	1 53E-03		
	21	6 30E 05	3 84E+01	11015 912	3 84E+01	1 58E-0C											27 706	0 002	311	0 002	3 47E+01	1 53E-03		
	22	6 60E-05	3 82E+01	10663 507	3 82E+01	1 60E-0C											27 751	0 002	31 082	0 002	3 46E+01	1 54E-03		
	23	6 90E-05	3 79E+01	10332 951	3 79E+01	1 62E-0C											27 769	0 002	31 038	0 002	3 45E+01	1 55E-03		
	24	7 20E-05	3 77E+01	10022 272	3 77E+01	1 65E-0C											27 764	0 002	30 971	0 002	3 44E+01	1 57E-03		
	25	7 50E 05	3 74E+01	9729 7297	3 74E+01	1 67E-0C											27 739	0 002	30 885	0 002	3 42E+01	1 58E-03		
	26	7 80E 05	3 72E+01	9453 7815	3 72E+01	1 70E-0C											27 696	0 002	30 782	0 002	3 40E+01	1 60E-03		
	27	8 10E 05	3 69E+01	9193 0541	3 69E+01	1 73E 03											27 637	0 002	30 666	0 002	3 38E+01	1 62E 03		
	28	8 40E-05	3 66E+01	8946 3221	3 66E+01	1 76E 03											27 566	0 002	30 537	0 002	3 36E+01	1 64E-03		
	29	8 70E-05	3 64E+01	8712 4879	3 64E+01	1 79E-03											27 483	0 002	30 399	0 002	3 34E+01	1 67E-03		
	30	9 00E 05	3 61E+01	8490 566	3 61E+01	1 83E-03											27 39	0 002	30 252	0 002				
	31	9 30E 05	3 58E+01	8279 6688	3 58E+01	1 86E-03											27 289	0 002	30 097	0 002				

E	deltak	ft				k=	0	E1=	45000 0		beta=	0 01											
45000 0	3 00E 06		55 7			n=	1	stress=	55 7		alpha=	7 00E-01											
																					stress=	122	
																					k=	2 3E 05	
	k	t	E	stress	strain																		
				0	0																0	0	
1	3 00E-06	1 69E+01	39647 6	1 69E+01	4 26E-04																0	0	
2	6 00E-06	2 85E+01	35433 1	2 85E+01	7 54E-04																9 23652	0 00031	11 4397
3	9 00E-06	3 66E+01	32028 5	3 66E+01	1 01E-03																16 2231	0 00056	19 8118
4	1 20E-05	4 25E+01	29220 8	4 25E+01	1 21E-03																21 58	0 00077	26 0403
5	1 50E-05	4 66E+01	26865 7	4 66E+01	1 36E-03																25 7302	0 00095	30 73
6	1 80E-05	4 96E+01	24861 9	4 96E+01	1 48E-03																28 9699	0 0011	34 2905
7	2 10E-05	5 18E+01	23136 2	5 18E+01	1 58E-03																31 5121	0 00122	37 0064
8	2 40E 05	5 33E+01	21634 6	5 33E+01	1 65E-03																33 5121	0 00132	39 081
9	2 70E-05	5 44E+01	20316	5 44E+01	1 70E-03																35 0861	0 00141	40 6616
10	3 00E-05	5 50E+01	19148 9	5 50E+01	1 73E-03																36 3216	0 00148	41 8576
11	3 30E-05	5 55E+01	18108 7	5 55E+01	1 76E-03																37 286	0 00154	42 751
12	3 60E-05	5 57E+01	17175 6	5 57E+01	1 77E-03																38 0314	0 00159	43 4044
13	3 90E-05	5 57E+01	16333 9	5 57E+01	1 77E-03																38 5988	0 00162	43 8661
14	4 20E-05	5 56E+01	15570 9	5 56E+01	1 78E-03																39 0206	0 00165	44 1737
15	4 50E-05	5 54E+01	14876	5 54E+01	1 79E-03																39 3227	0 00167	44 3569
16	4 80E-05	5 51E+01	14240 5	5 51E+01	1 81E-03																39 526	0 00169	44 439
17	5 10E-05	5 48E+01	13657 1	5 48E+01	1 83E-03																39 6475	0 0017	44 4391
18	5 40E-05	5 44E+01	13119 5	5 44E+01	1 86E-03																39 7009	0 0017	44 3722
19	5 70E-05	5 40E+01	12622 7	5 40E+01	1 90E-03																39 6978	0 0017	44 2506
20	6 00E-05	5 35E+01	12162 2	5 35E+01	1 93E-03																39 6473	0 00171	44 0843
21	6 30E-05	5 31E+01	11734	5 31E+01	1 97E-03																39 5575	0 00172	43 8817
22	6 60E 05	5 26E+01	11335	5 26E+01	2 02E 03																39 4347	0 00173	43 6495
23	6 90E-05	5 21E+01	10962 2	5 21E+01	2 06E-03																39 2844	0 00174	43 3932
24	7 20E-05	5 16E+01	10613 2	5 16E+01	2 11E-03																39 1112	0 00176	43 1175
25	7 50E-05	5 11E+01	10285 7	5 11E+01	2 16E-03																38 9189	0 00178	42 8264
26	7 80E-05	5 06E+01	9977 83	5 06E+01	2 21E-03																38 7109	0 0018	42 5229
27	8 10E-05	5 01E+01	9687 84	5 01E+01	2 26E-03																38 4898	0 00183	42 2099
28	8 40E-05	4 96E+01	9414 23	4 96E+01	2 32E-03																38 258	0 00185	41 8896
29	8 70E-05	4 91E+01	9155 65	4 91E+01	2 37E-03																38 0176	0 00188	41 5639
30	9 00E-05	4 86E+01	8910 89	4 86E+01	2 43E-03																37 7703	0 00191	41 2344
31	9 30E-05	4 81E+01	8678 88	4 81E+01	2 48E-03																37 5174	0 00194	40 9025

A	B	C	D	E	F	G	H	I	J	K	L	M	N	O	P	Q	R	T	U	V	W	X
E	deltak	ft				k=	0		E1=	40000		beta=	0 01									
40000	3 00E 06	58 43				n=	1		stress=	58 43		rapha=	0 7									

i	k	t	E	stress	strain
				0	0
1	3 00E 06	1 61E+01	35714 286	1 61E+01	4 50E-04
2	6 00E-06	2 76E+01	32258 065	2 76E+01	8 06E-04
3	9 00E 06	3 59E+01	29411 765	3 59E+01	1 09E 03
4	1 20E 05	4 21E+01	27027 027	4 21E+01	1 32E-03
5	1 50E 05	4 67E+01	25000	4 67E+01	1 50E-03
6	1 80E 05	5 01E+01	23255 814	5 01E+01	1 65E 03
7	2 10E 05	5 26E+01	21739 13	5 26E+01	1 77E-03
8	2 40E 05	5 45E+01	20408 163	5 45E+01	1 86E-03
9	2 70E 05	5 59E+01	19230 769	5 59E+01	1 93E-03
10	3 00E 05	5 69E+01	18181 818	5 69E+01	1 99E 03
11	3 30E-05	5 76E+01	17241 379	5 76E+01	2 03E-03
12	3 60E-05	5 81E+01	16393 443	5 81E+01	2 05E-03
13	3 90E-05	5 83E+01	15625	5 83E+01	2 07E-03
14	4 20E-05	5 84E+01	14925 373	5 84E+01	2 08E 03
15	4 50E-05	5 84E+01	14285 714	5 84E+01	2 08E-03
16	4 80E 05	5 83E+01	13698 63	5 83E+01	2 09E-03
17	5 10E-05	5 81E+01	13157 895	5 81E+01	2 10E 03
18	5 40E 05	5 78E+01	12658 228	5 78E+01	2 12E-03
19	5 70E-05	5 75E+01	12195 122	5 75E+01	2 15E 03
20	6 00E 05	5 72E+01	11764 706	5 72E+01	2 18E-03
21	6 30E-05	5 68E+01	11363 636	5 68E+01	2 21E 03
22	6 60E-05	5 64E+01	10989 011	5 64E+01	2 25E 03
23	6 90E-05	5 59E+01	10638 298	5 59E+01	2 29E 03
24	7 20E-05	5 55E+01	10309 278	5 55E+01	2 33E-03
25	7 50E 05	5 50E+01	10000	5 50E+01	2 38E 03
26	7 80E 05	5 46E+01	9708 7379	5 46E+01	2 43E-03
27	8 10E 05	5 41E+01	9433 9623	5 41E+01	2 48E 03
28	8 40E-05	5 36E+01	9174 3119	5 36E+01	2 53E-03
29	8 70E-05	5 32E+01	8928 5714	5 32E+01	2 58E-03
30	9 00E-05	5 27E+01	8695 6522	5 27E+01	2 63E-03
31	9 30E-05	5 22E+01	8474 5763	5 22E+01	2 69E-03

0 0125	217 7
0 0126	218 8
0 0127	219 7
0 0128	220 5
0 0129	221 2

stress=	125	stress=	158	stress=	198
k=	5E 05	k=	3E-05	k=	1E-05
0	0	0	0	0	0
9 2259	0 0003	11 134	0 0004	13 397	0 0004
16 307	0 0006	19 487	0 0007	23 211	0 0007
21 81	0 0008	25 845	0 0009	30 518	0 001
26 127	0 001	30 735	0 0011	36 025	0 0012
29 538	0 0012	34 527	0 0013	40 209	0 0014
32 248	0 0013	37 482	0 0014	43 403	0 0015
34 407	0 0014	39 79	0 0015	45 845	0 0016
36 129	0 0015	41 592	0 0016	47 708	0 0017
37 501	0 0016	42 995	0 0017	49 118	0 0018
38 59	0 0017	44 079	0 0018	50 174	0 0019
39 448	0 0017	44 907	0 0018	50 947	0 0019
40 118	0 0018	45 528	0 0019	51 495	0 002
40 632	0 0018	45 979	0 0019	51 861	0 002
41 017	0 0018	46 293	0 0019	52 082	0 002
41 295	0 0019	46 492	0 0019	52 183	0 002
41 483	0 0019	46 598	0 0019	52 187	0 002
41 597	0 0019	46 627	0 0019	52 112	0 002
41 647	0 0019	46 591	0 0019	51 973	0 002
41 645	0 0019	46 501	0 002	51 782	0 002
41 598	0 0019	46 368	0 002	51 547	0 0021
41 513	0 0019	46 198	0 002	51 277	0 0021
41 397	0 0019	45 997	0 002	50 979	0 0021
41 254	0 0019	45 771	0 002	50 658	0 0021
41 088	0 0019	45 524	0 002	50 318	0 0022
40 904	0 002	45 26	0 0021	49 964	0 0022
40 703	0 002	44 982	0 0021	49 598	0 0023
40 49	0 002	44 693	0 0021	49 224	0 0023
40 265	0 002	44 394	0 0022	48 843	0 0023
40 031	0 0021	44 089	0 0022	48 458	0 0024
39 79	0 0021	43 778	0 0022	48 07	0 0024

APPENDIX D

1. Comparison between power function and logarithm function for softening function for stress ratio 1:0

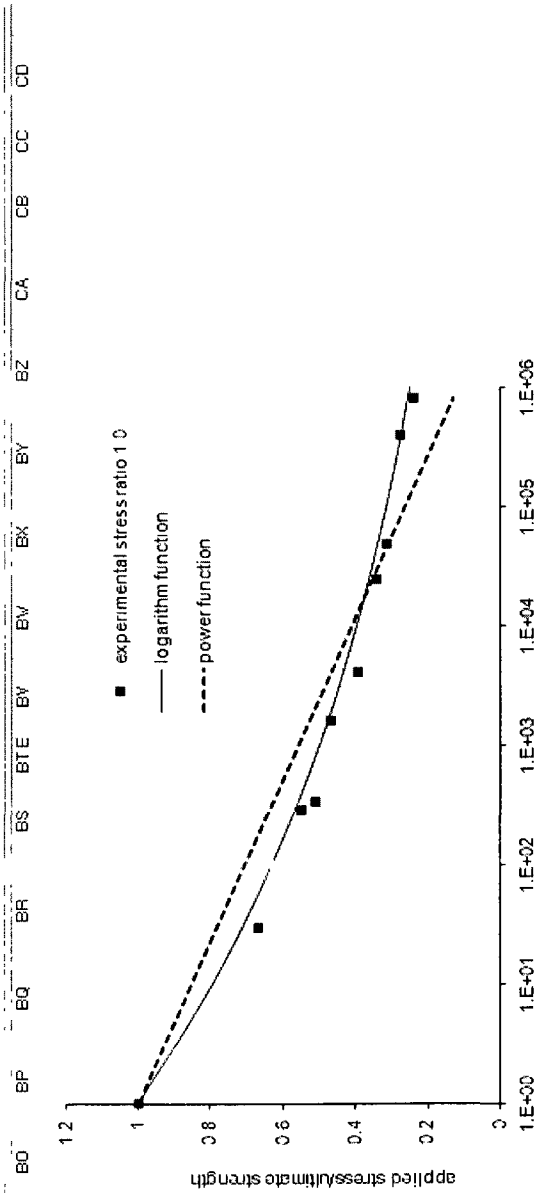

stres ratio	Logarithm function: t=n^A						Power function t=1+Bln(n)			Regression analysis			
	A	n	Sexp	Sexp/ft	Sthe	he-Sexp/ft)^2	B	Sthe	)exp/ft)^2	Sexp*ln(n	ln(n)	(ln(n))^2	
1 to 0	-0.1	1	257	1	1	0	-0.064	1	0	0	0	0	
		29	171	0.6654	0.7141	0 0024		0 7846	0 0142	2 2405	3.3673	11 339	
		280	141	0 5486	0 5692	0.0004		0.6396	0.0083	3 0915	5.6348	31.751	
		330	131	0.5097	0.5599	0.0025		0.629	0.0142	2.956	5.7991	33.629	
		1600	121	0.4708	0 4782	5E-05		0.5281	0 0033	3 4736	7.3778	54 431	
		4000	101	0 393	0 4363	0.0019		0 4694	0 0058	3 2595	8.294	68.791	
		24000	88	0.3424	0.3647	0.0005		0.3548	0 0002	3 4535	10.086	101 72	
		48000	81	0.3152	0 3403	0.0006		0.3105	2E-05	3 3973	10.779	116.19	
		390000	71	0.2763	0.276	8E-08		0.1765	0.01	3 5566	12.874	165.74	
		800000	61	0.2374	0.2569	0.0004		0.1305	0 0114	3 2262	13.592	184.75	
				RMS=	S^2=	0 0011	RMS=	S^2=	0 0084	SUM:	28.655	77.804	768 34	B= -0 064

2. Comparison between power function and logarithm function for softening function for stress ratio 1:1

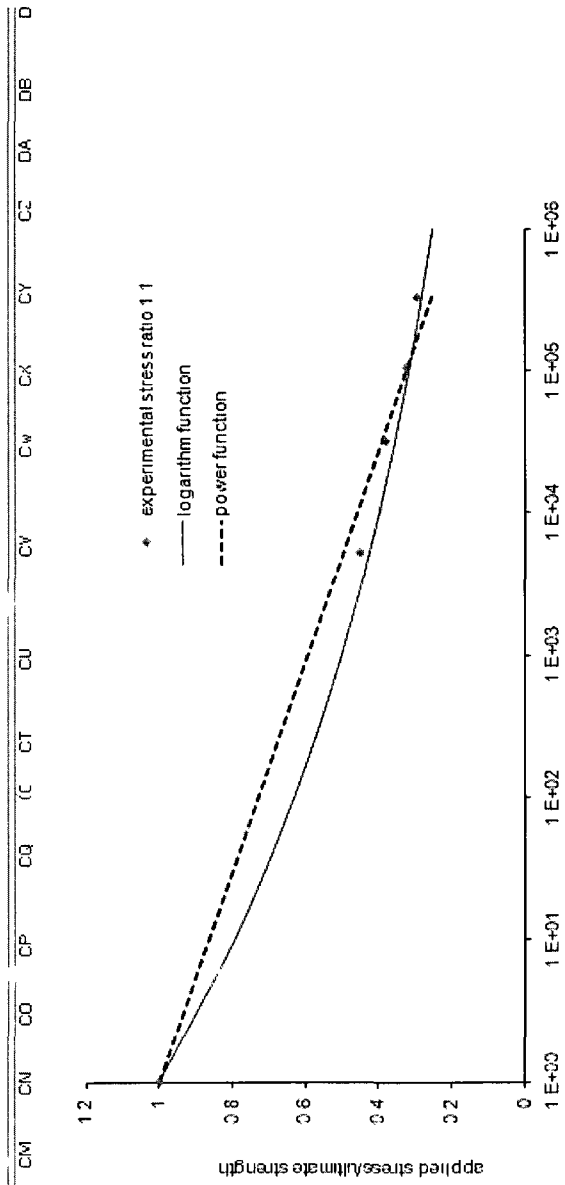

stres ratio	Logarithm function t=n^A						Power function t=1+Bln(n)				Regression analysis			
	A	n	Sexp	Sexp/ft	Sthe	(the-Sexp/ft)^2	B	Sthe	(Sthe-Sexp/ft)^2		Sexp*ln(n	ln(n)	(ln(n))^2	
1 to 0 5	-0 1	1	223	1	1	0	-0 065	1	0		0	0	0	
		19	146	0 655	0 745	0 008143		0 8072	0 023264277		1 9277	2 9444	8 6697	
		170	131	0 587	0 598	0 000119		0 6638	0 005825962		3 017	5 1358	26 376	
		400	113	0 507	0 549	0 001811		0 6078	0 01020648		3 036	5 9915	35 898	
		3000	90	0 404	0 449	0 002066		0 4758	0 005220843		3 2313	8 0064	64 102	
		4000	86	0 386	0 436	0 002566		0 457	0 005092076		3 1986	8 294	68 791	
		23000	77	0 345	0 366	0 000441		0 3425	7 83033E-06		3 4678	10 043	100 87	
		1E+05	65	0 291	0 308	0 000274		0 2291	0 003891142		3 4323	11 775	138 66	
		9E+05	53	0 238	0 254	0 000262		0 1024	0 018289289		3 2585	13 71	187 97	
				RMS=	S^2=	0 00224	RMS=	S^2=	0 010256843	SUM	24 569	65 901	631 33	B= -0 065

3. Comparison between power function and logarithm function for softening function for stress ratio 1:0.5

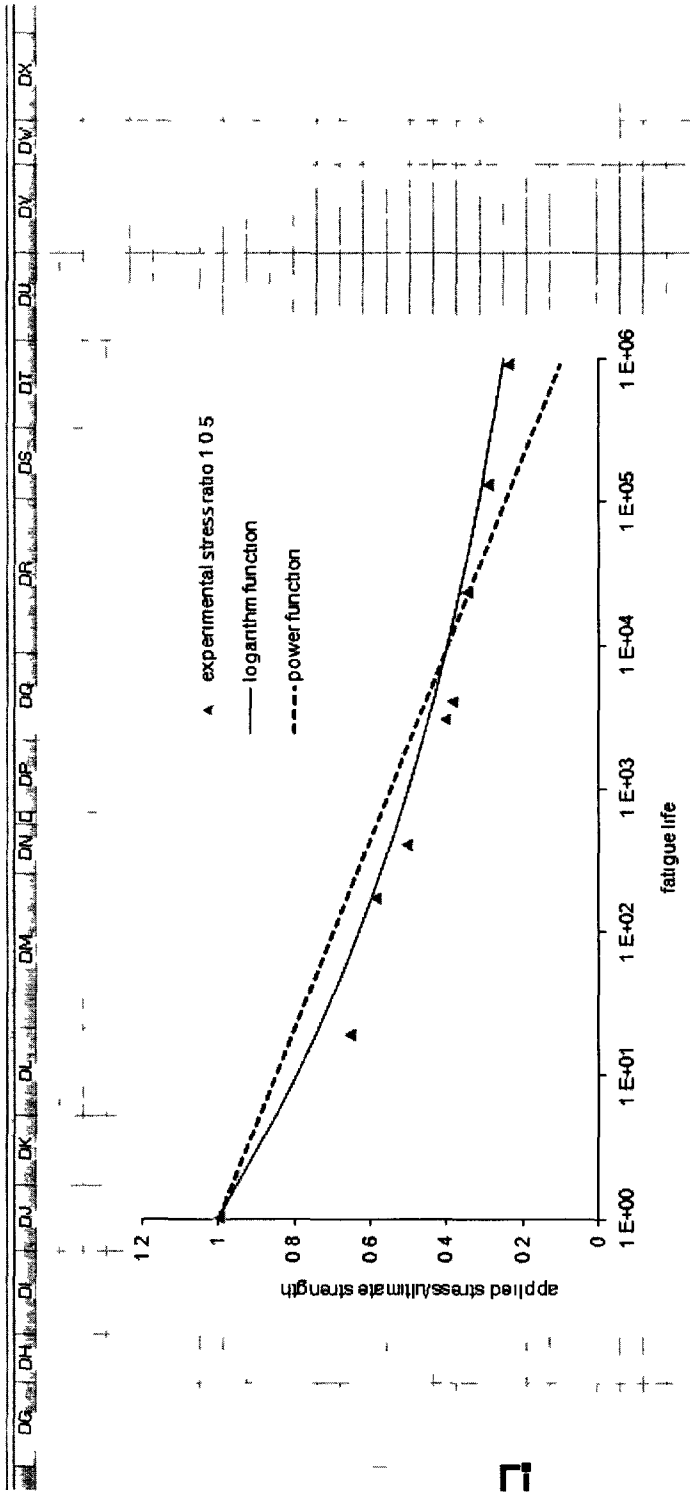

stres ratio	Logarithm function t=n^A						Power function t=1+Bln(n)			Regression analysis			
	A	n	Sexp	Sexp/ft	Sthe	(Sthe-Sexp/ft)^2	B	Sthe	(Sthe-Sexp/ft)^2	Sexp*ln(n	ln(n)	(ln(n))^2	
1 to 1	-0	1	250	1	1	0	-0 06	1	0	0	0	0	
		5200	113	0 45	0 425	0 000728433		0 4988	0 002186732	3 8675	8 5564	73 212	
		32000	95	0 38	0 3544	0 000655724		0 3923	0 000151721	3 9419	10 373	107 61	
		105000	81	0 32	0 3147	8 67014E-05		0 3227	1 66164E-06	3 746	11 562	133 67	
		330000	74	0 3	0 2806	0 000235949		0 2556	0 001629839	3 7612	12 707	161 46	
				RMS=	S^2=	-0 029290162	RMS=	S^2=	0 001984977	SUM	15 317	43 198	475 96 B= -0 059